

Chapter 3

STAGGERED FERMIONS ON THE LATTICE

Stephen R. Sharpe

Physics Department, University of Washington, Seattle, WA 98195, USA

3.1 OVERVIEW

This Chapter explains how one calculates weak amplitudes using staggered fermions, and why such calculations are interesting. Numerical results are discussed separately, in Chapter 8.

The fundamental motivation for using staggered fermions is that there is a chiral symmetry even at finite lattice spacing. This is in contrast to Wilson fermions, for which the chiral symmetry is completely broken. Staggered fermions are thus well suited to studying quantities constrained by chiral symmetry. Two such quantities are of particular interest: the chiral condensate $\langle \bar{\psi}\psi \rangle$, and the amplitudes for weak decays involving kaons and pions.

The price one pays for the chiral symmetry is that a single lattice fermion represents more than one continuum quark. This is a manifestation of the fermion doubling problem. In the Hamiltonian formulation there is a two-fold degeneracy in the continuum limit [1], while the Euclidean formulation is four-fold degenerate in this limit [2, 3]. We concentrate here on Euclidean staggered fermions since numerical calculations use this formulation. To highlight the appearance of the degeneracy factor, we often refer to it as N_f . This does not indicate that we could choose other values—we always mean $N_f = 4$.

It turns out that to make use of the lattice chiral symmetry we must introduce one lattice fermion for each continuum quark. In the continuum limit, the lattice theory thus represents four degenerate up quarks, four degenerate down quarks, etc. We call this continuum theory QCDN_f. To extract matrix elements we must first relate the lattice theory at finite lattice spacing to QCDN_f, and then relate the latter

to QCD. These steps make the calculations more complicated to set up than those with Wilson fermions. This is the price we pay for the axial symmetry. Numerical results indicate that it is worth paying this price when calculating kaon decay and mixing amplitudes.

This Chapter is organized as follows. In the three subsequent sections we explain how QCD matrix elements are transcribed onto the lattice. Section 3.2 introduces staggered fermions, explains how the N_f continuum fermions arise, and how the full $SU(N_f)$ flavor symmetry appears in the continuum limit. Section 3.3 explains how matrix elements in QCD are related to those in QCDN_f , while section 3.4 discusses the relationship between lattice and QCDN_f matrix elements. We then turn to the rewards for using staggered fermions. Section 3.5 explains how the lattice axial symmetry implies Ward identities, which in turn can be used to show that suitably chosen lattice amplitudes have the same chiral behavior as their continuum counterparts. This chiral behavior includes the presence of chiral logarithms due to pion and kaon loops, and these are discussed separately in section 3.6. We close with a brief discussion of the outlook for future calculations.

Partial reviews of the subjects covered here are to be found in Refs. [4] and [5].

3.2 ACTION AND SYMMETRIES

To understand staggered fermions it is useful to begin with the naive discretization of the continuum fermion action, which describes so-called “naive” fermions,

$$S_F = \sum_n \left[\bar{\psi}(n) \sum_{\mu} \frac{1}{2} \gamma_{\mu} \left(U_{\mu}(n) \psi(n+\mu) - U_{\mu}(n-\mu)^{\dagger} \psi(n-\mu) \right) + m \bar{\psi}(n) \psi(n) \right]. \quad (3.1)$$

Here n is a four-vector of integers labeling the lattice points, and $U_{\mu}(n)$ are the gauge fields residing on links. The lattice spacing is set equal to unity. Throughout this Chapter we work in Euclidean space, with $\mu = 1-4$, and with hermitian gamma matrices satisfying $\{\gamma_{\mu}, \gamma_{\nu}\} = 2\delta_{\mu\nu}$. Naively one expects that, in the continuum limit, this action will describe a single Dirac fermion. Instead, the fermion propagator

$$G(k) = \frac{1}{m + \sum_{\mu} i \gamma_{\mu} \sin k_{\mu}} \quad \left(-\frac{\pi}{2} < k_{\mu} \leq \frac{3\pi}{2} \right) \quad (3.2)$$

has poles close to the 16 positions in the Brillouin zone where all components of $\sin k_{\mu}$ vanish. Each pole represents a separate fermion with mass m in the continuum limit. This is the fermion doubling problem.

To label the poles we use four-vectors A_{μ} with components either 0 or 1: the A 'th pole is close to $k_{\mu} = \pi A_{\mu}$. The 16 possible vectors A correspond to the corners of a 2^4 hypercube, so we call A a “hypercube vector”. The addition of two such vectors is defined by combining components modulo 2, $C_{\mu} =_2 A_{\mu} + B_{\mu}$.

To reduce the degeneracy, we use the trick of spin-diagonalization. Performing the change of variables [2]

$$\psi(n) = \gamma_n \chi(n) , \quad \bar{\psi}(n) = \bar{\chi}(n) \gamma_n^\dagger , \quad \gamma_n = \gamma_1^{n_1} \gamma_2^{n_2} \gamma_3^{n_3} \gamma_4^{n_4} , \quad (3.3)$$

in which γ_n depends only on $\text{mod}_2(n_\mu)$, one finds

$$S_F = \sum_n \left[\bar{\chi}(n) \sum_\mu \frac{1}{2} \eta_\mu(n) \left(U_\mu(n) \chi(n+\mu) - U_\mu(n-\mu)^\dagger \chi(n-\mu) \right) + m \bar{\chi}(n) \chi(n) \right] . \quad (3.4)$$

The gamma matrices have been replaced by the phases¹

$$\eta_\mu(n) = (-)^{\sum_{\nu < \mu} n_\nu} , \quad (3.5)$$

so that the four spinor components of χ are only coupled by gluon exchanges. Staggered fermions result from simply deleting three of the four components of χ , leaving a one component fermion on each site. This reduces the number of continuum fermions from 16 to $N_f = 4$.

This theory still does not seem useful for studying QCD, which, after all, has only two nearly degenerate quarks. We discuss in the next section how one can overcome this problem while retaining the N_f -fold degeneracy. We note here two alternative approaches. First, it is possible to reduce the degeneracy by a further factor of two [3, 7], thus producing a theory with two fermions. Second, one can add extra mass terms so as to break the degeneracy [8], and then use the four flavors to represent u , d , s and c quarks. Unfortunately, both of these alternatives remove the lattice axial symmetry which, as we shall see, is crucial to the study of weak matrix elements. For such studies it is better to use the N_f -fold degenerate theory.

Staggered fermions represent four degenerate flavors in the continuum limit, but at finite lattice spacing the flavor symmetry is broken. The only continuous symmetry of the action Eq. 3.4 is that corresponding to fermion number

$$\chi(n) \rightarrow \exp[i\theta_V] \chi(n) , \quad \bar{\chi}(n) \rightarrow \bar{\chi}(n) \exp[-i\theta_V] , \quad (3.6)$$

which we refer to as $U(1)_V$. In the massless limit, the continuum symmetry enlarges to $SU(4)_L \times SU(4)_R$, while the lattice action has an additional symmetry

$$\chi(n) \rightarrow \exp[i(-)^n \theta_A] \chi(n) , \quad \bar{\chi}(n) \rightarrow \bar{\chi}(n) \exp[i(-)^n \theta_A] , \quad (3.7)$$

where $(-)^n = (-)^{n_1+n_2+n_3+n_4}$. As we will see, this is a flavor non-singlet axial symmetry in the continuum limit, and we refer to it as $U(1)_A$. The remaining symmetries are translations, rotations, reflections and charge conjugation [7]. These are the discrete remains of the flavor and Poincaré symmetries.

To use staggered fermions, we must learn how to identify the continuum spin and flavor transformation properties of fields constructed from χ and $\bar{\chi}$. We also

¹Other choices of phases are possible, but all are equivalent [6].

need to know how the full symmetry group is broken at finite lattice spacing. To do this requires some notation. We denote quark fields in a continuum theory with four degenerate fermions using upper case letters, e.g. $Q_{\alpha,a}$. These have a spinor index (here α) and a flavor index (here a), both running from 1 to 4. Quark bilinears in this theory are of the general form $\overline{Q}_{\alpha,a}\gamma_S^{\alpha\beta}\xi_F^{ab}Q_{\beta,b}$. Here γ_S determines the spin of the bilinear, ξ_F the flavor. S is one of the 16 hypercube vectors, and labels Dirac matrices as in Eq. 3.3. We also use gamma matrices as the generators of the U(4) flavor group. More precisely, we follow the notation of Ref. [9] and use $\xi_F \equiv \gamma_F^*$, with F another hypercube vector. To keep the notation as clear as possible, we always use the ξ matrices for flavor, and γ matrices for spin. It is convenient to combine spin and flavor matrices into a single 16×16 matrix ($\gamma_S \otimes \xi_F$). The general bilinear is thus

$$\overline{Q}_{\alpha,a}\gamma_S^{\alpha\beta}\xi_F^{ab}Q_{\beta,b} \equiv \overline{Q}_{\alpha,a}(\gamma_S \otimes \xi_F)^{\alpha a, \beta b}Q_{\beta,b} . \quad (3.8)$$

We usually abbreviate the notation to $\overline{Q}(\gamma_S \otimes \xi_F)Q$, treating Q as a 16 component column vector. For example, the scalar-isoscalar bilinear $\overline{Q}_{\alpha,a}Q_{\alpha,a}$ is written $\gamma_S \otimes \xi_F$ with $S = F = (0000)$, or equivalently as $1 \otimes 1$. Color indices play no role in the discussion of this section, and we do not show them explicitly.

We also need two other sets of matrices which are unitarily equivalent to $(\gamma_S \otimes \xi_F)$. Both sets trade the indices $[\alpha, a]$ for a hypercube vector. In the notation of Refs. [10, 9], the sets are first the ‘‘hypercube’’ matrices

$$\overline{(\gamma_S \otimes \xi_F)}_{AB} \equiv \frac{1}{4}\text{Tr}[\gamma_A^\dagger \gamma_S \gamma_B \gamma_F^\dagger] \quad (3.9)$$

$$= \left(\frac{1}{2}\gamma_A^*\right)^{\alpha a}(\gamma_S \otimes \xi_F)^{\alpha a, \beta b}\left(\frac{1}{2}\gamma_B\right)^{\beta b} , \quad (3.10)$$

and second the ‘‘pole-space’’ matrices

$$\overline{\overline{(\gamma_S \otimes \xi_F)}}_{AB} \equiv \sum_{CD} \frac{1}{4}(-)^{A.C} \overline{(\gamma_S \otimes \xi_F)}_{CD} \frac{1}{4}(-)^{D.B} . \quad (3.11)$$

Here $A.C = \sum_{\mu} A_{\mu}C_{\mu}$. The reasons for the choice of names will become apparent shortly. The multiplication rule for each of the representations is as for a direct product, for example

$$\overline{(\gamma_S \otimes \xi_F)} \overline{(\gamma_{S'} \otimes \xi_{F'})} = \overline{(\gamma_S \gamma_{S'} \otimes \xi_F \xi_{F'})} \equiv \overline{(\gamma_{SS'} \otimes \xi_{FF'})} . \quad (3.12)$$

In the last equality we use the abbreviation $\gamma_S \gamma_{S'} = \gamma_{SS'}$. Either of these new sets of matrices could appear in bilinears in place of $(\gamma_S \otimes \xi_F)$ without changing the physical content of the theory.

With this notation in hand we discuss first the symmetries of the free staggered action. This is best done in momentum space. Since continuum fermions are constructed from the 16 poles close to $k_{\mu} = \pi A_{\mu}$, it is convenient to use the decomposition

$$k_{\mu} = k'_{\mu} + \pi A_{\mu} ; \quad -\pi/2 < k'_{\mu} \leq \pi/2 . \quad (3.13)$$



Figure 3.1: Notation for Feynman diagrams.

For physical quarks the “small” component k' is close to zero: if k_{phys} is the physical momentum and a is the lattice spacing then $k' = ak_{\text{phys}}$. k' is conserved by the action, Eq. 3.4, whereas the alternating phases $\eta_\mu(n)$ cause the large component $A\pi$ to change. The fermion propagator is thus a matrix acting on the indices A , and can be written [7, 8] (see Fig. 3.1 for notation)

$$G^{-1}(q, p) = G^{-1}(q' + \pi B, p' + \pi A) \quad (3.14)$$

$$= \bar{\delta}(q' + p') \left[\overline{m(1 \otimes 1)}_{BA} + i \sum_{\mu} \sin q'_{\mu} \overline{(\gamma_{\mu} \otimes 1)}_{BA} \right], \quad (3.15)$$

where $\bar{\delta}(q' + p')$ is the periodic delta function, which sets $q'_{\mu} + p'_{\mu} = 0 \pmod{2\pi}$.

There are various noteworthy features of this result.

1. The propagator has exactly the same form in spin and flavor space as a free continuum propagator, except that the matrices are in the “pole-space” basis. Thus the free lattice action is invariant under an $SU(4)$ flavor group, which we identify with the corresponding group in the continuum. Furthermore, if $m = 0$ the symmetry is the full chiral $SU(4)_L \times SU(4)_R$. Thus, in the continuum limit, the 16 components of $\chi(p' + \pi A)$ for fixed p' become equivalent to the continuum field $Q(p')_A$, where the latter has been rotated into the pole-space basis.

2. The lattice propagator does not have the full Euclidean symmetry because of the appearance of $\sin p_{\mu}$ in place of p_{μ} . Since $\sin p'_{\mu} = p'_{\mu} + O(p'^3)$, and $p' = O(a)$, the symmetry is broken only by corrections of $O(a^2)$. This should be compared to Wilson fermions, which have corrections of $O(a)$.

3. Because the flavor symmetries are momentum dependent, almost all involve non-local transformations in position space [6]. This explains the lack of corresponding local, continuous symmetries of the action Eq. 3.4. The non-local symmetries are not useful, however, as they do not survive the introduction of interactions.²

4. The only flavor symmetries which correspond to local transformations are $U(1)_V$ and $U(1)_A$. In momentum space the vector symmetry becomes

$$\chi(p' + \pi C) \rightarrow \exp[i\theta_V \overline{(1 \otimes 1)}_{CD}] \chi(p' + \pi D); \quad (3.16)$$

$$\bar{\chi}(q' + \pi D) \rightarrow \bar{\chi}(q' + \pi C) \exp[-i\theta_V \overline{(1 \otimes 1)}_{CD}], \quad (3.17)$$

²The appearance of non-local symmetries is nothing new for free fermions: there are an infinite number of the form $\psi(p) \rightarrow \exp(i\omega(p))\psi(p)$.

while the axial symmetry is

$$\chi(p' + \pi C) \rightarrow \exp[i\theta_A \overline{(\gamma_5 \otimes \xi_5)}_{CD}] \chi(p' + \pi D) , \quad (3.18)$$

$$\bar{\chi}(q' + \pi D) \rightarrow \bar{\chi}(q' + \pi C) \exp[i\theta_A \overline{(\gamma_5 \otimes \xi_5)}_{CD}] . \quad (3.19)$$

These are both symmetries of the full action including interactions. Eq. 3.18 shows that the axial symmetry is a flavor non-singlet, and is thus not anomalous in the continuum limit. It plays a crucial role in the study of weak amplitudes.

5. A discrete subgroup of the flavor and spin symmetries correspond to local transformations, and survive in the presence of interactions. For example, the symmetry transformation corresponding to a shift in the μ direction is a pure flavor rotation [8]

$$\chi(p' + \pi A) \rightarrow \exp[ip'] \overline{(1 \otimes \xi_\mu)}_{AB} \chi(p' + \pi B) . \quad (3.20)$$

Note that here the matrix is an element of the flavor group, and not its Lie algebra.

That the non-local flavor $SU(4)$ is broken by the interactions can be seen by looking at the quark-gluon vertex. Aside from color factors this can be written as [8, 9]

$$V_\mu(q' + \pi B, p' + \pi A, k) = -ig\bar{\delta}(p' + q' + k) \cos(q'_\mu + k_\mu/2) \overline{(\gamma_\mu \otimes 1)}_{AB} , \quad (3.21)$$

where μ is the gluon polarization direction, and the momenta are defined in Fig. 3.1. For physical quark and gluon momenta (i.e. $p', q', k = O(a)$), the vertex conserves flavor and agrees with the continuum vertex up to corrections of $O(a^2)$. In loop diagrams, however, the momenta need not be physical. For example, if the gluon momentum is $k = k' + \pi C$, with $C_\nu \neq 0$ for some $\nu \neq \mu$, and $k' = O(a)$ (k' has no physical significance for the gluon), then the vertex becomes

$$V_\mu(q' + \pi B, p' + \pi A, k' + \pi C) = -ig\bar{\delta}(p' + q' + k') \cos(q'_\mu + k'_\mu/2) \overline{(\gamma_{\mu\tilde{C}} \otimes \xi_{\tilde{C}})}_{AB} . \quad (3.22)$$

Here we follow Ref. [9] and define $\tilde{C}_\mu =_2 \sum_{\nu \neq \mu} C_\nu$. The appearance of the flavor matrix $\xi_{\tilde{C}}$ means that the vertex does not conserve flavor. This flavor symmetry breaking is not suppressed by powers of a .

Thus we see that gluons with “large” momenta cause a large breaking of the non-local flavor symmetry. It is important to understand how this affects physical amplitudes, i.e. those in which all external particles have physical momenta. To address this question, we imagine making the lattice spacing very small, and then integrating out quarks and gluons with physical momenta above a scale μ . We choose μ to be far below the cutoff, i.e. $\mu a \ll 1$, but large enough that perturbation theory is valid. The only subtlety is that for quarks the physical momentum is the distance from the nearest of the 16 poles. The integration yields the effective action, and we

are interested in its symmetries.³ The leading term in the effective action is simply the tree-level Lagrangian, and we have already seen that two and three point vertices do not break the flavor symmetries for low momentum quarks and gluons. Potential flavor breaking comes from two sources. First, from the exchange of a gluon with one or more components close to π . This leads, for example, to a four fermion vertex which does break the flavor symmetry [1]. It is, however, suppressed by $O(a^2)$, because the gluon energy is of $O(1/a)$. The second source is loop corrections involving large momentum gluons, e.g. self energy and vertex corrections. These are potentially dangerous as they are suppressed only by powers of g^2 , not by powers of a . They turn out, however, not to break flavor symmetry at $O(a^0)$, because the flavor breaking vertices always come in pairs. It is relatively simple to see that the flavor breaking “cancels” in 1-loop corrections. In Ref. [3] it is argued that, due to the discrete symmetries of the action, flavor symmetry breaking does not occur at $O(a^0)$ to all orders in g^2 . A more explicit demonstration of this result for the quark propagator has been given in Ref. [12].

In summary, flavor symmetry breaking in physical amplitudes vanishes in the continuum limit. It is reasonable to assume that the leading flavor breaking terms are of $O(a^2)$, since there are only $O(a^2)$ corrections to vertices and propagators. Recent numerical evidence supports this assumption [13]. We do not, however, know of a proof.

A related claim of Ref. [3] is that perturbative diagrams can be written so that there is an explicit factor of N_f for each fermion loop, with an integrand which is the same as for naive lattice fermions (Eq. 3.1) except that the range of integration is restricted to $-\pi/2 < k_\mu \leq \pi/2$, and thus includes only a single pole. This shows that, in a certain sense, there are N_f fermions even at finite lattice spacing. Furthermore, it makes taking the N_f 'th root of the fermion determinant, which is the standard method for reducing the degeneracy in fermion loops, seem more reasonable.

The pole-space representation of the symmetry group is useful in perturbative calculations, but we need a position space representation for numerical simulations. This is provided by the work of Ref. [6]. The lattice is divided into 2^4 hypercubes in one of the 16 possible ways. Points on the original lattice are specified by a vector y labeling the hypercubes (with all components even), and a vector A determining the position within the hypercube (with all components 0 or 1). We collect the 16 components of χ for a given y into a “hypercube field”

$$\chi(y)_A = \frac{1}{4}\chi(y + A) , \tag{3.23}$$

³This is equivalent to the following renormalization group approach [11]. The continuum symmetries are those of theories on the renormalized trajectory. This is the trajectory in the space of actions that one flows towards as one integrates out the high momentum quarks and gluons. By starting with a small enough lattice spacing, and integrating far enough, one approaches exponentially close to this trajectory. This assumes that the mass term, which is the only relevant operator, is tuned to zero appropriately.

where we have used the notation and normalization of Ref. [10]. It is shown in Ref. [6] that, in the continuum limit, $\chi(y)_A$ becomes equal to the continuum field $Q(y)$, if the latter is in the hypercube basis. Thus, the bilinear

$$\mathcal{O}_{SF}(y) = \sum_{A,B} \bar{\chi}(y)_A \overline{(\gamma_S \otimes \xi_F)_{AB}} \chi(y)_B \quad (3.24)$$

has the same flavor, spin and normalization as $\overline{Q}(y)(\gamma_S \otimes \xi_F)Q(y)$ in the continuum limit. We often refer to \mathcal{O}_{SF} by the abbreviated form $\overline{\chi}(\gamma_S \otimes \xi_F)\chi$. We also use $\overline{(\gamma_S \otimes \xi_F)}$, when confusion with the matrix that this notation also defines is unlikely.

The equivalence of χ_A and Q is established by showing that the Fourier transform of $\chi(y)_A$ is equivalent to $\chi(p' + \pi A)$, which we have already seen is equivalent to $Q(p')_A$. All of these equivalences hold only in the continuum limit. These relationships are in momentum space, which on the lattice extends only to $\pi/2$. This means that in position space, $\chi(y)_A$ is related to the continuum field $Q(y)_A$ smeared over the hypercube.

To establish the relationship between $\chi(y)_A$ and $\chi(p' + \pi A)$, we change the former to the pole-space basis and then Fourier transform

$$\chi(p')_A = 16 \sum_{y,B} \exp(-ip' \cdot y) \frac{1}{4} (-)^{A \cdot B} \chi(y)_B, \quad \frac{\pi}{2} < p' \leq \frac{\pi}{2}. \quad (3.25)$$

The factor of 16 accounts for the fact that the hypercube has a volume of $(2)^4$ in lattice units [10]. Using the even-ness of y we can rewrite Eq. 3.25 as

$$\chi(p')_A = \sum_{y,B} \exp[-i(p' + A\pi) \cdot (y + B)] \exp(ip' \cdot B) \chi(y + B). \quad (3.26)$$

This differs from the standard Fourier transform,

$$\chi(p' + \pi A) = \sum_{y,B} \exp[-i(p' + A\pi) \cdot (y + B)] \chi(y + B), \quad (3.27)$$

only by the factor of $\exp(ip' \cdot B)$ in Eq. 3.26. In the continuum limit, when $p' \rightarrow 0$ for physical quarks, the two sets of fields are the same.

It is important to determine how quickly the position space bilinears approach their continuum limits. We have argued above that amplitudes involving the momentum space fields (with physical momenta) differ from their continuum limits by terms of $O(a^2)$. But when we take matrix elements of \mathcal{O}_{SF} (Eq. 3.24) between quarks and antiquarks with definite physical momenta, we are, in effect, using $\chi(p')_A$ rather than the exact Fourier transform $\chi(p' + \pi A)$. It is easy to see from Eqs. 3.26 and 3.27 the difference between these fields is proportional to $\exp(ip' \cdot B) - 1 \propto p'$, and is thus of $O(a)$. This means that matrix elements of the operators \mathcal{O}_{SF} have $O(a)$ corrections, which will, in general, be larger than the $O(a^2)$ flavor breaking corrections coming from the action. Thus we expect larger scaling corrections in matrix elements than in hadron mass ratios.

It is quite simple to improve the operators so as to remove the $O(a)$ corrections [14]. One of many methods is to make the replacement

$$\chi(y)_A \rightarrow \frac{1}{16} \sum_{\mu} \chi(y + A + 2\hat{\mu}[1 - 2A_{\mu}]) , \quad (3.28)$$

where $\hat{\mu}$ is a vector whose μ 'th component is 1 while all other components zero. Such improved operators should be used as numerical work progresses.

It is instructive to display some hypercube operators explicitly. The analog of $\bar{u}u + \bar{d}d$ in QCD is the flavor singlet scalar density,

$$\overline{(1 \otimes 1)}(y) = \sum_A \bar{\chi}(y + A)\chi(y + A) . \quad (3.29)$$

Numerical simulations indicate that it gets a vacuum expectation value, which breaks the $U(1)_A$ symmetry dynamically.⁴ Results are shown in Chapter 8. This means that the pion with flavor ξ_5 is a pseudo-Goldstone boson. In fact, using the axial symmetry one can derive Ward identities from which it follows that the ξ_5 pion mass satisfies $m_{\pi}^2 \propto m_q$, with the form of the relationship the same as in the continuum [15]. Such Ward identities are discussed further in section 3.5. We will refer to the flavor ξ_5 pion simply as the Goldstone pion. A field which creates this pion is

$$\overline{(\gamma_5 \otimes \xi_5)}(y) = \sum_A \bar{\chi}(y + A)\chi(y + A)(-)^A . \quad (3.30)$$

Both this operator and that in Eq. 3.29 are completely local in terms of χ , whereas most of the \mathcal{O}_{SF} are slightly non-local. One can see from the definition of the hypercube fields (Eqs. 3.24 and 3.10) that if $S_{\mu+2} F_{\mu} = 1$, then the fields are separated by a link in the μ direction. Thus the fields in the axial current associated with the dynamically broken symmetry, $\overline{(\gamma_{\mu 5} \otimes \xi_5)}$, are separated by 1 link, while those in the flavor singlet current $\overline{(\gamma_{\mu 5} \otimes 1)}$ are separated by 3 links. Non-local operators such as these must be made gauge invariant in some way. Various possibilities are discussed in section 4.

In the remainder of this section we collect various facts about staggered fermions which are needed in the subsequent discussion. For further details readers should consult the references given above, and also Refs. [16].

Aside from the $U(1)_V \times U(1)_A$ currents, all flavor currents are broken by the action. In particular the other axial currents are not conserved, so that the corresponding pion fields are not pseudo-Goldstone bosons. They should become degenerate with the Goldstone pion in the continuum limit, with the mass splitting falling as a^2 . The numerical results show a clear drop in the splitting, consistent with the expected dependence on a , though the errors are large [17].

⁴For $m = 0$ one can choose how to combine left and right handed fermions into Dirac fermions, which means that the assignment of non-singlet symmetries as vector or axial is arbitrary. Thus, in a certain basis $U(1)_A$ is a vector symmetry. The fact that the flavor singlet field has an expectation value, however, does fix the $U(1)_A$ symmetry to be axial.

The mass of the flavor singlet “pion” (i.e. that created by $\overline{(\gamma_5 \otimes 1)}$, a 4 link operator) should not be degenerate with the other pions in the continuum limit, because of the axial anomaly. This enters with staggered fermions in much the same way as for Wilson fermions, i.e. through the regulator terms [3]. It is this pion which has an anomalous three point vertex with two $U(1)_V$ currents analogous to the $\pi_0\gamma\gamma$ vertex in QCD, as has been shown explicitly in Ref. [18]. The Goldstone pion has no such vertex because the triangle graph has a vanishing flavor trace.

At finite a , lattice states lie in representations of the discrete symmetry group consisting of shifts, rotations, translations and charge conjugation. The representations of this group for states at zero and non-zero momentum are worked out in Refs. [16] and [15] respectively. It is also known how the discrete group is embedded in the continuum spin and flavor group, so that continuum representations can be decomposed into their lattice parts. For example, the 14 non-singlet non-Goldstone pions with zero spatial momentum fall into four three-dimensional and two one-dimensional representations. Using these symmetries allows one to construct meson and baryon operators which couple to only a single lattice representation [16], and to understand which states are created by the extended sources that are in common use in numerical simulations [19].

The symmetries are also useful as a check when studying the possible mixing amongst lattice operators [8, 9, 20]. As discussed above, we know that mixing of the flavor-singlet operators in the action with flavor non-singlet operators is suppressed by a^2 . This suppression is not true in general when we renormalize an external operator. The flavor mixing is generically of $O(g^2)$, and may be substantial in present numerical simulations. We discuss this in detail in section 3.4.

3.3 TRANSCRIBING OPERATORS

In this section we explain how staggered fermions can be used to calculate QCD matrix elements [21]. It turns out that there are many ways to transcribe a particular continuum matrix element onto the lattice, and in general there is no clear reason to prefer one choice over the others. For matrix elements involving pseudo-Goldstone bosons—pions, kaons and etas—there is, however, a subset of preferred choices, those which make maximum possible use of the lattice axial symmetry. These are the matrix elements for which staggered fermions are at an advantage compared to Wilson fermions, and we concentrate entirely on such matrix elements in this Chapter. Exactly how the lattice axial symmetry constrains the results is explained in section 3.5. For a discussion of other approaches see Refs. [5] and [22].

The method can be broken down into a number of rules, which we explain by working out the lattice transcription of a variety of QCD matrix elements. Further applications of the method are discussed in sections 3.4 and 3.5.

The first rule is to introduce a separate lattice fermion for each continuum quark, i.e. for three flavor QCD we use χ_u , χ_d and χ_s . This means that in the continuum

limit the theory we obtain is not QCD but QCDN_f, i.e. QCD with N_f degenerate copies of each quark. The transcription of continuum matrix elements onto the lattice thus breaks up into two stages. First, we match QCD matrix elements to those of QCDN_f. This matching is the subject of this section. It is designed so that there are no perturbative corrections: the contractions in the two theories are formally equal diagram by diagram. Second, we match operators in QCDN_f to those on the lattice. In the previous section we explained how to do this at tree level, and we give further examples of tree-level matching in this section. In the following section we extend the matching to 1-loop order.

The reason for the first rule is that it allows us to take lattice matrix elements between lattice pseudo-Goldstone bosons. A single lattice fermion produces only a single Goldstone pion, but with three staggered fermions there are $3 \times 3 = 9$, more than enough for the eight pions, kaons and etas. The second rule is to transcribe continuum pions, kaons and etas into QCDN_f pseudoscalars with flavor ξ_5 , so that on the lattice they become the Goldstone pions. For example, the QCDN_f version of the K^0 is created by $\overline{D}(\gamma_5 \otimes \xi_5)S$, while the lattice “kaon” is created by $\overline{\chi}_d(\gamma_5 \otimes \xi_5)\chi_s$. (Recall that the upper case letters represent the four flavor fermions of QCDN_f.) This rule is crucial if we are to use the lattice axial symmetry to constrain the amplitudes.

The third rule concerns the flavor of the operators to be used: it should be chosen so that the matrix element does not have a vanishing flavor trace. We illustrate this with two examples. The first is the kaon decay constant

$$\sqrt{2}f_K p_\mu = \langle 0 | \overline{s}\gamma_\mu\gamma_5 d | K^0 \rangle . \quad (3.31)$$

According to the second rule, the QCDN_f kaon has flavor ξ_5 . This means that the QCDN_f transcription of the axial current must also have this flavor, and thus is $\overline{S}(\gamma_\mu\gamma_5 \otimes \xi_5)D$. Any other flavor would yield a vanishing flavor trace. At tree level this QCDN_f operator matches onto the lattice operator $\overline{\chi}_s(\gamma_{\mu 5} \otimes \xi_5)\chi_d$. It turns out that, because of the discrete lattice symmetries, loop diagrams do not cause mixing with other operators. Their only effect is to change the relative normalization of the lattice and QCDN_f operators [9].

The second example is the pion scalar transition matrix element $\langle \pi^+ | \overline{u}u | \pi^+ \rangle$. The QCDN_f equivalent uses $\overline{U}(\gamma_5 \otimes \xi_5)D$ to create the pion, and the conjugate operator to destroy it. The scalar operator acts between two pions of flavor ξ_5 , and thus, for the flavor trace to be non-zero, the QCDN_f operator must be the flavor singlet $\overline{U}(1 \otimes 1)U$. This transcribes onto the lattice as $\chi_u(1 \otimes 1)\chi_u$, again with loops only changing the normalization but not causing mixing.

In each of these examples there are N_f quarks flowing in the quark propagators of the QCDN_f contraction, as compared to a single quark for QCD. The fourth rule is to divide the QCDN_f matrix element by a factor of N_f for each fermion loop. When we transcribe the matrix elements onto the lattice we continue to divide by the same factors of N_f .

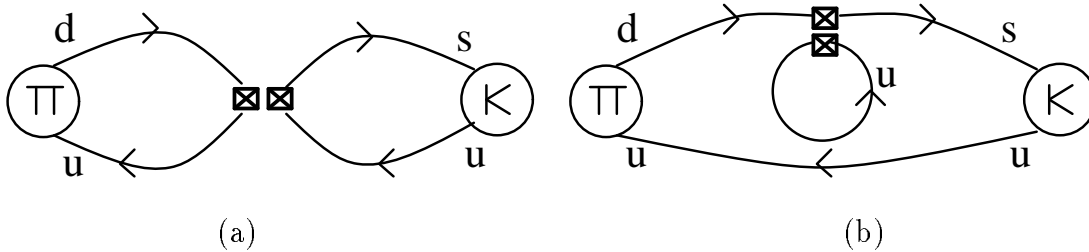


Figure 3.2: Contractions contributing to $\langle \pi^+ | \mathcal{O}_1 | K^+ \rangle$. (a) eight and (b) eye diagrams.

This rule also applies to the disconnected quark loops produced by the fermion determinant. It is equivalent to taking the N_f 'th root of the QCDN_f determinant, which does yield the QCD determinant. To match QCDN_f onto the lattice theory, we simply take the N_f 'th root of the lattice determinant.

This procedure has aroused some controversy, because, once we take the N_f 'th root of the lattice determinant, we do not know what the lattice action is. Nevertheless, the lattice action differs from that of QCDN_f only by terms of $O(a^2)$, so that in the continuum limit it does describe N_f flavors, and taking the root is legitimate. At finite lattice spacing there are corrections, but these are no different in character from the those introduced by discretizing the continuum theory. In particular, taking the root does not break any of the lattice symmetries discussed above. In fact, in perturbation theory, it is claimed in Ref. [3] that loop diagrams come naturally with an overall factor of N_f^{loop} . Altogether, then, taking the N_f 'th root of the determinant seems reasonable, though it is of considerable interest to check this claim with explicit calculations.

To illustrate why we take matrix elements between lattice Goldstone pions, we consider the continuum relationship

$$\langle \pi^+ | \bar{u}u | \pi^+ \rangle = \sqrt{2} f_\pi \langle 0 | \bar{d} \gamma_5 u | \pi^+ \rangle \left(1 + O(m_\pi^2 / (4\pi f_\pi)^2) \right), \quad (3.32)$$

which follows from the approximate chiral symmetry of QCD. If we transcribe the matrix elements using our rules then the lattice axial symmetry guarantees that this equation holds also for the lattice quantities [15].

The fifth and final rule applies to matrix elements in which the operators have more than one contraction with the external states. This is the case for some four fermion operators. The rule is that the transcription is to be done separately for each contraction. Different contractions will in general require different operators. There is not a one-to-one mapping between QCD and QCDN_f operators.

We illustrate this with our final example. We consider

$$\langle \pi^+ | \mathcal{O}_1 | K^+ \rangle = \langle \pi^+ | [\bar{u}_a \gamma_\mu (1 + \gamma_5) d_a] [\bar{s}_b \gamma_\mu (1 + \gamma_5) u_b] | K^+ \rangle, \quad (3.33)$$

where we have reinstated the color indices. The operator \mathcal{O}_1 plays a major role in the weak decays of kaons. There are two types of contractions, illustrated in Fig.

3.2, and colloquially referred to as “eights” and “eyes”. Consider the eight-diagram first. In this, $\bar{s}_b \gamma_\mu (1 + \gamma_5) u_b$ is contracted with the K^+ , $\bar{u}_a \gamma_\mu (1 + \gamma_5) d_a$ with the π^+ . Each of these contractions consists of two parts, that with the axial current $\gamma_\mu \gamma_5$, and that with the vector current γ_μ . Because of parity, only the “vector-vector” and “axial-axial” contractions survive.⁵ These are transcribed to QCDN_f using two different operators. First consider the vector-vector contraction. As always, the QCDN_f external states have flavor ξ_5 . This means that both bilinears must also have this flavor. The same is true for the axial-axial contraction, so that

$$\text{vector–vector eight: } \mathcal{O}_1 \rightarrow [\bar{U}_a(\gamma_\mu \otimes \xi_5)D_a] [\bar{S}_b(\gamma_\mu \otimes \xi_5)U_b]/N_f^2, \quad (3.34)$$

$$\text{axial–axial eight: } \mathcal{O}_1 \rightarrow [\bar{U}_a(\gamma_\mu \gamma_5 \otimes \xi_5)D_a] [\bar{S}_b(\gamma_\mu \gamma_5 \otimes \xi_5)U_b]/N_f^2. \quad (3.35)$$

There are three important points to note here

1. The factors of $1/N_f^2$ cancel the flavor factors from the two loops.
2. The two QCDN_f operators have different lattice transcriptions, the first (Eq. 3.34) consisting of 3-link bilinears, the second (Eq. 3.35) of 1-link bilinears.
3. Each of the QCDN_f operators themselves have both an eight and an eye type contraction with the external states, but we keep only the eight contraction.

This takes care of the eight diagrams. For the eye diagrams we face a new decision, namely whether or not to Fierz transform the continuum operator to

$$\mathcal{O}_1 = [\bar{u}_a \gamma_\mu (1 + \gamma_5) u_b] [\bar{s}_b \gamma_\mu (1 + \gamma_5) d_a]. \quad (3.36)$$

(We have included the sign from fermion anticommutation in the Fierz transform.) We choose to use the Fierz transformed operator, because then both eight and eye contractions contains two traces over spinor indices. We indicate this in Fig. 3.2 by splitting the operator up into two bilinears. We choose the same number of spinor traces for each contraction since this is necessary for the derivation of Ward identities [15]. These identities also hold, however, if we Fierz transform the operator so that there is only a single spinor trace in all contractions. There is no strong reason to prefer two spinor traces over a single trace, but, since present numerical calculations use the two-trace transcription, we adopt it exclusively in the following sections.

Having made this choice, there are again vector-vector and axial-axial contractions. In this case, however, the QCDN_f operators should be flavor singlets in order that the contractions have a non-vanishing flavor trace. Thus we use

$$\text{vector–vector eye: } \mathcal{O}_1 \rightarrow [\bar{U}_a(\gamma_\mu \otimes 1)U_b] [\bar{S}_b(\gamma_\mu \otimes 1)D_a]/N_f^2, \quad (3.37)$$

$$\text{axial–axial eye: } \mathcal{O}_1 \rightarrow [\bar{U}_a(\gamma_\mu \gamma_5 \otimes 1)U_b] [\bar{S}_b(\gamma_\mu \gamma_5 \otimes 1)D_a]/N_f^2. \quad (3.38)$$

⁵This solves a puzzle that may have occurred to the reader. How can the chiral weak interactions be put on the lattice, given that the lattice theories are vector-like? The answer is that, since the strong interactions conserve parity, one only has to transcribe non-chiral quantities such as the vector-vector contractions onto the lattice.

Each of these QCDN_f operators has both eight and eye contractions, but we keep only the latter.

Taking into account color indices, we end up needing four different QCDN_f operators, one per contraction. Beyond tree-level, the matching of these operators with lattice operators does involve mixing, and such mixing forms the main topic of the following section.

3.4 RENORMALIZATION

In this section we discuss the $O(g^2)$ corrections to the tree-level relationships between lattice and continuum operators. We consider one loop corrections to fermion bilinear and quadrilinear operators. These corrections vanish logarithmically in the continuum limit, and thus dominate over scaling violations of $O(a)$ for small enough lattice spacing. As explained in the previous section, the lattice operators are to be matched with those in QCDN_f , the continuum theory with N_f degenerate versions of each quark. Thus we adopt the following notation in this section: “continuum” operators ($\mathcal{O}^{\text{CONT}}$) are from QCDN_f and not QCD.

Perturbative calculations with staggered fermions were pioneered in Refs. [3] and [2] and extended in Refs. [8], [9] and [20]. It is possible to write the expressions for loop diagrams in such a way that they are similar to those in QCDN_f . The main difference is that the lattice gluon can change the flavor of the quark it couples to, if the gluon has a momentum with one or more components close to π . These contributions break the flavor symmetry, so that operators which do not mix in QCDN_f can mix on the lattice. The size of this flavor symmetry breaking is, however, perturbatively calculable for small enough lattice spacing, since it is momenta close to the cut-off that are responsible for the mixing. For more discussion of the reliability of lattice perturbation theory see Ref. [23].

The general form of the relationship between QCDN_f and lattice operators is

$$\mathcal{O}_i^{\text{CONT}} = \mathcal{O}_i^{\text{LATT}} + \sum_j \frac{g^2}{16\pi^2} (d_{ij}L_\mu + c_{ij}) \mathcal{O}_j^{\text{LATT}} + O(g^4) + O(a) , \quad (3.39)$$

where \mathcal{O}_i is a set of operators, and $L_\mu = 2 \ln(\mu a/\pi)$. Such relations are derived by comparing the matrix elements of lattice and continuum operators between external quark and antiquark states. On the lattice the momenta of external particles must be physical, i.e. each component should lie close to zero or π . The coefficients c_{ij} and d_{ij} do not depend on the external momenta except through terms suppressed by powers of the lattice spacing. Similarly, the mass dependence is suppressed by powers of $O(ma)$. We do not discuss these corrections here.

The matrix elements of the continuum and lattice operators between external quark and antiquark states are ultraviolet and infrared divergent. The infrared divergences are handled by adding a gluon mass in one loop calculations. The ultraviolet divergences can be removed in the continuum using one of the standard

renormalization prescriptions. We follow Ref. [24] and use dimensional reduction with a renormalization scale μ . On the lattice the ultraviolet cut-off is $1/a$. If one has transcribed the continuum operators correctly onto the lattice then the infrared divergences cancel, and the ultraviolet divergences combine to give finite factors proportional to $\ln(\mu a)$. This cancellation has been assumed in writing Eq. 3.39. The coefficient of the logarithm, d_{ij} , is proportional to the anomalous dimension matrix. The remaining finite terms are contained in the coefficients c_{ij} .

With staggered fermions the operators are quasi-local rather than local, and must be made gauge invariant in some way. We discuss three alternatives. In Refs. [8, 9, 20] gauge invariance is insured by inserting the appropriate product of gauge links between quark and antiquark, and averaging over paths so as to maintain rotational invariance. A second approach is to project the average of the products of gauge links back into the gauge group $SU(3)$. This only affects operators with two or more links, but reduces the fluctuations in these operators. In numerical calculations using staggered fermions it is more convenient to use a third method: fix to Landau gauge and simply leave out the gauge links. As we will see, this not only reduces fluctuations due to gauge links, but also considerably simplifies the perturbative calculations [25]. The disadvantage of Landau gauge operators is that they may not be well defined due to Gribov copies. Such copies do not show up in perturbation theory, but could effect non-perturbative quantities such as weak matrix elements. This topic is under active investigation.

We present results for all three types of operator for fermion bilinears, since the comparison between them is instructive. For quadrilinear operators we give results only for Landau gauge operators.

3.4.1 Bilinear Operators

The one-loop diagrams one must calculate on the lattice are shown in Fig. 3.3. The three diagrams in the top line are common to all types of operators, while those of the second line are absent for Landau gauge operators. For calculations involving Landau gauge operators one must use the lattice Landau gauge gluon propagator, while the gauge choice is irrelevant for the gauge invariant operators. The continuum calculations require only the first two diagrams of the top line.

In the continuum, the logarithmic divergence does not mix the bilinears, and its coefficient depends only on the spin of the operator and not its flavor. It is a non-trivial check of the transcription of operators onto the lattice that the same is true for the lattice operators. Thus lattice and continuum bilinears have the same anomalous dimensions (as has been implicitly assumed in writing Eq. 3.39), with $d_{ij} = 0$ for $i \neq j$. Results for d_{ii} are given in Table 3.1.

The finite part of the correction does cause mixing amongst bilinears. Mixing occurs for vector, axial-vector and tensor operators, and is always between operators having the same spin but different flavor. For example, $\overline{(\gamma_\mu \otimes \xi_\nu)}$ ($\mu \neq \nu$) mixes with $\overline{(\gamma_\mu \otimes \xi_\mu)}$ (no sum on μ). It turns out, however, that present numerical calculations

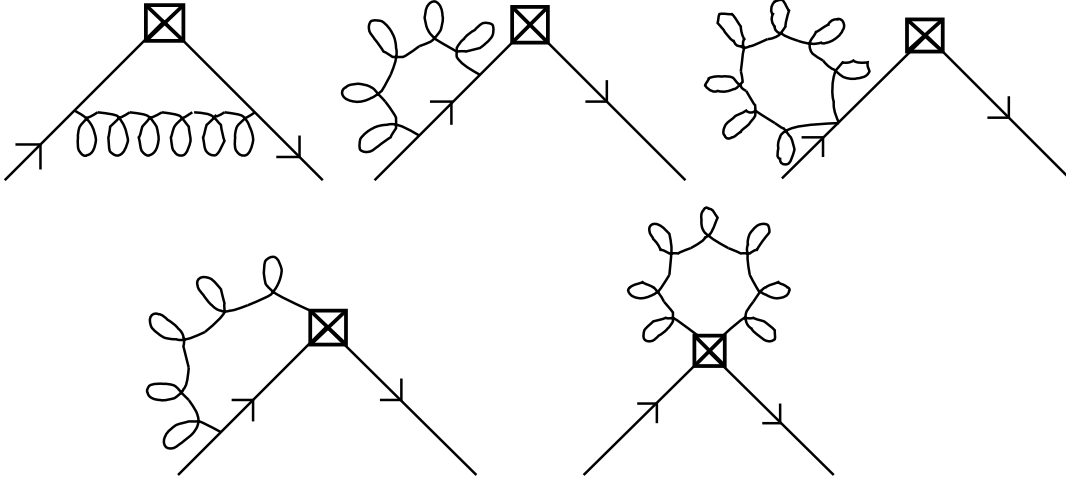


Figure 3.3: Diagrams contributing to the renormalization of fermion bilinears.

Spin	Flavor	d	Name	(a)	(b)	(c)
1	1	3	c_{SS}	-35.36	-35.36	-35.36
1	γ_5	3	c_{SP}	42.22	6.34	-3.22
1	γ_μ	3	c_{SV}	-4.77	-4.77	-13.95
1	$\gamma_{\mu 5}$	3	c_{SA}	28.84	6.33	-4.42
1	$\gamma_{\mu\nu}$	3	c_{ST}	14.30	4.43	-6.81
γ_μ	1	0	c_{VS}	0	0	-10.18
γ_μ	γ_5	0	c_{VP}	21.51	-1.01	-11.76
γ_μ	γ_μ	0	c_{VV0}	-15.78	-15.78	-15.78
γ_μ	γ_ν	0	c_{VV2}	9.04	-0.83	-12.08
γ_μ	$\gamma_{\mu 5}$	0	c_{VA4}	33.50	-2.38	-11.95
γ_μ	$\gamma_{\nu 5}$	0	c_{VA2}	9.06	-0.81	-12.06
γ_μ	$\gamma_{\mu\nu}$	0	c_{VT1}	-4.40	-4.40	-13.57
γ_μ	$\gamma_{\nu\rho}$	0	c_{VT3}	21.24	-1.28	-12.02

Table 3.1: Results for the diagonal part of renormalization constants at one-loop, i.e. $d = d_{ii}$ and c_{ii} . An overall color factor of $C_F = 4/3$ has been taken out. The components μ , ν and ρ are all different. The finite parts c_{ii} are given for three choices of operator: (a) with gauge links [9]; (b) projected gauge links [25]; and (c) Landau gauge [25].

do not require knowledge of the off-diagonal corrections. Nor do we need either the diagonal or off-diagonal corrections for tensor operators. Thus in Table 3.1 we give results for the diagonal corrections for scalar and vector operators. Because of the $U(1)$ axial symmetry, the corrections are the same for the two operators $(\overline{\gamma_S \otimes \xi_F})$ and $(\overline{\gamma_{S5} \otimes \xi_{F5}})$. Thus the table applies also to pseudoscalar and axial-vector operators, e.g. $c_{AP} = c_{VS}$.

To evaluate the corrections we need to choose a value for μ and a scheme for g^2 . A one-loop calculation gives no guidance as to how to make these choices, so we rely on the general arguments of Ref. [23]. The renormalization scale μ should be a typical loop momentum, and we take $\mu = \pi/a$. This choice causes the d_{ij} term in Eq. 3.39 to vanish. Other reasonable choices do not change the correction by much. More important is the choice of scheme for g^2 . In present simulations the bare lattice coupling is $g^2 \approx 1$. It is argued in Ref. [23] that one should not use the bare coupling, but instead pick a coupling constant evaluated in a continuum scheme such as \overline{MS} , which is larger by a factor of about 2. Using the bare lattice constant a typical correction ($c \sim 10$) is about 8%, while the largest corrections are $\sim 35\%$. With a continuum g^2 , the corrections range from -60% to $+70\%$.

The major cause of the large range of the corrections is the fluctuations in the gauge links in the non-local operators. This is shown by the increase in c as the number of links in the operator varies from zero (c_{SS}) to four (c_{SP} and c_{VA4}). This variation is reduced substantially using the projected gauge links, and is reduced still further with Landau gauge operators. In fact, aside from c_{SS} , the corrections to Landau gauge operators are uniform and relatively small. The large size of c_{SS} does, however, make a calculation of the condensate potentially unreliable. This issue is considered further in Chapter 8.

3.4.2 Four Fermion Operators

The calculation for four-fermion operators with (unprojected) gauge links has been done in Ref. [20], and that for Landau gauge operators in Ref. [25]. We focus on Landau gauge operators, and in particular those needed for the calculation of B_K , since the numerical calculations are well advanced [26]. The method we outline can be used for all four-fermion operators, except that some operators require the calculation of penguin diagrams, which are discussed in Ref. [25], but which we do not discuss here.

The mixing of four fermion operators is very messy, because huge numbers of operators can mix with one another. To begin we must introduce a compact notation for the operators. We will only consider the 256 operators of the type $(\overline{\gamma_S \otimes \xi_F}) (\overline{\gamma_S \otimes \xi_F})$, i.e. those in which the spins of the two bilinears are the same, as are the flavors. (Strictly speaking, we also need those of the form $(\overline{\gamma_S \otimes \xi_F}) (\overline{\gamma_{S5} \otimes \xi_{F5}})$, but the corrections for these can be obtained with no additional calculation.) In fact, we are only interested in those linear combinations of these operators which are scalars under the Euclidean lattice rotation group [27].

There are 35 such operators. To define them we first consider spin and flavor separately. The five scalar operators for spin alone are

$$S = I \cdot I ; \quad P = \gamma_5 \cdot \gamma_5 ; \quad T = \sum_{\mu < \nu} T_{\mu\nu} ; \quad V = \sum_{\mu} V_{\mu} ; \quad A = \sum_{\mu} A_{\mu} , \quad (3.40)$$

where (no sum over repeated indices)

$$V_{\mu} \equiv \gamma_{\mu} \cdot \gamma_{\mu} ; \quad A_{\mu} \equiv \gamma_{\mu} \gamma_5 \cdot \gamma_5 \gamma_{\mu} ; \quad T_{\mu\nu} \equiv \gamma_{\mu} \gamma_{\nu} \cdot \gamma_{\nu} \gamma_{\mu} . \quad (3.41)$$

The dot separates the matrices in the two bilinears. Exactly the same list applies for flavor, and the first 25 diagonal singlets are the products of the five spin singlets with the five flavor singlets. The notation we use for these products is exemplified by

$$[A \times P] = \sum_{\mu} \overline{(\gamma_{\mu 5} \otimes \xi_5)} \overline{(\gamma_{5\mu} \otimes \xi_5)} . \quad (3.42)$$

The remaining 10 operators are somewhat more complicated. They are

$$[V_{\mu} \times V_{\mu}] = \sum_{\mu} \overline{(\gamma_{\mu} \otimes \xi_{\mu})} \overline{(\gamma_{\mu} \otimes \xi_{\mu})} , \quad (3.43)$$

with $[V_{\mu} \times A_{\mu}]$, $[A_{\mu} \times V_{\mu}]$ and $[A_{\mu} \times A_{\mu}]$ defined similarly;

$$[V_{\mu} \times T_{\mu}] = \sum_{\substack{\mu, \nu \\ \mu \neq \nu}} \overline{(\gamma_{\mu} \otimes \xi_{\mu\nu})} \overline{(\gamma_{\nu} \otimes \xi_{\nu\mu})} - \overline{(\gamma_{\mu} \otimes \xi_{\mu\nu 5})} \overline{(\gamma_{\nu} \otimes \xi_{5\nu\mu})} , \quad (3.44)$$

and the analogous $[A_{\mu} \times T_{\mu}]$, $[T_{\mu} \times V_{\mu}]$ and $[T_{\mu} \times A_{\mu}]$; and finally

$$\begin{aligned} [T_{-} \times T_{-}] &= \sum_{\mu < \nu} \overline{(\gamma_{\mu\nu} \otimes \xi_{\mu\nu})} \overline{(\gamma_{\nu\mu} \otimes \xi_{\nu\mu})} + \overline{(\gamma_{\mu\nu 5} \otimes \xi_{\mu\nu 5})} \overline{(\gamma_{5\nu\mu} \otimes \xi_{5\nu\mu})} \\ &\quad - \overline{(\gamma_{\mu\nu} \otimes \xi_{\mu\nu 5})} \overline{(\gamma_{\nu\mu} \otimes \xi_{5\nu\mu})} - \overline{(\gamma_{\mu\nu 5} \otimes \xi_{\mu\nu})} \overline{(\gamma_{5\nu\mu} \otimes \xi_{\nu\mu})} \end{aligned}$$

with $[T_{+} \times T_{+}]$ defined analogously. Linear combinations of these operators are concisely written as

$$[(V + A)_{\mu} \times T_{\mu}] = [V_{\mu} \times T_{\mu}] + [A_{\mu} \times T_{\mu}] . \quad (3.45)$$

Finally, we consider the color indices. These can be contracted either between the bilinears or within each bilinear. These we label color-types (I) and (II) respectively:

$$\mathcal{O}_I = \overline{(\gamma_S \otimes \xi_F)_{ab}} \overline{(\gamma_S \otimes \xi_F)_{ba}} ; \quad \mathcal{O}_{II} = \overline{(\gamma_S \otimes \xi_F)_{aa}} \overline{(\gamma_S \otimes \xi_F)_{bb}} . \quad (3.46)$$

This notation is used because, when the operators are contracted with external color singlet mesons, those of type (I) give rise to a single color trace, while those of type (II) produce two traces.

3.4.3 Corrections Needed For B_K

We illustrate the calculation for the lattice transcription of the QCD matrix element needed to calculate B_K

$$\mathcal{M}_K = \langle \bar{K}^0 | [\bar{s}_a \gamma_\mu (1 + \gamma_5) d_a] [\bar{s}_b \gamma_\mu (1 + \gamma_5) d_b] | K_0 \rangle . \quad (3.47)$$

We must first write down an equivalent matrix element in QCDN_f. Using the rules of the previous section we find that the operator we need is $2\mathcal{O}_B/N_f^2$, where

$$\mathcal{O}_B = \mathcal{O}_1 + \mathcal{O}_2 ; \quad \mathcal{O}_1 = [(V - A) \times P]_I , \quad \mathcal{O}_2 = [(V - A) \times P]_{II} . \quad (3.48)$$

The minus sign multiplying A appears because the continuum operator has the form $\gamma_\mu \gamma_5 \cdot \gamma_\mu \gamma_5$ whereas $A = \gamma_\mu \gamma_5 \cdot \gamma_5 \gamma_\mu$. The matrix elements of \mathcal{O}_B are to be taken between kaons with flavor ξ_5 . Furthermore, we must only use the contractions in which the quark and antiquark from one bilinear are connected to the external K_0 , while those from the other bilinear are connected to the \bar{K}_0 . It is because of this restriction that \mathcal{O}_B must have the flavor $P = \xi_5 \cdot \xi_5$.

At 1-loop, the continuum operator \mathcal{O}_B^{CONT} does not mix under renormalization: \mathcal{O}_1^{CONT} and \mathcal{O}_2^{CONT} mix into one another, but do so in such a way that their sum receives only an overall renormalization. On the other hand, the lattice operator \mathcal{O}_B^{LAT} does mix with many of the 35 operators discussed above, as well as with flavor off-diagonal operators. The only constraint comes from the $U(1)_A$ symmetry, which restricts the mixing to be with operators that, like \mathcal{O}_B , have an odd number of links in each of their bilinears. Even with this constraint, it would appear that numerical calculations would have to include a large number of operators to take into account perturbative corrections even at 1-loop. This would make such calculations all but intractable.

In fact, one does not need to include all the operators when projecting the external states onto a definite flavor. Here we project onto flavor ξ_5 . If there were no flavor-symmetry breaking, the lattice kaons would only couple to operators with flavor P . The flavor symmetry breaking at large momenta is taken into account by the perturbative calculation to be described. The remaining symmetry breaking is from small loop momenta, and this is suppressed by powers of the lattice spacing. If we ignore such scaling violations, we can restrict ourselves to the operators with flavor P . Combining this with the restriction that all bilinears have an odd number of links, we see that we need only keep track of the mixing between the four operators $\mathcal{O}_1, \mathcal{O}_2,$

$$\mathcal{O}_3 = [(V + A) \times P]_I \quad \text{and} \quad \mathcal{O}_4 = [(V + A) \times P]_{II} . \quad (3.49)$$

This is why we discarded off-diagonal flavor mixing when discussing fermion bilinears, for at one-loop such mixing always leads to four-fermion operators which are flavor off-diagonal. In a two loop calculation, however, one would have to keep all operators at intermediate stages.

For the Landau gauge version of \mathcal{O}_B , the corrections to four-fermion operators can be obtained from those for bilinears, as for Wilson fermions [28]. There are three

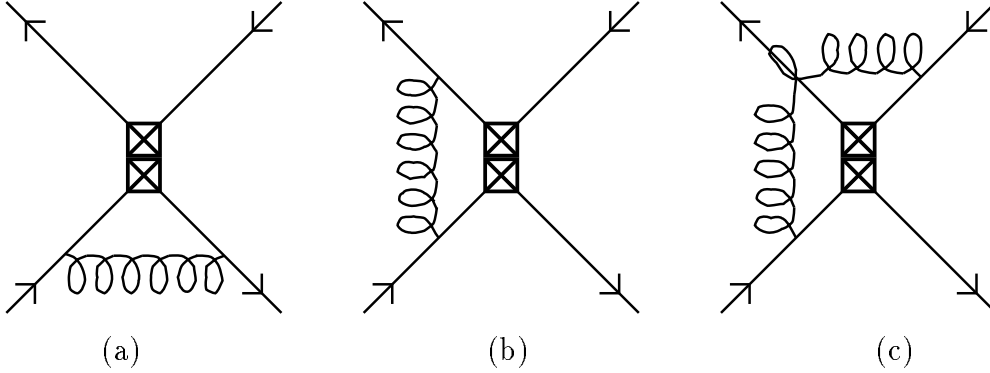


Figure 3.4: Diagrams contributing to renormalization of four fermion operators for Landau gauge operators.

types of diagram involving a gluon connecting two external legs, as shown in Figure 3.4. The two boxes in the figures represent the two bilinears in the operators. In addition, there are the external leg renormalizations (not shown). It turns out that these combine with the gluon exchange diagrams with the correct factors to make the calculations the same as for bilinears.

The simplest part of the calculation is the evaluation of the color factor, i.e. the term of the form $\sum_{\alpha} T^{\alpha} \cdot T^{\alpha}$, where T^{α} are the color group generators. This is just as in the continuum, and mixes the color types as follows

$$\begin{aligned}
 \text{Fig. 3.4a :} & \quad (\text{I}) \rightarrow -\frac{1}{6}(\text{I}) + \frac{1}{2}(\text{II}) & (\text{II}) \rightarrow & \quad \frac{4}{3}(\text{II}) \\
 \text{Fig. 3.4b :} & \quad (\text{I}) \rightarrow \frac{4}{3}(\text{I}) & (\text{II}) \rightarrow & \quad \frac{1}{2}(\text{I}) - \frac{1}{6}(\text{II}) \\
 \text{Fig. 3.4c :} & \quad (\text{I}) \rightarrow -\frac{1}{6}(\text{I}) + \frac{1}{2}(\text{II}) & (\text{II}) \rightarrow & \quad \frac{1}{2}(\text{I}) - \frac{1}{6}(\text{II}) .
 \end{aligned}$$

Since mixing between color types is independent of the spin and flavor mixing, we can ignore color factors until we collect the results at the end.

We now turn to the calculation of spin and flavor mixing. The calculation of Fig. 3.4a is identical to that for bilinears. For the example of the operator $\mathcal{O} = [(V - A) \times P]$, the correction due to this diagram is

$$\delta_a \mathcal{O} = 2c_{VP} [V \times P] - 2c_{VS} [A \times P] \tag{3.50}$$

$$= (c_{VP} + c_{VS}) [(V - A) \times P] + (c_{VP} - c_{VS}) [(V + A) \times P] . \tag{3.51}$$

The notation here is as follows: $\delta_a \mathcal{O}$ is the contribution to $\mathcal{O}^{CONT} - \mathcal{O}^{LAT}$ from Fig. 3.4a, except that we have extracted an overall factor of $g^2/16\pi^2$, and removed all color factors. We have also set $\mu a = \pi$ so that the d_{ij} terms are absent. We can always reconstruct the d_{ij} since they appear with the c_{ij} in the same proportion as in Eq. 3.39. The factors of 2 in Eq. 3.50 arise because each four fermion

operator consists of two bilinears, both of which are renormalized. Since $c_{VP} \neq c_{VS}$, the mixing brings in $[(V + A) \times P]$. The coefficient of this operator contains no logarithms, however, because $d_{VP} = d_{VS}$.

The calculation of Fig. 3.4b is more involved. To bring the calculation into the form of a bilinear correction one must first do a Fierz transformation of the spin-flavor indices. It is here that the complications of staggered fermions enter. The Fierz transformations for spin or flavor alone are

$$\begin{aligned} V - A &\leftrightarrow A - V \\ V + A &\leftrightarrow 2(S - P) \\ 2(S + P) &\leftrightarrow S + P + T \\ 2T &\leftrightarrow 3S + 3P - T . \end{aligned}$$

It does not matter whether we treat the fermions as anticommuting (we have not done so in the above relations), because any sign cancels when we Fierz transform back. For the 25 scalar operators built as products of S, P, V, A and T the Fierz transforms are obtained by simultaneous transformation of the spin and flavor parts, for example

$$\mathcal{O} \rightarrow \mathcal{O}' = \frac{1}{4} [(A - V) \times (S + P + T - V - A)] . \quad (3.52)$$

The corrections to the Fierz bilinear can now be calculated. In this example we have

$$\begin{aligned} 4\delta_b \mathcal{O}' &= 2c_{VP}([A \times S] - [V \times P]) + 2c_{VS}([A \times P] - [V \times S]) \\ &2c_{VV_2}([V \times V] - [A \times A]) + 2(c_{VV_0} - c_{VV_2})([V_\mu \times V_\mu] - [A_\mu \times A_\mu]) \\ &2c_{VA_2}([V \times A] - [A \times V]) + 2(c_{VA_4} - c_{VA_2})([V_\mu \times A_\mu] - [A_\mu \times V_\mu]) \\ &(c_{VT_1} + c_{VT_3})[(A - V) \times T] + (c_{VT_3} - c_{VT_1})[(A_\mu + V_\mu) \times T_\mu] \\ &+ \text{off-diagonal} . \end{aligned}$$

The result is then Fierz transformed back, giving

$$\delta_b \mathcal{O} = C_b [(V - A) \times P] + \dots , \quad (3.53)$$

where

$$8C_b = c_{VS} + c_{VP} + 3c_{VV_2} + c_{VV_0} + 3c_{VA_2} + c_{VA_4} + 3c_{VT_1} + 3c_{VT_3} . \quad (3.54)$$

The ellipsis in Eq. 3.53 represents the operators with flavors other than P . Note that this diagram does not cause mixing with $[(V + A) \times P]$.

To bring the third type of diagram (Fig. 3.4c) into canonical form, we have to follow a series of steps. First, one of the propagators appearing in the loop must be “charge conjugated”, which results in an overall sign because the momentum flow is opposite for quark and antiquark propagators. Second, one of the bilinears must be conjugated, using

$$\overline{(\gamma_S \otimes \xi_F)_{AB}} = \overline{(\gamma_{S^\dagger} \otimes \xi_{F^\dagger})_{BA}} . \quad (3.55)$$

Next one does the Fierz transformation, calculates the correction, Fierz transforms back, and finally conjugates again. In our example, the result is

$$8\delta_c\mathcal{O} = -(c_{SS} + c_{SP} + 6c_{ST} + 4c_{SV} + 4c_{SA}) [(V - A) \times P] + \dots, \quad (3.56)$$

where again we have kept only those terms with flavor P .

We now collect together the corrections to the operator \mathcal{O}_B , including the color factors and the logarithmic terms. With the definition

$$\mathcal{O}_B^{CONT} = \mathcal{O}_B^{LAT} + \frac{g^2}{16\pi^2} \sum_j C_j \mathcal{O}_j^{LAT}, \quad (3.57)$$

we have

$$C_1 = -2L_\mu - 35.54, \quad C_2 = -2L_\mu - 29.69, \quad C_3 = -0.26, \quad C_4 = 2.90.$$

Since $C_1 \approx C_2$ and $C_3 \approx C_4 \approx 0$, the major effect is a diagonal renormalization of \mathcal{O}_B . This is exactly true for the anomalous dimension matrix, i.e. the terms proportional to L_μ . The corrections are relatively large, 30-50% depending on the choice of g^2 .

In practice, however, we calculate B_K , which is proportional to the ratio of the matrix element of \mathcal{O}_B to that of $[A \times P]_{II}$ evaluated in vacuum saturation approximation. In this approximation only Fig. 3.4a contributes, so that the correction is just twice that for the bilinear $(\overline{\gamma_A} \otimes \xi_P)$. Including color factors the correction to the vacuum saturation calculation is $2C_{FCVS} = -27.133$. Since this is a diagonal correction, it does not affect C_3 and C_4 , but should be subtracted from C_1 and C_2 , giving $C'_1 = -2L_\mu - 8.41$ and $C'_2 = -2L_\mu - 2.56$. Thus there is a large cancellation, and the perturbative corrections to a calculation of B_K are small.

We have presented the results for B_K in detail to illustrate the issues and the problems. Other results are given in Refs. [20] and [25]. In particular the latter reference contains a discussion of the penguin diagrams which are needed in the calculation of the $\Delta I = 1/2$ amplitudes in kaon decays.

Since these calculations are an important ingredient in all matrix element calculations, it is important to test their reliability. This can be done by comparing results with operators which should differ only by normalization factors. Only very limited testing has been done to date. One can also test how effectively the external states project onto operators of a given flavor by comparing matrix elements of operators which differ only by terms which should vanish upon projection.

3.5 WARD IDENTITIES

In the study of weak amplitudes involving pseudo-Goldstone bosons, the approximate $SU(3)_L \times SU(3)_R$ symmetry plays a central role. The symmetry relates amplitudes differing by one pseudo-Goldstone boson, e.g. $\mathcal{A}(K \rightarrow 3\pi)$ and $\mathcal{A}(K \rightarrow 2\pi)$,

and predicts the momentum dependence of the amplitudes for small momenta, i.e. the “chiral behavior” of the amplitudes. The various predictions are most easily derived using the chiral Lagrangian. In many instances the predictions are successful at the $\sim 25\%$ level for processes involving kaons and pions.

The major advantage of staggered fermions for the calculation of weak amplitudes is the existence of the axial $U(1)_A$ symmetry at all lattice spacings. This symmetry implies Ward identities which constrain the behavior of amplitudes involving external pseudo-Goldstone pions. With a suitable transcription of operators, the lattice amplitudes satisfy similar Ward Identities to their continuum counterparts, and have the same chiral behavior, even at finite lattice spacing. This is in contrast with Wilson fermions, for which the amplitudes have the correct chiral behavior only in the continuum limit, so that at finite lattice spacing the continuum amplitude can be obscured by lattice artifacts.

In this section we discuss two examples of the Ward identities and their consequences. The first concerns the calculation of B_K . While a partial analysis has been given previously [21], the full analysis involving non-degenerate quarks is new. The second example is the calculation of matrix elements of \mathcal{O}_6 , which are needed to predict the CP violating part of the $K \rightarrow \pi\pi$ amplitude, i.e. the quantity ϵ' . This example is more complicated, and has not previously been presented, although it is similar to the analysis of Ref. [15] for the operators needed to discuss the $\Delta I = 1/2$ rule.

The basic tools are two identities for quark propagators which show the effect of zero momentum insertions of the Goldstone pion ($\bar{\chi}(n)\chi(n)(-1)^n$) and the scalar density ($\bar{\chi}(n)\chi(n)$)

$$(m_1+m_2) \sum_n G_1(n_2; n)(-1)^n G_2(n; n_1) = (-1)^{n_2} G_2(n_2; n_1) + G_1(n_2; n_1)(-1)^{n_1} \quad (3.58)$$

$$(m_1-m_2) \sum_n G_1(n_2; n)G_2(n; n_1) = G_2(n_2; n_1) - G_1(n_2; n_1) . \quad (3.59)$$

Here $G_i(n_2; n_1)$ is the propagator from n_1 to n_2 of a quark of mass m_i . Color indices are suppressed, since they play no role in the following discussion. These identities can be established, for example, using the hopping parameter expansion [15].

3.5.1 B_K And Related Matrix Elements

To extract the kaon B-parameter we need to calculate \mathcal{M}_K (Eq. 3.47). Using the chiral Lagrangian one can show that

$$\mathcal{M}_K = \langle \bar{K}^0 | [\bar{s}\gamma_\mu(1+\gamma_5)d] [\bar{s}\gamma_\mu(1+\gamma_5)d] | K^0 \rangle \quad (3.60)$$

$$= -\gamma m_{\bar{K}} m_K + O(m_K^4 \ln m_K) , \quad (3.61)$$

where γ is an unknown constant. The fact that \mathcal{M}_K vanishes in the chiral limit causes a potential problem for lattice calculations. If there are corrections, suppressed by powers of the lattice spacing, which do not vanish in the chiral limit,

then these corrections can obscure the physical amplitude γ . What we show here is that, with staggered fermions, the lattice transcription of \mathcal{M}_K has the chiral behavior of Eq. 3.60 for any lattice spacing.

We have discussed the transcription of the \mathcal{M}_K onto the lattice in the previous section. There are three important features:

1. The transcription requires a combination of the operators $[A \times P]_I$, $[A \times P]_{II}$, $[V \times P]_I$ and $[V \times P]_{II}$. Many other operators are produced by mixing, but none has the correct flavor to give matrix elements in the continuum limit. It turns out, however, that the Ward identities apply separately to each of the operators which appear in the mixing calculation. All that is needed is that there be an odd number of links between quark and antiquark fields in both bilinears. In the following we use \mathcal{O} to refer to any operator with this property.
2. The matrix elements are to be taken between lattice kaons having flavor ξ_5 . In numerical calculations one can create the kaons with any operator having the appropriate symmetries. To derive the Ward identities, however, one must use the local pseudoscalar operators, for example

$$K(t) = \sum_{\vec{n}} \bar{\chi}_d(\vec{n}, t) \chi_s(\vec{n}, t) (-1)^n . \quad (3.62)$$

We have set the spatial momentum to zero since this is necessary for the following derivation.

3. Only one of the contractions between the operators and the external kaons is to be kept. This restriction is illustrated in Fig. 3.5. The operators consist of two bilinears, shown by the two squares. The quark-antiquark pair emanating from the operator creating each external kaon must be contracted with one of the bilinears. It is useful to define the matrix element so that the restriction on contractions is automatic. This requires the introduction of two additional quarks fields s' and d' , with masses equal to those of the s and d quarks, respectively. One of the bilinears and one of the external kaons are constructed from these primed quarks. Thus the operator $[A \times P]$ becomes (ignoring color indices)

$$\sum_{\mu} [\bar{\chi}_{s'} (\overline{\gamma_{\mu 5} \otimes \xi_5}) \chi_{d'}] [\bar{\chi}_s (\overline{\gamma_{\mu 5} \otimes \xi_5}) \chi_d] . \quad (3.63)$$

The primed fermions are not to be included in internal loops.

The complete correlator is thus

$$C_{\text{KK}}(t, t') = \langle K(t) \mathcal{O}(0) K'(t') \rangle , \quad (3.64)$$

where the expectation value represents the functional integral over gauge and fermion fields. The operator \mathcal{O} is placed with the corner of its hypercube at the origin. When we formally integrate out the fermions fields, the correlator becomes the product of

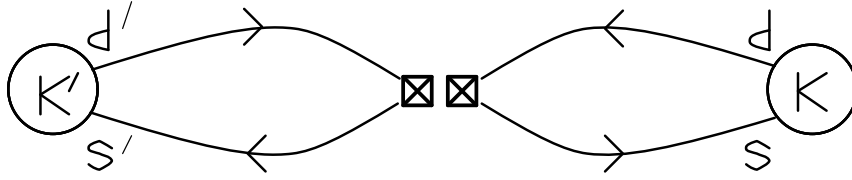


Figure 3.5: The correlator C_{KK} .

quark propagators shown in Fig. 3.5. By adding the contribution from a gauge configuration and its conjugate, one can see that C_{KK} is real.

To derive the Ward identities we make repeated use of Eq. 3.58. Each application reduces the number of kaons by one, and changes the flavor-spin of one of the bilinears in the operator. This is analogous to continuum PCAC calculations in which one reduces in a pion or kaon and obtains commutator terms which change the parity and flavor of the operator. To make use of the Ward identities, we must, as in the continuum, expand the amplitudes as a function of the quark masses and kaon momenta, keeping terms only up to a given order. Quark masses count as two powers of energy, since for both continuum and lattice theories Ward identities imply that $m_K^2 \propto m_s + m_d$. For reasons which will become clear, we must keep all terms up to quartic order in momenta.

We begin by Fourier transforming C_{KK} to energy space

$$C_{KK}(E, E') = \sum_{t, t'} e^{+iEt} C_{KK}(t, t') e^{-iE't'} , \quad (3.65)$$

and using the parameterization

$$C_{KK}(E, E') = \frac{\sqrt{Z_K}}{(E^2 + m_K^2)} \frac{\sqrt{Z_{K'}}}{(E'^2 + m_{K'}^2)} N_f \mathcal{A}_{KK}(E, E') . \quad (3.66)$$

In writing this equation we have dropped all terms of $O(a)$, as we do throughout this section. This means that, for example, we do not distinguish between $\sinh E$ and E . The lattice correlator differs from the corresponding QCD correlator by an overall factor of N_f^2 . Our parameterization is chosen so that the factors of N_f do not appear in \mathcal{A}_{KK} . One factor of N_f is explicit, while the other is contained in the Z -factors, each of which are proportional to $\sqrt{N_f}$. The Z -factors and masses are obtained in the standard way from two point functions. Using axial Ward identities one can show that [15]

$$\sqrt{\frac{Z_K}{2N_f}} = f_K \frac{m_K^2}{(m_s + m_d)} \left(1 + O(m_K^2)\right) , \quad (3.67)$$

a relation we use frequently in the following derivations.

Applying the reduction theorem, we see that $\mathcal{A}_{KK}(-im_K, -im_{K'})$ is the on-shell matrix element we are interested in. To use the Ward identities, however, we must

parameterize \mathcal{A}_{KK} for off-shell energies extending from the kaon poles down to zero. We assume that \mathcal{A}_{KK} varies smoothly in this range, and can be expanded in a power series in the energies. A necessary condition for this to hold is that the poles from excited states, which are contained in \mathcal{A}_{KK} , are at energies much higher than m_K . The fact that $C_{\text{KK}}(t, t')$ is real restricts the expansion to even powers of energy

$$\mathcal{A}_{\text{KK}} = \alpha + \beta E^2 + \beta' E'^2 + \gamma EE' + \delta E^4 + \delta' E'^4 + \epsilon E^3 E' + \epsilon' EE'^3 + \eta E^2 E'^2 + O(E^6). \quad (3.68)$$

The coefficients α, β, \dots are themselves expansions in the quark masses. To the order we are working, α is a quadratic function of m , while β, β' and γ are linear functions, and the remaining coefficients are constants.

We have left out of Eq. 3.68 the non-analytic terms which are generated by Goldstone-boson loops. These turn out to be non-leading for the combination of operators which corresponds to the matrix element \mathcal{M}_K , the matrix element in which we are mainly interested. For other operators, however, the non-analytic terms are dominant. We discuss them in the following section.

With the tools in hand, we now proceed to the Ward identities. Summing over t , and using Eq. 3.58, gives

$$(m_s + m_d) \sum_t C_{\text{KK}}(t, t') = \langle [\mathcal{O}_s^-(0) - \mathcal{O}_d^-(0)] K'(t') \rangle \equiv C_{\text{KO}}(t'). \quad (3.69)$$

The new operators $\mathcal{O}_{s,d}^-$ are related to \mathcal{O} as follows: the bilinear in \mathcal{O} with flavor $\bar{s}d$ has both its flavor-spin multiplied by $(\gamma_5 \otimes \xi_5)$, and its flavor changed to $\bar{s}s$ (for \mathcal{O}_s^-) or $\bar{d}d$ (for \mathcal{O}_d^-). For example, if $\mathcal{O} = [A \times P]$ then

$$\mathcal{O}_s^- = \sum_{\mu} \bar{\chi}_s (\gamma_{\mu} \otimes 1) \chi_s \bar{\chi}_{s'} (\gamma_{5\mu} \otimes \xi_5) \chi_{d'}. \quad (3.70)$$

The superscript indicates that these correspond to negative parity continuum operators.

The correlator C_{KO} in Eq. 3.69 vanishes explicitly when $m_s = m_d$: the two terms in the Ward identity Eq. 3.58 cancel because the bilinears have an odd number of links between quark and antiquark fields. C_{KO} also vanishes when $m_{s'} = m_{d'}$, for then one can show that on each configuration the result is purely imaginary, and so cancels between a configuration and its conjugate. Thus, we can parameterize the Fourier transform as

$$C_{\text{KO}}(E') = \sum_{t'} C_{\text{KO}}(t') e^{-iE't'} = \frac{\sqrt{Z_{K'}}}{E'^2 + m_{K'}^2} N_f^{3/2} (m_s - m_d)(m_{s'} - m_{d'}) \mathcal{A}_{\text{KO}}. \quad (3.71)$$

The amplitude \mathcal{A}_{KO} is independent of quark masses at the order we are working, and has been constructed so as to have no dependence on N_f in the continuum limit.

Substituting the parameterizations of C_{KK} and C_{KO} into Eq. 3.69, we find

$$\sqrt{2} f_K (\alpha + \beta' E'^2 + \delta' E'^4) = (m_s - m_d)(m_{s'} - m_{d'}) \mathcal{A}_{\text{KO}}. \quad (3.72)$$

Thus at the order we are working, we find

$$\beta' = \delta' = 0, \quad \text{and} \quad \sqrt{2}f_K\alpha = (m_s - m_d)(m_{s'} - m_{d'})\mathcal{A}_{K\mathcal{O}}. \quad (3.73)$$

The latter relation shows why we had to keep all terms of $O(m^2, E^4)$ in \mathcal{A}_{KK} .

Summing over t' rather than t gives the same result, except that primed and unprimed fields are interchanged. This does not effect α , but shows that $\beta = \delta = 0$. The upshot is that the only term of $O(m, E^2)$ that survives in C_{KK} is $\gamma EE'$. Thus the on-shell matrix element is

$$\mathcal{A}_{KK}^{\text{on-shell}} = -\gamma' m_K m_{K'} + (m_s - m_d)(m_{s'} - m_{d'}) \frac{\mathcal{A}_{K\mathcal{O}}}{\sqrt{2}f_K} + O(m_K^6). \quad (3.74)$$

We have collected into γ' the contributions from γ , ϵ , ϵ' and η , so that γ' is the most general quadratic function of m_K and $m_{K'}$.

The main conclusion of this analysis is that the lattice amplitudes \mathcal{A}_{KK} vanish in the chiral limit. We also see that there are complicated quartic corrections, one of which is related to $C_{K\mathcal{O}}$. Both of these results are identical to those which apply to QCD amplitude we wish to calculate. The only flaw in the analysis is the omission of non-analytic terms due to pion loops, a flaw we correct in the next section.

3.5.2 \mathcal{O}_6

One of the major contributions to the imaginary part of the $K \rightarrow \pi\pi$ amplitude is from the ‘‘penguin’’ operator

$$\mathcal{O}_6 = -2 \sum_{q=u,d,s} \bar{s}_c(1-\gamma_5)q_c \bar{q}_d(1+\gamma_5)d_d. \quad (3.75)$$

The color indices c and d are dropped in the following. Under the $SU(3)_L \times SU(3)_R$ symmetry \mathcal{O}_6 transforms as $(8_L, 1_R)$, which implies that its matrix elements vanish in the chiral limit. This is easily seen using the chiral Lagrangian. At lowest order, only a single operator contributes to the physical $K \rightarrow \pi\pi$ amplitudes [29]. For example, the $K^0 \rightarrow \pi^0\pi^0$ amplitude is

$$\mathcal{A}_{000}^{\text{on-shell}} = \frac{\sqrt{2}a}{f_\pi^3} (m_K^2 - m_\pi^2) + O(m_K^4), \quad (3.76)$$

with only the single coefficient a undetermined.⁶

In principle we can transcribe \mathcal{O}_6 onto the lattice and directly calculate \mathcal{A}_{000} . The continuum Ward identities which guarantee the chiral behavior of Eq. 3.76 can also be derived on the lattice. In practice, however, this calculation is difficult because, among other things, one must understand final state interactions between

⁶The notation is standard but unfortunate. There should, however, be no possibility of confusing this coefficient with the lattice spacing, for the latter equals unity throughout this section.

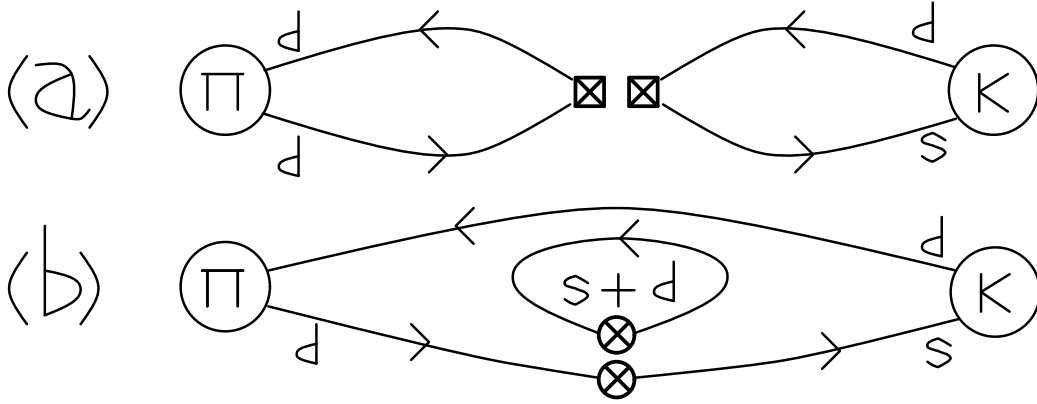


Figure 3.6: Contractions contributing to the $K^0 \rightarrow \pi^0$ correlator of \mathcal{O}_6 : (a) eight diagram; (b) eye diagram. For the specific example discussed in the text, the square and circular boxes represent pseudoscalar and scalar operators, respectively.

the pions. This approach has been pushed further with Wilson than with staggered fermions, and we do not discuss it further.

Instead, we focus on the less ambitious but more practical calculation which aims to extract the leading chiral coefficient a . We use the method of Ref. [29], the strategy of which is to relate \mathcal{A}_{000} to the $K^0 \rightarrow \pi^0$ matrix element of \mathcal{O}_6 , which we call \mathcal{A}_{00} . This method is based on the Ward identity

$$\mathcal{A}_{000}(p_1=0) = \frac{1}{2f_\pi} \mathcal{A}_{00} + \text{non-pole terms} , \quad (3.77)$$

where p_1 is the outgoing Euclidean momenta of one of the pions, and the “non-pole terms” vanish when the K^0 and the second π^0 are on-shell. This relation is true both in the continuum and, with staggered fermions, on the lattice. To use it requires an off-shell parameterization of \mathcal{A}_{000} . In the chiral Lagrangian, the operator which gives rise to the on-shell amplitude gives

$$\mathcal{A}_{000} = -\frac{a}{\sqrt{2}f_\pi^3} (p_K \cdot (p_1 + p_2) + 2p_1 \cdot p_2) + O(p^4) , \quad (3.78)$$

with p_K the incoming kaon momentum, and p_2 , like p_1 , an outgoing pion momentum. Combining this with the Ward identity Eq. 3.77 yields

$$\mathcal{A}_{00}^{\text{on-shell}} = \frac{a\sqrt{2}}{f_\pi^2} m_K m_\pi + O(m_K^4) (?) , \quad (3.79)$$

from which it appears that one can calculate a simply by evaluating \mathcal{A}_{00} . Unfortunately, the parameterization of Eq. 3.78 is not complete, so that Eq. 3.79 is wrong. The calculation of a turns out to be far less straightforward.

To set the stage for the lattice calculation, we first discuss the difficulties with Eq. 3.78 in the continuum. We summarize the analysis of Ref. [29]. Both eight and

eye diagrams contribute to \mathcal{A}_{00} , examples being shown in Fig. 3.6. In addition to the usual mixing with other dimension 6 operators, the eye-diagrams allow mixing with bilinear operators of lower dimension, i.e. $\bar{s}d$ and $\bar{s}\gamma_5 d$. The mixing coefficients are divergent, i.e. proportional to inverse powers of the lattice spacing. We do not normally worry about such mixing, for it can be absorbed, by a chiral rotation, into a redefinition of the mass matrix and vacuum [30]. Indeed, in continuum calculations using dimensional regularization such divergences are automatically ignored. But in lattice calculations the weak interactions are not included in the action, instead being added by hand. Thus the mass matrix and vacuum are not affected by the perturbation, and we must manually subtract the effects of the mixing.

In the continuum, \mathcal{O}_6 can only mix with $(8_L, 1_R)$ operators, and the only example with dimension less than six is (in Euclidean space)

$$\mathcal{O}_{\text{sub}} = \bar{s}\gamma_\mu(1+\gamma_5)(\vec{D}_\mu - \overleftarrow{D}_\mu)d . \quad (3.80)$$

Using the equations of motion (valid for on-shell correlators) this can be written as

$$\mathcal{O}_{\text{sub}} = (m_s+m_d)\bar{s}d + (m_s-m_d)\bar{s}\gamma_5 d \quad (3.81)$$

$$= \frac{(m_s+m_d)}{(m_s-m_d)}\partial_\mu(\bar{s}\gamma_\mu d) + \frac{(m_s-m_d)}{(m_s+m_d)}\partial_\mu(\bar{s}\gamma_\mu\gamma_5 d) . \quad (3.82)$$

From this we see that \mathcal{O}_{sub} has the following properties [29].

1. For $m_s \neq m_d$ it is a total derivative. Thus it cannot contribute to amplitudes in which the operator inserts no momentum. In particular, it makes no contribution to the physical amplitude \mathcal{A}_{000} , so one need not be concerned about \mathcal{O}_{sub} if one directly calculates the $K \rightarrow \pi\pi$ amplitude.
2. \mathcal{O}_{sub} does contribute to $K \rightarrow \pi$ matrix elements, for the operator inserts momentum (proportional to (m_s-m_d)). In fact, it contributes even when $m_s = m_d$ because of the singular denominator multiplying $\bar{s}\gamma_\mu d$. The contribution to \mathcal{A}_{00} is proportional to (m_s+m_d) .

Thus the mixing with \mathcal{O}_{sub} introduces an additional term in \mathcal{A}_{00} which invalidates Eq. 3.79. Since the new term is proportional to (m_s+m_d) , it does not affect the a term. The corrected relation is ⁷

$$\mathcal{A}_{00} = -a\frac{\sqrt{2}}{f_\pi^2}p_K \cdot p_\pi - b\frac{(m_s+m_d)}{\sqrt{2}f_\pi^2} + O(p^4) , \quad (3.83)$$

with b being the new constant. The matrix element still vanishes in the chiral limit, but contains a term unrelated to $\mathcal{A}_{000}^{\text{on-shell}}$. It is important to realize that the Ward

⁷In the following discussion, some results differ from those in Ref. [15]. This is partly due to the use of $K^0 \rightarrow \pi_0$ rather than $K^+ \rightarrow \pi^+$ matrix elements, and partly due to the use of $(1+\gamma_5)$ instead of $(1-\gamma_5)$ as the left handed projector. There are also, however, some sign errors in [15] which are corrected here.

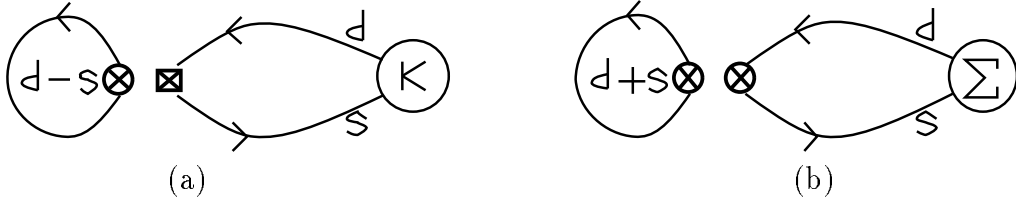


Figure 3.7: Contractions contributing to matrix elements of \mathcal{O}_6 (a) K^0 to vacuum and (b) Σ to vacuum. For the specific example discussed in the text, the square and circular boxes represent pseudoscalar and scalar operators, respectively.

identity Eq. 3.77 remains valid; it is the parameterization of \mathcal{A}_{000} (Eq. 3.78) which is incomplete.

We are not interested in the b term, which is an unphysical, cut-off dependent quantity. To remove it, we form the subtracted operator $\mathcal{O}_6^{\text{sub}} = \mathcal{O}_6 - \rho \mathcal{O}_{\text{sub}}$, and find the coefficient ρ such that there is no b term in its $K \rightarrow \pi$ matrix element. Various methods have been suggested for doing this subtraction [29, 15, 31, 32]. In practice, the most successful for staggered fermions has been that of Ref. [29]. Chiral symmetry relates the matrix elements of positive and negative parity parts of $\mathcal{O}_6^{\text{sub}}$, and it is shown in Ref. [29] that removing the b term from \mathcal{A}_{00} is equivalent to the condition

$$\langle 0 | \mathcal{O}_6^{\text{sub}} | K^0 \rangle = 0 . \quad (3.84)$$

Physically, this means that the kaons are orthogonal to the vacuum, which is a non-perturbative analog of the requirement that there be no mixing between the s and d quarks. There are corrections at $O(m_K^4)$, so this condition can only be used to extract the leading coefficients in the chiral expansion. At the same level of accuracy, Eqs. 3.83 and 3.84 can be combined to give an equation for b

$$\langle 0 | \mathcal{O}_6 | K^0 \rangle = b \frac{\sqrt{2}(m_s - m_d)}{f_\pi} . \quad (3.85)$$

Figure 3.7a shows an example of the contractions which contribute to this matrix element. One can see from the figure that $\langle 0 | \mathcal{O}_6 | K^0 \rangle$ vanishes when $m_s = m_d$, so that b has a finite chiral limit.

A straightforward transcription of the preceding analysis onto the lattice faces the following possible problems. First, the fact that \mathcal{A}_{00} vanishes in the chiral limit requires a cancellation between eight and eye diagrams. This cancellation might work only in the continuum limit, with corrections having the wrong chiral behavior appearing at finite lattice spacing. Second, there could be more than one lower dimension operator to subtract on the lattice, so that the continuum subtraction method would not work. Finally, even if there is only a single operator to subtract, the method using Eq. 3.85 may only work in the continuum limit. At finite lattice spacing the subtraction might remove part of the a -term in addition to the b -term. Since b is a quadratically divergent quantity, the ratio a/b vanishes as the square

of the lattice spacing, so that any contamination of b in a could have disastrous consequences.

It turns out that, with staggered fermions, all these problems can be avoided, at least for gauge invariant operators. This is entirely due to the $U(1)_A$ symmetry. We transcribe the matrix elements in Eqs. 3.83 and 3.85 onto the lattice using the rules of section 3.2, extract the lattice coefficients a_L and b_L , and in the continuum limit a_L becomes equal to the desired coefficient a . To demonstrate this, we show first that the lattice $K \rightarrow \pi$ matrix elements have the form of Eq. 3.83, with b_L defined by the lattice transcription of Eq. 3.85. This shows that \mathcal{A}_{00} is not contaminated with corrections having the wrong chiral behavior. Since the lattice and continuum matrix elements have the same form and relationships, it also suggests that a_L should be identified with a . To really establish this, however, we show that the eye diagrams cause mixing with a single lower dimension operator, and that subtracting this operator in the manner described above removes the b_L term from \mathcal{A}_{00} without affecting the a_L term.

These results follow from lattice Ward identities, and to discuss these we must define various correlators. In addition to the kaon field defined in Eq. 3.62, we need pion and scalar fields

$$\Pi^0(t) = \sum_{\vec{n}} \frac{(-1)^n}{\sqrt{2}} [\bar{\chi}_u(\vec{n}, t)\chi_u(\vec{n}, t) - \bar{\chi}_d(\vec{n}, t)\chi_d(\vec{n}, t)] , \quad \Sigma(t) = \sum_{\vec{n}} \bar{\chi}_d(\vec{n}, t)\chi_s(\vec{n}, t) . \quad (3.86)$$

The correlators of interest are (with the superscript on \mathcal{O}_6 indicating the parity)

$$C_{K\pi}(t_K, t_\pi) = \langle K^0(t_K)\mathcal{O}_6^+(0)\Pi^0(t_\pi) \rangle , \quad (3.87)$$

$$C_K(t_K) = \langle \mathcal{O}_6^-(0)K^0(t_K) \rangle , \quad (3.88)$$

$$C_\Sigma(t) = \langle \mathcal{O}_6^+(0)\Sigma(t) \rangle . \quad (3.89)$$

Strictly speaking the operator in C_K should be the commutator of the pion axial charge with \mathcal{O}_6^+ , but this is proportional \mathcal{O}_6^- . In the continuum, there are many contractions contributing to each of these correlators, the general form of which is shown in Figs. 3.6 and 3.7. As discussed previously, we Fierz rearrange the operators so that the contractions all have two spinor traces. There are contractions in which the bilinears are scalars, pseudoscalars, vectors and axial-vectors. We focus here on the dominant contribution, that in which the external pions or kaons are connected to pseudoscalars, while the remaining bilinears are scalars. To make clear which contractions we are considering, Figs. 3.6 and 3.7 show the scalar bilinears as circles and the pseudoscalars as squares.

To transcribe these contractions onto the lattice, we must use the staggered flavors appropriate to the external flavor ξ_5 states. The resulting operators are

$$\mathcal{O}_6^- = -2\overline{\chi_s(\gamma_5 \otimes \xi_5)}\chi_d \left[\overline{\chi_s(1 \otimes 1)}\chi_s - \overline{\chi_d(1 \otimes 1)}\chi_d \right] , \quad (3.90)$$

$$\mathcal{O}_6^+ = \mathcal{O}_6^a - \mathcal{O}_6^b , \quad (3.91)$$

$$\mathcal{O}_6^a = -2\overline{\chi_s(1 \otimes 1)}\chi_d \left[\overline{\chi_s(1 \otimes 1)}\chi_s + \overline{\chi_d(1 \otimes 1)}\chi_d \right] , \quad (3.92)$$

$$\mathcal{O}_6^b = -2\overline{\chi_s(\gamma_5 \otimes \xi_5)}\chi_d \left[\overline{\chi_s(\gamma_5 \otimes \xi_5)}\chi_s + \overline{\chi_d(\gamma_5 \otimes \xi_5)}\chi_d \right] . \quad (3.93)$$

The contractions of these operators are constrained: we use only those shown in Figs. 3.6 and 3.7. In addition, only the \mathcal{O}_6^a part of \mathcal{O}_6^+ contributes to C_Σ . Thus in the lattice matrix elements, the circles in the figures represent $\overline{(1 \otimes 1)}$, the boxes $\overline{(\gamma_5 \otimes \xi_5)}$.

These contractions are the only ones leading to operators without gauge links. The transcriptions of other contractions require operators whose bilinears have 1, 3 and 4 links. It turns out that the following analysis applies separately for operators with a given number of links. For 4-link operators the steps are essentially identical to those below. The analysis for 1 and 3 link operators is slightly different, and is given in Ref. [15].

The Ward identities we need follow from repeated use of Eq. 3.58

$$\sqrt{2}(m_s+m_d) \sum_{t_K} C_{K\pi}(t_K, t_\pi) = -C_\Sigma(t_\pi) \quad (3.94)$$

$$2\sqrt{2}m_d \sum_{t_\pi} C_{K\pi}(t_K, t_\pi) = -C_K(t_K) - C_\Sigma(t_K) , \quad (3.95)$$

while from Eq. 3.59 we find

$$(m_s+m_d) \sum_{t_K} C_K(t_K) = (m_d-m_s) \sum_t C_\Sigma(t) . \quad (3.96)$$

These identities are the transcriptions of those one gets in the continuum using the standard PCAC method of reducing pions.

To use these identities we define an amplitude from $C_{K\pi}$

$$C_{K\pi}(E_K, E_\pi) = \sum_{t_K, t_\pi} e^{+iE_K t_K} C_{K\pi}(t_K, t_\pi) e^{-iE_\pi t_\pi} = \frac{\sqrt{Z_K}}{(E_K^2 + m_K^2)} \frac{\sqrt{Z_\pi}}{(E_\pi^2 + m_\pi^2)} N_f \mathcal{A}_{00} . \quad (3.97)$$

and then use the most general quadratic form for this amplitude

$$\mathcal{A}_{00} = \alpha + \beta_\pi E_\pi^2 + \beta_K E_K^2 - \frac{\sqrt{2}a_L}{f_\pi^2} E_K E_\pi . \quad (3.98)$$

We have chosen the coefficient of $E_K E_\pi$ to match with the continuum definition, Eq. 3.83. The on-shell amplitude is thus ($E_\pi = im_\pi$, $E_K = im_K$)

$$\mathcal{A}_{00}^{\text{on-shell}} = \alpha - \beta_\pi m_\pi^2 - \beta_K m_K^2 + \frac{\sqrt{2}a_L}{f_\pi^2} m_K m_\pi . \quad (3.99)$$

We also must parameterize the K to vacuum amplitude

$$C_K(E_K) = \sum_{t_K} e^{-iE_K t_K} C_K(t_K) = \frac{\sqrt{Z_K}}{E_K^2 + m_K^2} N_f^{3/2} \frac{\sqrt{2}(m_s - m_d)}{f_\pi} b_L , \quad (3.100)$$

where b_L is the lattice transcription of b (Eq. 3.85). Here we are using the fact that, as in the continuum, the matrix element vanishes when $m_s = m_d$. This can be seen directly from Fig. 3.7. Finally, we must parameterize C_Σ . This has no pion or kaon pole, and thus, to the order we are working, is independent of E

$$C_\Sigma(E) = N_f^2 \mathcal{A}_\Sigma ; \quad N_f^2 \mathcal{A}_\Sigma = \sum_t C_\Sigma(t) . \quad (3.101)$$

It is now simply a matter of plugging the parameterizations into the Ward identities. From Eq. 3.94 (i.e. setting $E_K = 0$) we find that $\alpha + \beta_\pi E_\pi^2$ must be proportional to $m_\pi^2 + E_\pi^2$ so as to cancel the pion pole on the left hand side. Thus

$$\alpha = \beta_\pi m_\pi^2 , \quad (3.102)$$

which means that α has no term of $O(1)$, and that the combination $\alpha - \beta_\pi m_\pi^2$ does not contribute to the on-shell matrix element. The vanishing of the $O(1)$ term in α is due to a cancellation between the eight and eye diagrams. Next we note that Eq. 3.96, together with Eq. 3.67, implies ⁸

$$2b_L = -\mathcal{A}_\Sigma . \quad (3.103)$$

Here we have set $f_K = f_\pi$, which is valid at leading order in the chiral expansion. Finally we use Eq. 3.95 (i.e. setting $E_\pi = 0$) and, after some algebra involving Eq. 3.103, obtain

$$m_K^2 \beta_K = \frac{(m_s + m_d)}{\sqrt{2} f_\pi^2} b_L . \quad (3.104)$$

Putting this all together, we find that the on-shell amplitude is

$$\mathcal{A}_{00}^{\text{on-shell}} = a_L \frac{\sqrt{2} m_\pi m_K}{f_\pi^2} - b_L \frac{(m_s + m_d)}{\sqrt{2} f_\pi^2} , \quad (3.105)$$

i.e. it has the same form as the continuum Eq. 3.83. It is important to realize that no approximations have been made aside from the usual ones needed to make PCAC arguments. Although the lattice current algebra is different from that in the continuum, because of the extra lattice flavors, the form of the result is the same as in the continuum.

We now show that the removal of the b_L term from \mathcal{A}_{00} corresponds to the subtraction of a lower dimension operator (which we call $\mathcal{O}_{\text{sub}}^L$) having the same properties as the continuum \mathcal{O}_{sub} . The eye-diagrams allow the lattice operators to mix with others of lower dimension. The positive parity part of the subtraction operator, $\mathcal{O}_{\text{sub}}^+$, appears in $C_{K\pi}$ and C_Σ , while the negative parity part, $\mathcal{O}_{\text{sub}}^-$, contributes to C_K . There are two constraints on $\mathcal{O}_{\text{sub}}^L$. First, it must satisfy the Ward identities Eqs. 3.94, 3.95 and 3.96. Second, under the discrete lattice symmetries, $\mathcal{O}_{\text{sub}}^+$ must transform as a scalar and $\mathcal{O}_{\text{sub}}^-$ as a pseudoscalar. In addition, we want

⁸This is an alternative method for calculating b [32].

$\mathcal{O}_{\text{sub}}^L$ to be as local as possible. Together, these conditions restrict $\mathcal{O}_{\text{sub}}^L$ to be the lattice transcription of the continuum operator \mathcal{O}_{sub} . Rather than write down this lattice operator, it is simpler to use the lattice equations of motion to obtain

$$\mathcal{O}_{\text{sub}}^L = (m_s + m_d) \overline{\chi}_s (1 \otimes 1) \chi_d + (m_s - m_d) \overline{\chi}_s (\gamma_5 \otimes \xi_5) \chi_d . \quad (3.106)$$

This is the operator actually used in practice to do the subtractions. It does not satisfy the Ward identities, but it has the same on-shell matrix elements as the true $\mathcal{O}_{\text{sub}}^L$, which is all that matters for doing the subtraction.

The operator $\mathcal{O}_{\text{sub}}^L$ has the same properties as its continuum counterpart \mathcal{O}_{sub} . In particular, it can be rotated into the mass term, and so does not contribute to physical amplitudes. Thus we want to subtract it, i.e. form $\mathcal{O}_6 - \rho \mathcal{O}_{\text{sub}}$, and adjust ρ so that there is no mixing between the s and d quarks. To do this we assume that the correct non-perturbative condition is as in the continuum, namely that the $K \rightarrow 0$ matrix element of the subtracted operator should vanish [29]. Since $\mathcal{O}_{\text{sub}}^L$ satisfies the same Ward identities as \mathcal{O}_6 , we know that its $K \rightarrow \pi$ matrix element must have the form of Eq. 3.105, with coefficients a_L^{sub} and b_L^{sub} , and with b_L^{sub} related to the $K \rightarrow 0$ matrix element as in Eq. 3.100. The only difference is that, because $\mathcal{O}_{\text{sub}}^+$ is explicitly proportional to $(m_s + m_d)$, $a_L^{\text{sub}} = 0$. This means that the subtraction removes the entire b_L term without changing the value of a_L . We conclude that a_L is the lattice correspondent of the continuum a .

We have made this argument for the contractions involving operators without gauge links. For operators with gauge links the same argument works as long as they are gauge invariant. For Landau gauge operators (i.e. those in which the links are set to the unit matrix) the second part of the argument fails. This is because \mathcal{O}_6 can mix not only with $\mathcal{O}_{\text{sub}}^L$ but also with an operator of the same form but with covariant derivatives replaced by ordinary derivatives. (One can see explicitly that this operator appears at one-loop [25].) The equations of motion cannot be used to simplify this operator, and thus one cannot show that its positive parity matrix elements are proportional to $m_d + m_s$. This leaves open the possibility that this operator may contribute to a_L . Further study of this issue is required. It is not very important, however, for \mathcal{O}_6 , as the dominant contributions involve operators without gauge links.

This concludes the analysis. We have shown that, for staggered fermions, one can take over the continuum analysis of Ref. [29]. All the lattice transcriptions of the $(8_L, 1_R)$ operators, including those needed for discussion of the $\Delta I = 1/2$ rule, satisfy the same Ward identities, and so the same subtraction method can be used for all. The only unresolved difficulty is that, for Landau gauge operators, the subtraction may not completely remove the mixing with lower dimension operators.

3.6 CHIRAL LOGARITHMS

In the previous section, we used analytic functions of momenta to parameterize the matrix elements under study. This leaves out the non-analytic terms which arise

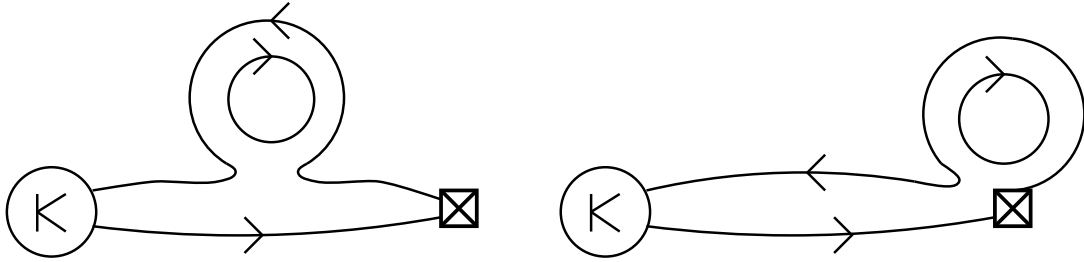


Figure 3.8: Diagrams giving chiral logs in f_K . The box is the axial vector current. The flavor of the quarks in the loop can be either u , d , or s .

from loops of pseudo-Goldstone bosons, the so-called chiral logarithms, or “chiral logs” for short. For example, in the limit $m_u = m_d = 0$, f_K has the expansion [33]

$$f_K = f \left(1 + \frac{5}{4} L_K + c m_K^2 \right); \quad L_K = \left(\frac{m_K}{4\pi f_\pi} \right)^2 \ln \left(\frac{\Lambda^2}{m_K^2} \right). \quad (3.107)$$

Chiral symmetry alone does not determine f , Λ or c (in fact c can be absorbed into Λ), but does fix the coefficient of the chiral log L_K . The diagrams giving rise to the chiral log are shown in Fig. 3.8.

There are three reasons for considering chiral logs. First, for quantities for which one calculates only the leading term in the chiral expansion, the chiral logs give an estimate of the higher order terms. For example, this would be useful for the calculation of the $K \rightarrow \pi\pi$ matrix element of \mathcal{O}_6 using the method explained in the previous section. To estimate the size of the logs we take $\Lambda = m_\rho$, for which $L_K(m_K) \approx 0.15$. This is actually very close to the maximal value of $L_K(m)$ as a function of m . Since the coefficient of L_K has a magnitude typically in the ranges $1 - 10$, the chiral log can be a very significant correction.

Second, if one is calculating a quantity without recourse to a chiral expansion, as in the example of B_K , then one can check the calculation by seeing whether the result contains the correct chiral log. This tests that the correct physics is being included. One searches for the chiral log not by looking at the variation with m_K^2 , which is difficult, but by looking at the dependence of the result on the volume of the box. As we explain below, associated with each chiral log is a known finite volume dependent correction.

Finally, chiral logs give an estimate of the size of the error introduced by the quenched approximation. In most quantities the chiral logs have a different coefficient in the quenched approximation and in the full theory. For example, the diagrams of Fig. 3.8 require internal quark loops, and thus are absent in the quenched approximation [34].⁹ This suggests that the quenched calculation of f_K may have a

⁹This is strictly true only for degenerate quarks, and thus for f_π , while not for f_K . The loops of the type shown in Fig. 3.10 do contribute chiral logs to f_K , as discussed below and in Ref. [37]. These logs are not, however, present in full QCD, and thus do not alter the basic observation that quenched chiral logs differ from those in full QCD.

systematic error of $\sim 20\%$. Part of this may be absorbed into an overall shift of scale, so it is more reasonable to consider dimensionless ratios, for example $R = f_K/f_\pi - 1$. Experimentally $R = 0.22$, whereas the chiral log is $0.75L_K \approx 0.12$ in full QCD [33]. Since there is no chiral log in the quenched theory, the latter may underestimate R by 50%.

The calculations are most simply done using the chiral Lagrangian (see Ref. [35] for a description of the method). In full QCD the logs are known for many amplitudes, e.g. for B_K see Ref. [36], and for $K \rightarrow \pi\pi$ amplitudes see Ref. [38]. For quenched QCD it is known that there are no chiral logs in f_π and $\bar{\psi}\psi$, except for the gauge group $SU(2)$ [39, 34]. The only other results are for B_K and related matrix elements [40, 41], and this is the calculation we discuss here. All calculations are done in the continuum, and can be applied to lattice calculations only if one has taken the continuum limit. In practice, the continuum results can be modified to account for some of the lattice artifacts. Although not dependent on the the type of lattice fermion, the results have been used so far only for staggered fermions.

The kaon B-parameter is defined as the ratio of \mathcal{M}_K to its value in vacuum saturation approximation

$$\mathcal{M}_K = \langle \bar{K}^0 | [(\bar{s}_a \gamma_\mu (1 + \gamma_5)) d_a] [(\bar{s}_b \gamma_\mu (1 + \gamma_5)) d_b] | K^0 \rangle = -\frac{16}{3} f_K^2 m_K^2 B_K, \quad (3.108)$$

where the normalization is such that $f_\pi = 93$ MeV. As discussed in the previous section, the lattice calculation is done contraction by contraction, and we pick out the contractions by substituting $d, s \rightarrow d', s'$ in one of the bilinears and one of the external kaons. Only the unprimed quarks are kept in disconnected loops. A check on this procedure is that the resulting chiral logs in B_K agree with those directly calculated in QCD [38].

With this device we can write $B_K = B_V + B_A$ with

$$B_V = B_{V,I} + B_{V,II} \quad (3.109)$$

$$\mathcal{M}_{V,I} = \langle \bar{K}^0 | [\bar{s}'_a \gamma_\mu d'_b] [\bar{s}_b \gamma_\mu d_a] | K^0 \rangle \equiv -\frac{8}{3} f_K^2 m_K^2 B_{V,I} \quad (3.110)$$

$$\mathcal{M}_{V,II} = \langle \bar{K}^0 | [\bar{s}'_a \gamma_\mu d'_a] [\bar{s}_b \gamma_\mu d_b] | K^0 \rangle \equiv -\frac{8}{3} f_K^2 m_K^2 B_{V,II}, \quad (3.111)$$

and B_A defined similarly with $\gamma_\mu \rightarrow \gamma_\mu \gamma_5$. The subscripts I and II refer to the number of traces over color indices. We label the operators appearing in the matrix element $\mathcal{M}_{V,I}$ as $\mathcal{O}_{V,I}$, etc. The arguments of the previous section apply to the lattice transcriptions of the individual matrix elements such as $\mathcal{M}_{V,I}$. If one ignores the chiral logarithms, each of these matrix elements was shown to vanish as m_K^2 .

The calculation of the chiral logs is standard [41], and we give only an overview. One begins with the chiral Lagrangian for the appropriate number of flavors. For example, if one is interested in the quenched logs there are four flavors: s, d, s' and d' . Then one finds the chiral operators which transform under the chiral symmetry as $\mathcal{O}_{V,I}$, etc. This fixes the form of the operators, but not their magnitudes. Finally,

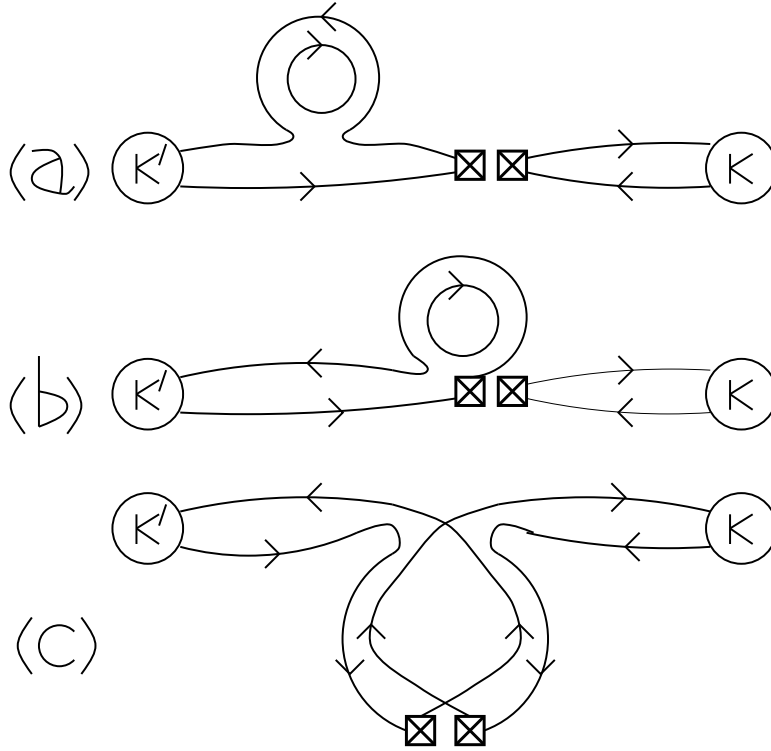


Figure 3.9: Quark diagrams giving chiral logs in \mathcal{M}_K , \mathcal{M}_V and \mathcal{M}_A .

one calculates the loop diagrams and extracts the chiral logs. The diagrams which contribute to \mathcal{M}_K , \mathcal{M}_V , etc. are shown in Fig. 3.9. Each quark-antiquark pair represents a pseudo-Goldstone boson. Given the definition of the B -parameters, one also needs to know the chiral logs in f_K^2 .

An important simplification is that the diagrams of Fig. 3.9a and 3.9b, which involve only one of the external kaon legs, do not contribute to the B -parameters. This is because they give the same multiplicative correction to the matrix elements as the diagrams of Fig. 3.8 give to f_K^2 . Chiral logs in B_K , B_V and B_A thus come only from diagrams of the type shown in Fig. 3.9c. Since these diagrams do not contain an internal quark loop, the logs are the same in full and quenched QCD. (Strictly speaking, this is only true for $m_s = m_d$, as discussed below.) This result is important for two reasons. First, we see that quenched B -parameters do contain chiral logs, and so we can test the calculation by checking for their presence. Second, the B -parameters should suffer from smaller systematic errors, when calculated in the quenched approximation, than quantities which have different logs in quenched and full QCD, e.g. f_K/f_π .

For simplicity, we present the results for $m_s = m_d$. For B_K we have [41]

$$B_K = B_K^0 \left(1 - \frac{2}{f_K^2} \int_k G(k) + \frac{m_K^2}{f_K^2} \int_k G(k)^2 + O(m_K^2) \right), \quad (3.112)$$

where $G = 1/(k^2 + m^2)$ is the kaon propagator, and $\int_k = \int d^4k/(2\pi)^4$. If we cut off the integrals at $|k| = \Lambda$, we find

$$B_K = B_K^0(1 + 3L_K + O(m_K^2)) . \quad (3.113)$$

Terms proportional to Λ^2 coming from quadratic divergences have been absorbed into B_K^0 . In the matrix element \mathcal{M}_K , the chiral log is proportional to $m_K^4 \ln(m_K)$, which is a correction to the leading m_K^2 behavior. Numerically, the correction is significant, roughly a 35% correction if $\Lambda = m_\rho$.

For B_V the result is

$$B_V = \frac{B_K^0}{2} - b_1 - b_2 \frac{\mu^2}{f_K^2} \int_k G(k)^2 + (1.5B_K^0 - b_3)L_K + O(m_K^2) , \quad (3.114)$$

where $\mu = m_K^2/(m_d + m_s)$, which tends to a constant in the chiral limit. The result for B_A is identical, except that the constants b_i flip sign, so that we recover Eq. 3.113 upon adding B_V and B_A . The most important feature of Eq. 3.114 is that the chiral log in the b_2 term ($16\pi^2 \int_k G(k)^2 = -\ln(m_K^2) + \dots$) is not multiplied by m_K^2 , and thus diverges in the chiral limit. The matrix element \mathcal{M}_V does not diverge, behaving as $m_K^2 \ln(m_K)$, and so vanishing in the chiral limit. Nevertheless, the non-analytic corrections dominate the analytic terms for small m_K .

The source of the enhanced chiral logs is the following. In Fig. 3.9c the kaons produced by the four-fermion operator have the flavor composition $s\bar{d}'$ and $s'\bar{d}$, i.e. they are produced with the wrong flavor to match onto the external kaons. The four kaon vertex reorganizes the flavors into $s\bar{d}$ and $s'\bar{d}'$. This means that the kaons in the loop are being produced by the Fierz rearranged operator. In the notation of section 3.4, we have $2V \rightarrow A - V + 2(S - P)$ and $-2A \rightarrow A - V - 2(S - P)$. (Recall that the operator in B_A is $-A$ in this notation.) The important point is that the Fierz operators include P , i.e. $(\bar{s}\gamma_5 d')(\bar{s}'\gamma_5 d)$. The matrix elements of this operator are enhanced by μ^2/m_K^2 over those of V and A . This factor changes the canonical chiral log, $m_K^4 \ln(m_K)$, into the enhanced form $\mu^2 m_K^2 \ln(m_K)$. The same is true for the scalar operator S , though its matrix elements are much smaller numerically. The enhanced chiral logs do not appear in B_K because $V - A$ does not contain S or P in its Fierz transform.

The analysis of lattice Ward identities given in the previous section can presumably be patched up to include the loop effects which give rise to the chiral logs. This should be possible because the lattice Ward identities are exact results, and are of the same form as the continuum Ward identities which underpin the use of the chiral Lagrangian. What needs to be changed are the parameterizations of the correlators.

The enhanced chiral log in B_V does not multiply the lowest order term, unlike the chiral log in B_K . Instead, the constant b_2 in Eq. 3.114 is given by

$$\mathcal{M}_P - \mathcal{M}_S = b_2 \frac{8}{3} f_K^2 \mu^2 [1 + O(m_K^2)] \quad (3.115)$$

$$\mathcal{M}_P = \langle \overline{K^0} | [\overline{s}'_a \gamma_5 d'_a] [\overline{s}_b \gamma_5 d_b] + [\overline{s}'_a \gamma_5 d'_b] [\overline{s}_b \gamma_5 d_a] | K^0 \rangle \quad (3.116)$$

$$\mathcal{M}_S = \langle \overline{K^0} | [\overline{s}'_a d'_a] [\overline{s}_b d_b] + [\overline{s}'_a d'_b] [\overline{s}_b d_a] | K^0 \rangle . \quad (3.117)$$

The normalization is chosen so that $b_2 = 1$ in vacuum saturation approximation, which we expect to give the right sign and correct order of magnitude. Since, for small m_K , $\int_k G(k)^2 \sim \ln(\Lambda/m_K) > 0$, the divergent part of B_V is negative. As discussed in Chapter 8, numerical results do see a negative divergence in B_V (and a corresponding positive divergence in B_A) with the divergence canceling in B_K (Ref. [40]).

It turns out to be difficult to extract the coefficient of the logarithm from fits to the B-parameters. For B_K , the range of m_K is too small, and does not extend to small enough values, so one cannot distinguish L_K from m_K^2 and m_K^4 terms. For B_V and B_A , a log term is needed, but its coefficient is poorly determined. A much better way of picking out the chiral log is to use the associated finite volume effects. This can be done using the methods of Ref. [42], as we now describe.

The basic loop integral can be rewritten

$$\int_k G(k) \equiv \int_{|k|<\Lambda} \frac{d^4k}{2\pi^4} G(k) \equiv G_\Lambda(x=0) , \quad (3.118)$$

where $G_\Lambda(x)$ is the configuration space kaon propagator smeared with a function of range $1/\Lambda$. In a finite box of size L , with periodic boundary conditions, the kaon propagator can be expanded in a sum over image terms involving the infinite volume propagator

$$G_\Lambda^L(0) = G_\Lambda(0) + G_\Lambda(L, 0, 0, 0) + G_\Lambda(0, L, 0, 0) + \dots + G_\Lambda(L, L, 0, 0) + \dots \quad (3.119)$$

Since $G(L) \sim \exp(-m_K L)$ for $m_K L \gg 1$, the expansion converges rapidly, and we need only keep the terms from the nearest images. Furthermore, the typical box is much longer in the time direction than in the spatial directions, so we need only keep the 6 adjacent spatial images. If $L \gg 1/\Lambda$ (which is true in practice) we can drop the smearing function for the image propagators, so that

$$\int_k G(k) \approx G_\Lambda(x=0) + 6G(L, 0, 0, 0) . \quad (3.120)$$

We have used the lattice rotational symmetry to collect terms.

To evaluate the image propagator we use

$$G(L, 0, 0, 0) = \int_0^\infty d\alpha I_0(2\alpha)^3 I_L(2\alpha) e^{-8\alpha} e^{-\alpha m_K^2} \quad (3.121)$$

$$\approx \int_0^\infty d\alpha \frac{1}{16\pi\alpha^2} e^{-L^2/4\alpha} e^{-\alpha m_K^2} \quad (3.122)$$

$$\approx \frac{1}{16\pi^2} \sqrt{\frac{8\pi m_K}{L^3}} e^{-m_K L} , \quad (3.123)$$

where I_L is the L 'th modified Bessel function. The first line is the exact lattice result, the continuum limit of which is given in the second line. The third line is the saddle point approximation to continuum integral. It is a reasonable approximation to the lattice result, differing by 10 – 15% for present parameters [26].

We also need the loop integral involving two kaon propagators

$$\int_k G(k)^2 = -\frac{d}{dm_K^2} \int_k G(k) \quad (3.124)$$

$$\approx -\frac{d}{dm_K^2} G_\Lambda(0) - 6 \frac{d}{dm_K^2} G(L, 0, 0, 0) . \quad (3.125)$$

Again we are interested in the finite volume dependent part of this

$$-\frac{d}{dm_K^2} G(L, 0, 0, 0) \approx \frac{1}{16\pi^2} \sqrt{\frac{2\pi}{m_K L}} e^{-m_K L} . \quad (3.126)$$

This analytic form approximates the true answer to within a few percent.

Collecting these results we find

$$\frac{B_K(L) - B_K(\infty)}{B_K^0} \approx -\frac{6m_K^2}{f_K^2} \left[\frac{d}{dm_K^2} G(L, 0, 0, 0) + 2G(L, 0, 0, 0) \right] \quad (3.127)$$

$$\approx \frac{6m_K^2 e^{-m_K L}}{(4\pi f_K)^2} \sqrt{\frac{2\pi}{m_K L}} \left[1 - \frac{4}{m_K L} \right] . \quad (3.128)$$

In present calculations $m_K L = 4 - 10$, so there is a large cancellation between the two terms in the last parenthesis, which makes the analytic approximation less reliable. This is not very important in practice, since the cancellation also reduces the size of the correction to a level significantly smaller than the statistical errors in present calculations [26].

The finite volume effect is much larger in B_V and B_A

$$B_V(L) - B_V(\infty) = -(B_A(L) - B_A(\infty)) \approx -b_2 \sqrt{\frac{2\pi}{m_K L}} \frac{6\mu^2 e^{-m_K L}}{(4\pi f_K)^2} . \quad (3.129)$$

Since the constant b_2 is not known precisely, the magnitude of the effect should be treated as a rough prediction. The shape of the curve as a function of m_K is, however, completely predicted. Testing this result provides an important check on the ability of lattices to properly include loop effects.

To apply this result to staggered fermion calculations there is one further subtlety that must be dealt with. As described in section 3.4, the Fierz rearrangement of the operator affects both the spin and staggered flavor. The flavor Fierzes as $4P \rightarrow S + P + T - V - A$, so that only a sixteenth of the loops contain Goldstone pions (which have flavor P), i.e.

$$G \rightarrow \frac{1}{16} G^{\text{Goldstone}} + \frac{15}{16} G^{\text{non-Goldstone}} . \quad (3.130)$$

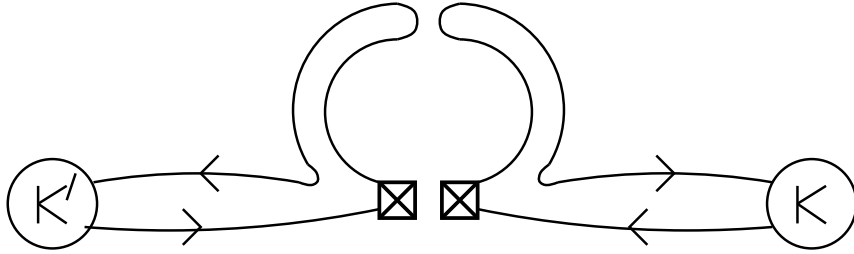


Figure 3.10: Additional diagrams contributing chiral logs to B_K in the quenched approximation for $m_s \neq m_d$.

For the non-Goldstone part of the loop, one should use the non-Goldstone pion masses. On present lattices all pions are degenerate within 10%, so this does not have a large effect. More important is the fact that matrix elements and scattering amplitudes involving non-Goldstone pions will differ from their Goldstone counterparts. This increases the uncertainty in the overall normalization.

We close by mentioning an unresolved question concerning quenched chiral logs. In the quenched approximation the flavor-singlet η' is a pseudo-Goldstone boson, in the sense that the diagrams which differentiate it from the flavor non-singlet pions are absent. This has two effects. First, the quenched mass eigenstates, for non-degenerate quarks, are $\bar{s}s$, $\bar{d}d$ and $\bar{u}u$ rather than the η' , η and π_0 of QCD. This affects the masses which enter in the loop diagrams, which in turn changes the coefficient of the chiral logs. For example in B_K , for $m_u = m_d = 0$, the coefficient of L_K in Eq. 3.113 is 10/3 in full QCD, while it is 4 in quenched QCD.

Secondly, there are additional diagrams such as those shown in Fig. 3.10. These violate the standard power counting rules which imply that each loop comes with an extra factor of m_K^2 . They do not contribute to f_K and B_K if the quarks are degenerate, but they do effect m_K and $\langle \bar{\psi}\psi \rangle$. These diagrams are under study [41, 37], but remain to be fully understood.

3.7 OPEN PROBLEMS

Many of the theoretical problems involved in setting up the calculation of weak matrix elements using staggered fermions have been understood. Numerical calculations have progressed in parallel with increases in theoretical understanding. Nevertheless, significant challenges remain. Particularly interesting is a direct calculation of $K \rightarrow \pi\pi$ decay amplitudes. Here we must face up to the problems of extracting complex amplitudes from Euclidean calculations [43], and the related problem of dealing with final state interactions [44]. Numerical calculations are in their infancy.

It is also essential to continue tests of the method of extracting QCD amplitudes with staggered fermions. To this end, some two loop calculations would be of con-

siderable interest, for they would allow one to test whether the factors of N_f are as harmless as claimed above.

Two loop calculations are also needed to fix the scale to be used in the 1-loop perturbative matching, and to reduce the scheme ambiguity. Although strong arguments have been made in favor of a particular choice of g^2 (Ref. [23]), these need to be backed up.

ACKNOWLEDGEMENTS

Thanks are due to Claude Bernard, Maarten Golterman, Rajan Gupta, Greg Kilcup, Guido Martinelli, Apoorva Patel, and Jan Smit for many helpful conversations over the past few years, to Rajan Gupta and Guido Martinelli for comments on the manuscript, and particularly to Keith Clay for a careful reading of the manuscript. This work is supported in part by an OJI award through grant DE-FG09-91ER40614 and an Alfred P. Sloan Fellowship.

Bibliography

- [1] Susskind, L., Phys. Rev. D16,3031(1977).
- [2] Kawamoto, N. and Smit, J., Nucl. Phys. B192,100(1981).
- [3] Sharatchandra, H.S., Thun, H.J. and Wiesz, P., Nucl. Phys. B192,205(1981).
- [4] Sharpe, S., Proceedings of the Ringberg Workshop, “Hadronic Matrix Elements and Weak Decays”, Ringberg, Germany, (4/88), Nucl. Phys. B (Proc. Suppl.)7A,255(1989).
- [5] Bernard, C., in “From Actions to Answers” (Proc. 1989 Theoretical Advanced Study Institute in Elementary Particle Physics), eds. DeGrand. T. and Tous-saint, D., (World Scientific, Singapore, 1990) pp. 233–292.
- [6] Kluberg-Stern, H., Morel, A., Napoly, O. and Petersson, B., Nucl. Phys. B220,447(1983).
- [7] van den Doel, C. and Smit, J., Nucl. Phys. B1983,122(228).
- [8] Golterman, M.F.L., and Smit, J., Nucl. Phys. B245,61(1984).
- [9] Daniel, D. and Sheard, S., Nucl. Phys. B302,471(1988).
- [10] Daniel, D. and Kieu, T.D., Phys. Lett. 175B,73(1986).
- [11] Wilson. K., and Kogut. J., Phys. Rep. 12,75(1974).
- [12] Joliceur, T., Morel, A. and Petersson, B., Nucl. Phys. B274,225(1986).
- [13] Sharpe, S., Proc. “LATTICE 91”, Tsukuba, Japan, Nov. 1991, Nucl. Phys. B (Proc. Suppl.), (1992), to appear, CEBAF preprint TH-92-01.
- [14] Sharpe, S., private communication.
- [15] Kilcup, G. and Sharpe, S., Nucl. Phys. B283,493(1987).
- [16] Golterman, M.F.L., and Smit, J., Nucl. Phys. B262,328(1984);
Golterman, M.F.L., Nucl. Phys. B273,663(1986).

- [17] Sharpe, S., Proc. “LATTICE 90”, Tallahassee, USA, Oct. 1990, Nucl. Phys. B (Proc. Suppl.)20,429(1991).
- [18] Coste, A., Korthals Altes, C. and Napoly, O., Nucl. Phys. B289,645(1987).
- [19] Gupta, R., Guralnik, G., Kilcup G. and Sharpe, S., Phys. Rev. D43,2003(1991).
- [20] Sheard, S., Nucl. Phys. B314,238(1989).
- [21] Sharpe, S., Patel, A., Gupta, R., Guralnik G. and Kilcup, G., Nucl. Phys. B286,253(1987).
- [22] Daniel, D., Hands, S., Kieu, T.D. and Sheard, S., Phys. Lett. 193B,85(1987).
- [23] Lepage, G.P. and Mackenzie, P., Proc. “LATTICE 90”, Tallahassee, USA, Oct. 1990, Nucl. Phys. B (Proc. Suppl.)20,173(1991).
- [24] Bernard, C., Draper, T. and Soni, A., Phys. Rev. D36,3224(1987).
- [25] Patel, A. and Sharpe, S., in preparation.
- [26] Kilcup, G., Sharpe, S., Gupta R. and Patel, A., Phys. Rev. Lett. 64,25(1990).
- [27] Verstegen, D., Nucl. Phys. B249,685(1985).
- [28] Martinelli, G., Phys. Lett. 141B,395(1984).
- [29] Bernard, C., Draper, T., Soni, A., Politzer, D. and Wise, M., Phys. Rev. D32,2343(1985).
- [30] Feinberg, G., Kabir, P. and Weinberg, S., Phys. Rev. Lett. 3,527(1959).
- [31] Maiani, L., Martinelli, G., Rossi, G.C. and Testa, M., Nucl. Phys. B289,505(1987).
- [32] Sharpe, S., Phys. Lett. 165B,371(1985).
- [33] Gasser, J. and Leutwyler, H., Nucl. Phys. B250,465(1985).
- [34] Sharpe, S., Phys. Rev. D41,3233(1990).
- [35] Georgi, H., “Weak Interactions and Modern Particle Theory”, Benjamin/Cummings, Menlo Park, 1984.
- [36] Bijnens, J., Sonoda, H. and Wise, M., Phys. Rev. Lett. 53,2367(1985).
- [37] Bernard, C. and Golterman, M., Proc. “LATTICE 91”, Tsukuba, Japan, Nov. 1991, Nucl. Phys. B (Proc. Suppl.),(1992), to appear, Washington University preprint HEP/91-31.

- [38] Bijnens, J., Phys. Lett. 152B,226(1985).
- [39] Morel, A., J. Physique, 48,1111(1987).
- [40] Sharpe, S., Proc. “LATTICE 89”, Capri, Italy, Sept. 1989, Nucl. Phys. B (Proc. Suppl.)17,146(1990).
- [41] Sharpe, S., in preparation.
- [42] Gasser, J. and Leutwyler, H., Phys. Lett. 184B,83(1987).
- [43] Maiani, L. and Testa, M., FSI Phys. Lett. 245B,585(1990).
- [44] Lüscher, M., Commun. Math. Phys. 104,177(1986); 105,153(1986); Nucl. Phys. B354,531(1991).

Chapter 8

KAON DECAYS WITH STAGGERED FERMIONS

Stephen R. Sharpe

Physics Department, University of Washington, Seattle, WA 98195, USA

8.1 OVERVIEW

This chapter describes the numerical calculations of weak matrix elements using staggered fermions. The theory behind these calculations is explained in Chapter 3. After a brief discussion of the numerical methods, we discuss results for $\langle \bar{\psi}\psi \rangle$, the kaon B-parameter (B_K), and the real and imaginary parts of $K \rightarrow \pi\pi$ decay amplitude. The bulk of the discussion concerns B_K , the results for which are by far the best and most comprehensive.

Nearly all present simulations use the quenched approximation, and thus suffer from an unknown systematic error. We have argued in Chapter 3 that this error is likely to be smaller for B_K than for most other quantities. Nevertheless, because of this unknown error, we do not stress the phenomenological implications of the results. Instead, we concentrate on the extent to which the sources of systematic error other than quenching have been controlled. These errors are due to finite volume, finite lattice spacing and unphysically heavy quark masses.

In Chapter 3 we explained how, in theory, the lattice axial symmetry makes it advantageous to use staggered fermions when calculating quantities constrained by chiral symmetry. The advantages come at the cost of requiring more complicated operators. The overall conclusion we draw from the results of this chapter is that the theoretical promise of staggered fermions is realized in practice. The complications can be dealt with, and the resulting amplitudes behave as expected in the chiral limit.

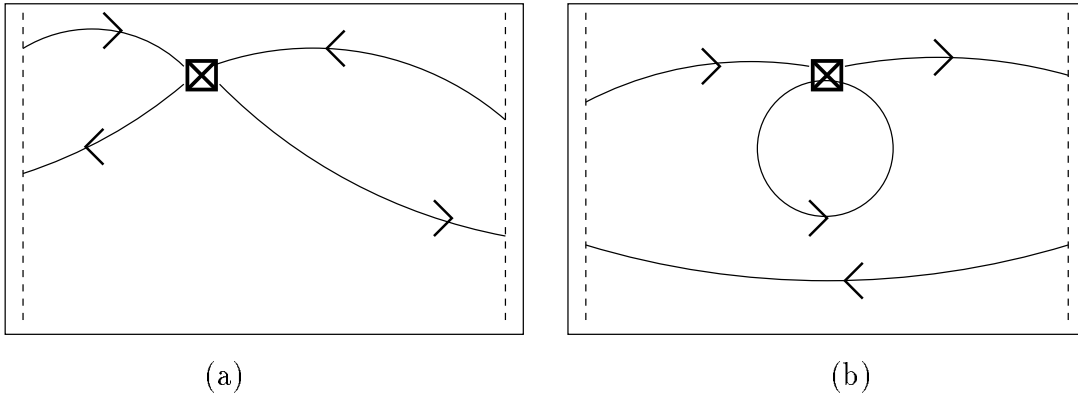


Figure 8.1: The method of calculation of matrix elements used for calculating (a) eight and (b) eye diagrams. The large box represents the lattice, with Euclidean time running horizontally. The small box represents the lattice operator. The vertical dashed lines represent the wall sources.

8.2 NUMERICAL METHODS

The most difficult aspect of calculations with staggered fermions is that the lattice transcriptions of local continuum operators are not themselves local. In the simplest transcription, explained in Chapter 3, bilinear operators involve quark and antiquark fields at different positions on a 2^4 hypercube. Thus the quark and antiquark can be separated by up to four gauge links. In addition, to project onto definite spin and staggered flavor the fields must be summed over the entire hypercube, keeping the same relative position.

The non-locality of the operators presents various problems for matrix element calculations. In such calculations one evaluates correlators involving the weak operator and a number of external particles. The most straightforward method of calculation is to place the operator at the origin of the quark and antiquark propagators. Most calculations with Wilson fermions can be done with local operators, and for these the method requires only a single propagator calculation (at least for eight-diagrams). With staggered fermions, on the other hand, the method requires the calculation of 16 propagators, one for each point in the hypercube. (One can use lattice symmetries to reduce the number of propagators for spectrum calculations, but not for those of matrix elements of four-fermion operators.)

A related problem is that one must make the non-local operator gauge invariant. Three possible methods are discussed in Chapter 3. The results presented here use only the simplest method in which the configurations are fixed to Landau gauge and the gauge links left out of the operator.

To reduce the number of propagators needed, present calculations with staggered fermions [1, 2, 3, 4, 5, 6] use the method illustrated, for eight-diagrams, in Fig. 8.1a. Two wall sources are placed far apart in time, and a quark-antiquark pair emanates from each. The four propagators are joined at the four-fermion operator in the center of the lattice. Since one calculates the propagators from the sources to all

points on the lattice, one has complete freedom to choose the form of the operator. There is thus no difficulty in using non-local hypercube operators. Furthermore, one can reduce the statistical errors by summing the operator over the entire timeslice, and, in addition, over a range of timeslices far enough from both sources that only the lightest state contributes to the matrix element.

Since antiquark propagators can be obtained with no extra work from quark propagators, this method requires only two propagator calculations, one from each source. The reduction in the number of calculations from sixteen to two does, however, come at a price: the projection onto definite external states has been lost. We are interested in the matrix elements of the operator between Goldstone pions having zero spatial momenta,¹ but there is contamination from all other states which couple to the sources. The main problem comes from other pion states, for these have only slightly more energy than the Goldstone pion. The problem is particularly serious for staggered fermions because there are fifteen non-Goldstone pions which become degenerate with the Goldstone pion in the continuum limit. Also potentially dangerous is the contamination from pions with non-zero momenta. Less problematic is the contribution of heavier mesons such as the ρ ; this can be reduced to an insignificant level by keeping the operator far enough from both sources.

The contamination from unwanted pion states can be removed using a combination of wall sources [2]. In these, the source timeslice is fixed to either Coulomb or Landau gauge, and the quark and antiquark sources are then independently summed over the timeslice. Thus both the quark and the antiquark have zero spatial momentum, so that the particle constructed from them also has zero momentum. This removes contamination from non-zero momentum pions. With staggered fermions, forcing the source to have zero spatial momentum stills leaves the choice of an alternating phase, corresponding to a choice of the spin and flavor of the source. It turns out that by combining propagators from two types of wall source one can project against all pions except the Goldstone pion. Thus, for a cost of only four propagators (two from each end) one eliminates all contamination. For a more detailed discussion of wall sources, see Ref. [2].

Lattices have a finite length in the time direction, and so one must take care that the calculation is not contaminated by pions propagating “around the world”. Two methods have been used to avoid this. The first uses Dirichlet boundary conditions in time, and places the source on or near the boundary [2]. This maximizes the number of time slices on which to calculate the matrix element, but at the price of losing a certain number of timeslices due to reflections off the boundary. The method is efficient because the timeslices lost to boundary reflections are also those in which there is contamination from ρ mesons.

This method is well suited to calculating ratios of matrix elements (such as the B -parameters discussed below). It is less good at calculating the matrix elements themselves. For example, the errors in f_K are much larger than those in B_K . To calculate matrix elements one needs to know the “strength” of the sources, i.e. the

¹Throughout this section “pion” refers to all pseudoscalar mesons, including kaons and etas.

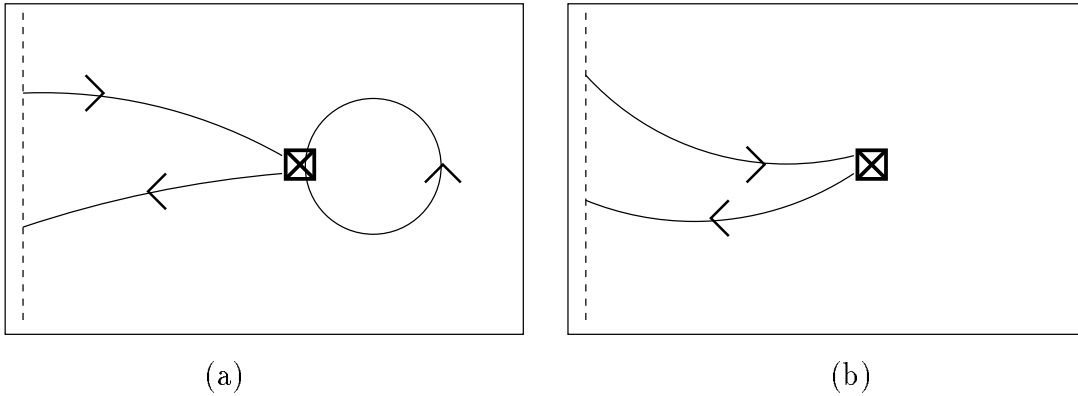


Figure 8.2: Correlators needed to calculate kaon to vacuum amplitudes needed for subtractions.

amplitude for the wall-source to create a pion. To extract this amplitude one must calculate the pion propagator from one wall source to the other, and the resulting signal is relatively poor [2].

A second method is designed to alleviate this problem [6]. The lattice is doubled in the time direction ($L_t \rightarrow 2L_t$), and periodic boundary conditions used for propagators on the doubled lattice. A single propagator from a wall-source now has a forward and backward component, both propagating over the same gauge links (in opposite directions) since the lattice is doubled. Thus the backward component can be shifted in time by L_t , and then combined with the forward component just as in Fig. 8.1a. The work required is essentially the same as for the first method, since a propagator on a doubled lattice takes roughly twice the computer time to calculate as two undoubled propagators. The advantage is that there are no boundary effects, so that the amplitude for the wall-source to create a pion can be obtained with good accuracy. We refer to this as the “FB” method.

A variant of this method combines the forward component of a propagator from a source at $t = 0$ with the backward part of a propagator from a source at $t = 1.5L_t$. This extends the distance between the sources. Since the second propagator emanates from the center of the lattice, we refer to this as the “FC” method.

As explained in Chapter 3, kaon decay amplitudes require the calculation of eye-diagrams in addition to eight-diagrams. The generic form of the eye-diagrams is shown in Fig. 8.1b. The extra ingredient needed is the quark loop. What one needs is the propagator from every lattice site to its nearby points. The present method of choice is to use pseudofermions, as explained in Ref. [4]. These give a noisy estimator of the propagator from all sites on the lattice to all others, the accuracy of which diminishes rapidly as the distance of propagation increases. For pseudoscalar and scalar operators (such as are needed in the calculation of B_5 and B_6 described below) one obtains sufficiently good statistics with 24 pseudofermions per lattice. For vector and axial operators (needed to study the $\Delta I = 1/2$ rule), the signal is poor with this many pseudofermions.

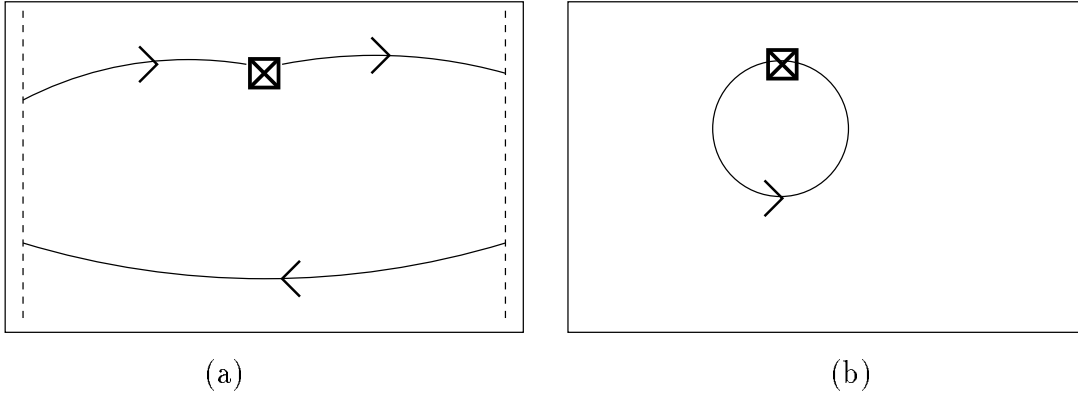


Figure 8.3: Correlators needed for vacuum saturation and subtraction matrix elements.

As explained in Chapter 3, eye-diagrams give rise to mixing with lower dimension operators, the contribution of which must be subtracted. This subtraction requires the calculation of the kaon to vacuum matrix elements illustrated in Fig. 8.2. Essentially what is needed is the ratio of Fig. 8.2a to that of Fig. 8.2b. The result is then multiplied by the bilinear matrix element shown in fig. 8.3a. To repeat the calculations in vacuum saturation approximation requires, in addition, the condensate of Fig. 8.3b.

The kaon to vacuum amplitude of Fig. 8.2a is proportional to $m_s - m_d$, and what is needed is the proportionality constant. In the degenerate limit this constant can be evaluated by replacing one of the propagators in the correlator with a “derivative propagator”, dG/dm . For the example of B_5 and B_6 discussed in Chapter 3, it is the propagator in the loop which is replaced by a derivative. Given G , the calculation of dG/dm uses

$$\frac{dG(n_2; n_1)}{dm} = - \sum_n G(n_2; n)G(n; n_1) , \quad (8.1)$$

and thus requires only one extra inversion [7].

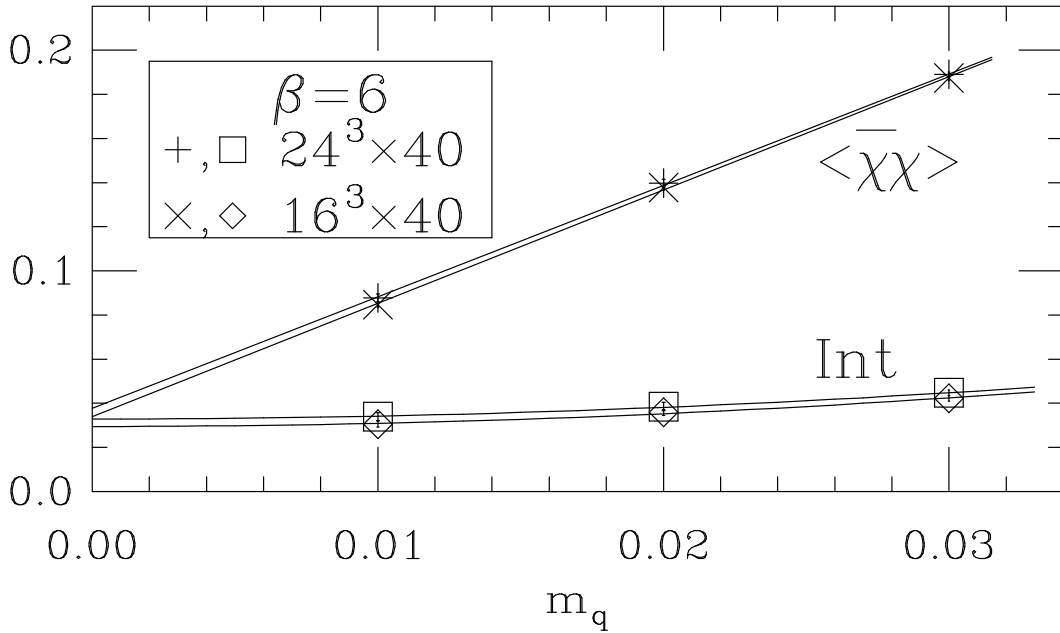


Figure 8.4: Results for the condensate at $\beta = 6$, together with linear fits. Results for the intercept are also shown, fit to $b + cm_q^2$.

8.3 CHIRAL SYMMETRY BREAKING

The major reason for using staggered fermions is the existence of a continuous chiral symmetry, similar to that of QCD. Numerical simulations show that this symmetry is broken dynamically. With staggered fermions the condensate, $\langle \bar{\chi}\chi \rangle \equiv \overline{\chi}(1 \times 1)\chi$ (for notation see Chapter 3), is an order parameter for chiral symmetry breaking in the massless limit. One expects, for a given lattice spacing, that

$$\langle \bar{\chi}\chi \rangle = \langle \bar{\chi}\chi \rangle_0 + cm_q + O(m_q^2), \quad (8.2)$$

where c is constant. A non-zero intercept, $\langle \bar{\chi}\chi \rangle_0$, indicates that chiral symmetry is broken. The quantities appearing in Eq. 8.2 are dimensionless, so that the relation to the physical condensate $\langle \bar{\psi}\psi \rangle$ is $\langle \bar{\chi}\chi \rangle_0 = N_f \langle \bar{\psi}\psi \rangle a^3 + O(a^4)$. (The factor of $N_f = 4$ appears since there are four staggered flavors propagating around the quark loop.) The factor of a^3 means that the intercept $\langle \bar{\chi}\chi \rangle_0$ decreases rapidly as the lattice spacing is reduced. The slope c , however, is not physical (it is a quadratic divergence cut-off by the lattice), and varies slowly with the lattice spacing. Thus it becomes increasingly difficult to extract $\langle \bar{\chi}\chi \rangle_0$ as one approaches the continuum limit.

For finite volume the symmetry cannot be broken, and, as m_q is reduced to zero, Eq. 8.2 eventually fails [8]. In practice one uses quark masses large enough that finite volume effects are small, and assumes a linear form for $\langle \bar{\chi}\chi \rangle$. An example of the results is shown in Fig. 8.4 (Ref. [2]). The lightest quark mass, $m_q = 0.1$, corresponds roughly to $0.5m_s$. The finite size effects are smaller than the statistical

errors, which are themselves small. It is clear that $\langle\bar{\chi}\chi\rangle$ has a non-zero intercept, with $\langle\bar{\chi}\chi\rangle_0 = 0.033(2)$ on the 24^3 lattice. As explained in Ref. [7], with no additional work one can also calculate $\text{Int} = \langle\bar{\chi}\chi\rangle - md\langle\bar{\chi}\chi\rangle/dm$. This removes the linear term in the expansion of the condensate [7]. Results for this quantity are also shown in the Fig. 8.4, and confirm the non-zero intercept.

To extract the physical condensate we need to know the lattice spacing. An average value, based on comparing a number of quantities to their experimental counterparts, is $1/a = 1.9$ GeV. The lattice result is then $\langle\bar{\chi}\chi\rangle_{\text{phys}} = 0.054(4)\text{GeV}^3$, three to four times larger than the continuum estimate of Ref. [9]: $\langle\bar{u}u\rangle = 0.0144\text{GeV}^3$ at a scale $\mu \sim 2\text{GeV}$. Part of this discrepancy can be explained by perturbation theory, as discussed in Chapter 3. The correction factor is $\sim 1 + g^2 35/16\pi^2$ which is ~ 1.4 if one uses $g^2 \sim 2$, as suggested by Lepage and Mackenzie [10]. This reduces the discrepancy to about a factor of two. A reasonable hypothesis is that this remaining factor is due to the use of the quenched approximation, as explained in Ref. [2].

Surprisingly, this discrepancy does not appear to affect many other quantities. For example, the ratios m_ρ/f_π and m_{proton}/m_ρ are close to their physical values [2, 11]. In addition, the value for the strange quark mass obtained from the vector mesons (i.e. comparing $(m_{K^*} - m_\rho)/m_\rho$ to experiment) is close to that obtained from the pseudoscalars (using m_K/f_π). It is very important, however, to try to understand why the large lattice condensate does not distort hadronic properties. Without such understanding, one does not know whether a given quenched result is likely to be wrong by a factor of three.

One aspect of the puzzle that can be understood is the effect on quark masses. When one uses m_K/f_π to fix the strange quark mass, one is, in effect, fixing the product $m_s\langle\bar{\chi}\chi\rangle_0$ to its physical value [2]. Since the lattice condensate is three times too large, the lattice quark mass must be smaller than continuum estimates by the same factor, as is indeed true. This is directly relevant for the continuum matrix elements of the operators \mathcal{O}_5 and \mathcal{O}_6 , as discussed below.

β	N_f	$a(\text{fm})$	$1/a(\text{GeV})$	L	L_t	BC	Configs
5.7	0	0.2	1	16	32	D	30
6.0	0	0.105	1.9	16	24	P+A	40
				16	40	D	14+17
				24	40	D	15+9
6.2	0	0.08	2.5	18	42	D	27
				32	48	P+A	12+11
6.4	0	0.06	3.4	32	48	P+A	8+8+7
5.7	2	0.1	2	16	32	D	40

Table 8.1: Parameters of simulations. N_f is the number of dynamical fermions. Lattices are of size $L^3 \times L_t$, with periodic boundary conditions (BC) on the gauge links. Fermionic BC are periodic in space, and either Dirichlet (D), periodic (P) or antiperiodic (A) in time, as given in the table. The numbers of configurations in independent streams are given.

8.4 DATA SAMPLE

We give a status report on the results for weak matrix elements as of March, 1992. Numerical results are available from the set of lattices shown in Table 8.1. The only unquenched lattices are those generated by the Columbia group, using quark masses $m_q = 0.01$ and $m_q = 0.025$, roughly $0.5m_s$ and $1.25m_s$ respectively [12]. Discussion of the lattice generation parameters for the quenched simulations, and of the calculation of propagators with Dirichlet boundary conditions in time, can be found in Ref. [2], while propagators with periodic and antiperiodic boundary conditions in time are discussed in Ref. [6].

When we present results we need to know the lattice spacing for each of these lattices. Various estimates can be made, using, for example, the rho mass or f_π extrapolated to zero quark mass. These estimates need not agree, however, because the calculations are done using an approximation to QCD. For definiteness, in much of the following we use the average of the estimates obtained using the nucleon and rho masses, which are given in the table. Other estimates differ by up to 20% from these values [2].

8.5 B_K AND RELATED MATRIX ELEMENTS

B_K , B_V and B_A have been discussed at length in Chapter 3. These are the best measured matrix elements, with results good enough to study volume, quark mass and lattice spacing dependence. The accuracy of the calculations is due to a number of factors. First, one can write the B -parameters as ratios, for example

$$B_K = \frac{3}{8} \frac{\langle \overline{K^0} | [\bar{s}_a \gamma_\mu (1 + \gamma_5) d_a] [\bar{s}_b \gamma_\mu (1 + \gamma_5) d_b] | K^0 \rangle}{\langle \overline{K^0} | [\bar{s}_a \gamma_\mu (1 + \gamma_5) d_a] | 0 \rangle \langle 0 | [\bar{s}_b \gamma_\mu (1 + \gamma_5) d_b] | K^0 \rangle}. \quad (8.3)$$

Such ratios have smaller statistical errors than the matrix elements themselves. Second, there are no noisy eye-diagram contributions. Third, the fact that the B -parameters are ratios means that they can be calculated using wall sources, for one only needs to have sources of K^0 and $\overline{K^0}$ mesons, but one does not need to know their strengths, since these cancel in the ratio. Wall sources have various advantages, as discussed in section 8.2.

To make use of the lattice results we must convert them to a continuum renormalization scheme. This involves two steps, which we discuss for the phenomenologically interesting quantity B_K . First we must calculate the perturbative Z -factors, i.e. match the lattice and continuum operators. The calculation is explained in Chapter 3, and yields the result that the corrections are small, $\sim 1 - 2\%$. They are, however, uncertain as it is not completely clear which value of the coupling constant g^2 should be used [10]. Because of this, we simply omit the perturbative corrections from the results presented here.

The second step is slightly more involved. Although B_K is dimensionless, it depends on the lattice spacing a through its non-zero anomalous dimension. At one loop, in the quenched approximation, the dependence is $B_K \propto g^{4/9} \propto |\ln a|^{-2/9}$. Thus the combination $B_K g^{-4/9}$, or a quantity proportional to this, is scale invariant. (In the full theory with four active flavors the anomalous dimension differs slightly and the invariant quantity is $B_K g^{-12/25}$.) It is this invariant quantity that we are ultimately interested in calculating, since the CP-violating parameter ϵ is proportional to it. In addition, it must be used when comparing results at different lattice spacings, and when comparing to continuum estimates of B_K . Unfortunately, the one-loop anomalous dimension does not determine which value of g to use, and this introduces some uncertainty in the comparisons. Possible choices are the bare lattice coupling (defined by $g^2 = 6/\beta$), and the coupling in a continuum scheme such as \overline{MS} . Arguments for the latter choice (with a scale $\sim \pi/a$) are given in Ref. [10]. The choice is important, since $g^2(\overline{MS})$ is roughly twice the bare lattice value.

What we do here is the following. When comparing results at different lattice spacings at a qualitative level we simply ignore the $g^{-4/9}$, since for our range of β it varies by only $\sim 2\%$. In quantitative comparisons we use $B_K g^{-4/9}$ with g being the bare lattice coupling. This probably underestimates the dependence on lattice spacing, but has the advantage of being entirely defined in terms of lattice quantities. In effect, we renormalize all results back to $g = 1$, i.e. to $\beta = 6$. Finally, to compare lattice and continuum estimates we use $\hat{B}_K = B_K \alpha_s(\mu)^{-6/25}$, which is the standard normalization used in the continuum. To be precise, we first use the bare lattice coupling to renormalize the results back to $\beta = 6$, and then, following Ref. [13], calculate \hat{B}_K using $\alpha_s(\beta = 6)^{-6/25} = 1.34$. This is the value obtained in the \overline{MS} scheme, with $\Lambda = 200$ MeV and the scale $\mu = 0.92/a$, with a given in Table 8.1.

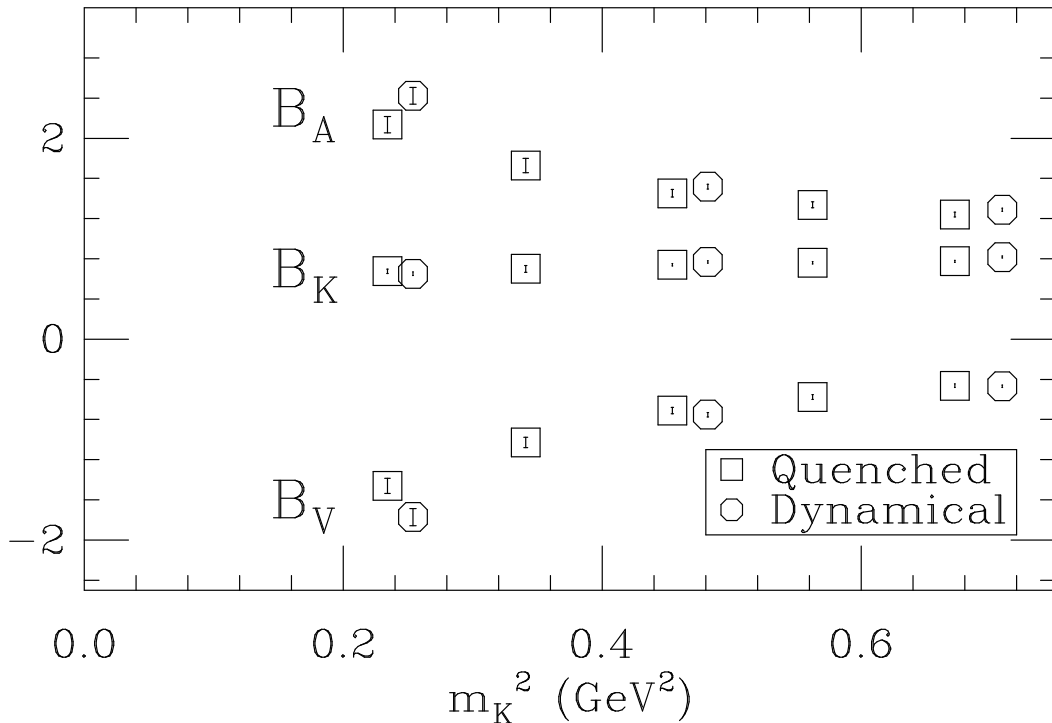


Figure 8.5: Results for B -parameters on $L = 16$ lattices. Quenched results at $\beta = 6$ from Ref. [1], unquenched from Ref. [5]. The kaon masses have been converted to physical units using $a^{-1} = 2$ GeV for both lattices.

8.5.1 The Effect of Quenching

Results from quenched and unquenched simulations on 16^3 lattices are shown in Fig. 8.5. The valence quark masses are $m_q = 0.01, 0.02$ and 0.03 in lattice units, which roughly correspond to $m_s/2, m_s$ and $1.5m_s$ respectively. The dynamical mass in the full QCD simulations is $m_q = 0.01$, so that only the lightest mass point has the same dynamical and valence quark masses.

The figure shows that the effect of dynamical fermions with $m_q = m_s/2$ is small. This is also true of the results with dynamical mass $m_q = .025 \approx 1.25m_s$ [5]. Indeed, with the accuracy of present calculations, it is difficult to distinguish between the quenched and dynamical lattices using either B_K or the spectrum. There is a small difference between quenched and full QCD results for B_V and B_A , but this could be due to an incorrect choice of lattice spacing for one or other of the theories.

It is not clear how to interpret the apparent unimportance of dynamical fermions. On the one hand it could indicate that quenched B_K is a good approximation to that in the full theory. This would be consistent with the fact that the chiral logarithms are the same. On the other hand, one does not expect large effects (other than changes in the overall scale) until the dynamical quark mass is considerably smaller than $m_s/2$. Clearly what is needed is results at smaller dynamical quark masses.

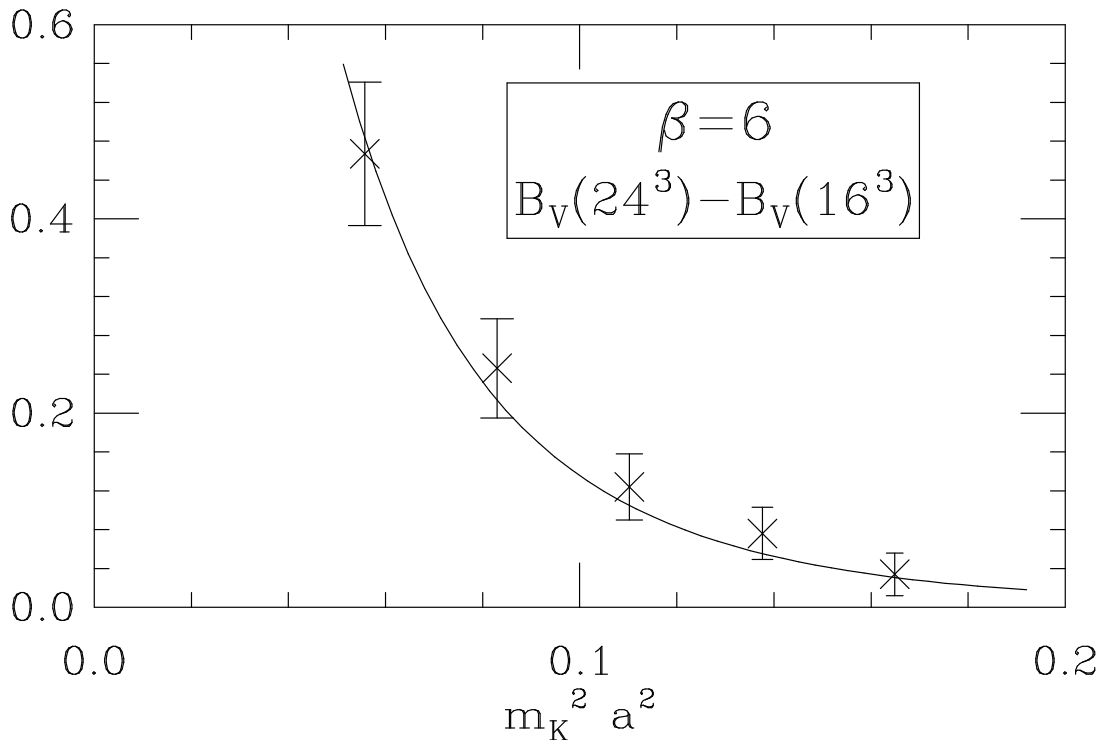


Figure 8.6: Finite volume effects in B_V [3].

8.5.2 Finite Volume Dependence and Chiral Logarithms

For the remainder of this section we concentrate on quenched calculations of B parameters, with the aim of showing the extent to which systematic errors are under control. As explained in Chapter 3, B_V and B_A are predicted to diverge as $\pm \ln(m_K)$, respectively, due to the contributions of chiral loops. The divergence should cancel in $B_K = B_V + B_A$, which is expected to have a finite chiral limit. Figure 8.5 shows that these expectations are qualitatively correct. The quantitative agreement is, however, less convincing [3]. Although B_V and B_A fit reasonably well to the expected form $c_1 \ln(m_K) + c_2 + c_3 m_K^2 + c_4 m_K^4$, the coefficients are large and poorly determined, and the truncation in the series is not justified. A fit to the simple form $c_0/m_K^2 + c_1$ is actually better. A power divergence is not expected, however, and, if present, would indicate a failure of the theoretical analysis explained in Chapter 3. Fortunately, as we discuss shortly, there is better evidence for the existence of the chiral logarithm from the finite volume dependence. If the case for presence of chiral logarithms is to be completely convincing, however, results at smaller quark masses are required, for these will be able to distinguish between the two fits.

The evidence for the existence of chiral logarithms is shown in Fig. 8.6. As discussed in Chapter 3, the chiral logs give rise to finite volume effects in B_V and B_A , the form of which can be predicted analytically. This has been tested at $\beta = 6$ using the lattices with $L = 16$ and 24. It turns out that $L = 24$ is indistinguishable from infinite volume with the present errors. Fig. 8.6 shows the difference in B_V between the two lattices together with the analytic form. The shape is completely predicted,

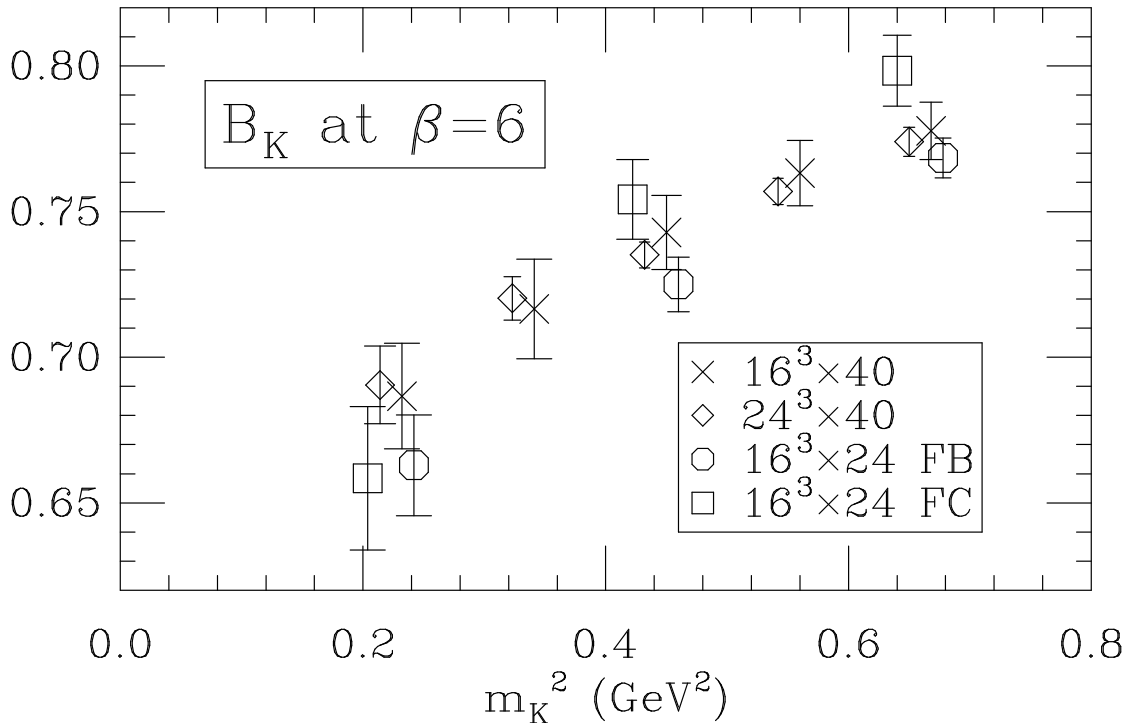


Figure 8.7: B_K at $\beta = 6$, using $a^{-1} = 2$ GeV. $16^3 \times 40$ and $24^3 \times 40$ results from Ref. [1], the remaining points from Ref. [14]. Some points are offset for clarity.

and is in good agreement with the results. The overall size of the effect is predicted only roughly, but agrees in sign and order of magnitude with expectations. This is a good example of the use of chiral logarithms as a diagnostic tool in calculations.

The analysis also predicts both the magnitude and shape of the finite volume effects in B_K . They turn out to be small, about a $\sim 0.5\%$ difference between $L = 16$ and $L = 24$ at the lightest kaon mass. As shown in Fig. 8.7, this is too small to be observed with present errors, and, indeed, there is no significant difference between the results from $L = 16$ and $L = 24$ lattices. In turn this means that, at $\beta = 6$, a lattice of size $L = 16$ is large enough to calculate B_K to better than 1% for $m_q \geq m_s/2$. Thus, at $\beta = 6.4$, where the lattice spacing is half that at $\beta = 6$, the lattices of size $L = 32$ should be large enough.

The figure shows that B_K has a smooth chiral limit, with no indication of a divergence at small m_K . This is expected with staggered fermions because of the lattice axial symmetry. The data are not good enough, however, to differentiate between analytic terms of the form $\alpha + \beta m_K^2 + \gamma m_K^4$ and chiral logarithms proportional to $m_K^4 \ln m_K$. Thus the prediction for the coefficient of the chiral logarithms discussed in Chapter 3 cannot yet be tested. This test is not crucial, however, because one does not need to extrapolate to extract the physical B_K . Since the lightest lattice kaon mass is close to the physical quark mass, one simply reads off $B_K(m_K^{\text{phys}})$.

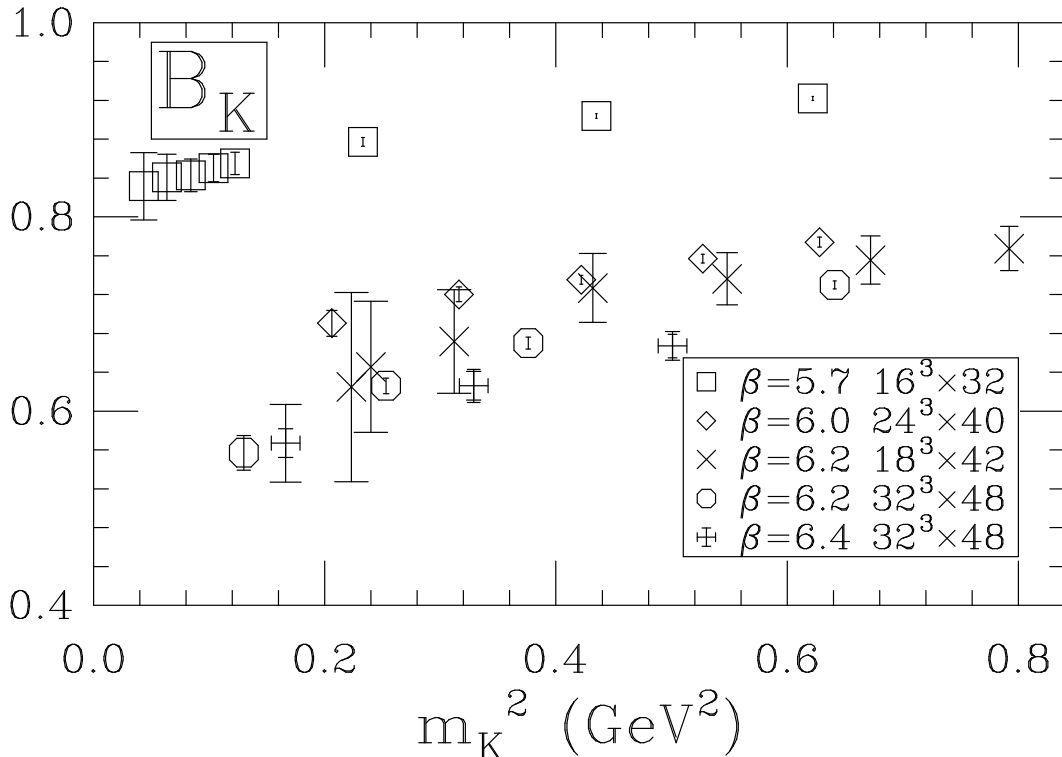


Figure 8.8: B_K for various β , with m_K converted to physical units using a^{-1} from Table 8.1.

8.5.3 Lattice Spacing Dependence

Also shown in Fig. 8.7 are preliminary data from $16^3 \times 24$ lattices [14]. These are chosen to have a physical size close to that of the $32^3 \times 48$ lattices at $\beta = 6.4$. They serve as a test bed for the new methods employed on the the latter lattices, and on $32^3 \times 48$ lattices at $\beta = 6.2$. For example, the new methods use wall sources in Landau gauge, as compared to the Coulomb gauge sources of the earlier calculations.² The fact that the two sets of results (labeled FB and FC in the figure) are consistent with each other and with the older results engenders confidence in the new methods.

The results for B_K from all values of β are collected in Fig. 8.8. For $\beta = 6$, only the $L = 24$ results are shown. These and the results at $\beta = 6.2$ on the $18^3 \times 42$ lattices are from Ref. [1]. The results at $\beta = 6.2$ and 6.4 from the $32^3 \times 48$ lattices are preliminary [14], and are the average of the results obtained from the FB and FC methods. At $\beta = 5.7$ the results for the heavier quark masses are also new [14], while those at the lighter quark masses are from a reanalysis of the data presented in Ref. [1]. The original analysis contained an error.

There is a clear trend visible from the figure: B_K falls with increasing β , which corresponds to decreasing lattice spacing. The evidence for this trend is strengthened by the new results at $\beta = 6.2$. These have smaller errors than the old results on $L = 18$ lattices, and give a lower estimate for $B_K(m_K)$, although the two sets of data are consistent within errors.

The trend is illustrated more clearly in Fig. 8.9. This shows the scale invariant

²For a discussion of the effect of this gauge choice see Ref. [2].

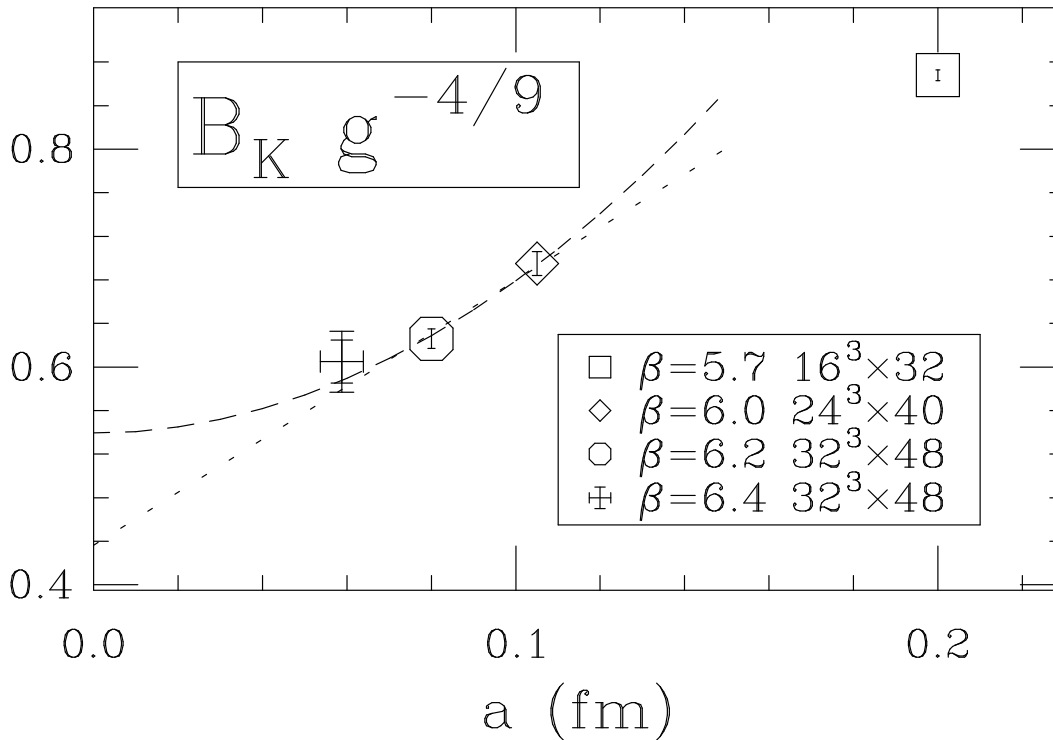


Figure 8.9: Scaling behavior of $B_K g^{-4/9}$, using a^{-1} from Table 8.1.

combination $B_K g^{-4/9}$, evaluated at the physical kaon mass, plotted versus lattice spacing. This quantity should approach its continuum value with corrections suppressed by powers of a . To extract the continuum value we need to know whether the dependence on a is linear or quadratic. As discussed in Chapter 3, the corrections from the staggered fermion action are most likely of $O(a^2)$, while the operators whose matrix elements we are calculating have, in general, corrections of $O(a)$. For the operators we use, however, the $O(a)$ terms vanish at tree level, and thus are suppressed by at least one power of α_s . Thus it is unclear whether the dominant correction should be linear or quadratic in a , or some combination thereof.

To investigate this, we make linear and quadratic fits to the first three points, i.e. we fit to

$$B_K g^{-4/9} = B_{\text{cont}}(1 + (a\Lambda_n)^n) ; \quad n = 1, 2 . \quad (8.4)$$

We do not include the point at $\beta = 5.7$, since the correction there is so large (80-100%) that it makes no sense to truncate the series in a . The fits are shown in the figure. The quadratic fit is slightly better ($\chi^2 = 0.5$ vs. $\chi^2 = 1.2$), but both fits are reasonable. The fits give $\Lambda_1 = 1.1$ GeV and $\Lambda_2 = 1.0$ GeV. Clearly, present data are not good enough to decide on the form of the dependence on a . This is a major source of uncertainty in B_K .

We collect the results from Fig. 8.9 in Table 8.2. We include the values of the continuum quantity \hat{B}_K . The results for \hat{B}_K are lower than previous estimates [1] because of the rapid dependence on a . This reduction is of considerable phenomenological significance [13]. This is particularly true if it indicates that there are large

β	$a(\text{fm})$	Size	Configs	$B_K(m_K)$	$B_K(m_K)g^{-4/9}$	\hat{B}_K
5.7	0.2	$16^3 \times 32$	30	0.88(1)	0.87(1)	1.20(1)
6.0	0.105	$24^3 \times 40$	15	0.70(1)	0.70(1)	0.96(2)
6.2	0.08	$32^3 \times 48$	12+11	0.62(1)	0.63(1)	0.86(2)
6.4	0.059	$32^3 \times 48$	8+8+7	0.60(3)	0.61(3)	0.84(4)
∞	0	Quadratic			0.54(2)	0.75(3)
∞	0	Linear			0.44(4)	0.61(5)

Table 8.2: Quenched results for B_K evaluated at the physical kaon mass.

$O(a)$ effects in all matrix elements, for then extracting continuum values will require smaller lattice spacings (and consequently larger lattices) than previously expected. Thus it is important to discuss possible sources of error. These include:

1. The results at $\beta = 6.2$ and 6.4 are preliminary, and so the errors are not completely trustworthy.
2. The quark and antiquark in the lattice kaon are almost degenerate, unlike those in the physical kaon. We discuss this effect below, and find that it appears to increase $B_K(m_K)$ by about 3%. We have included this factor in the values of \hat{B}_K given in Table 8.2. This enhancement factor is, however, quite uncertain.
3. When calculating $B_K g^{-4/9}$, one must choose whether to use the bare lattice value of g^2 , or a continuum value such as that in the \overline{MS} scheme. The latter is about a factor of two larger [10]. As discussed above, we use the bare lattice value for the results presented in the figures and the table. With the boosted g^2 the extrapolated results for \hat{B}_K increase to 0.78(3) and 0.66(6) for quadratic and linear fits, respectively. These numbers include the 3% increase due to non-degenerate quarks, and thus can be directly compared to those in Table 8.2. There is a few percent increase.
4. The use of Landau gauge operators. As explained in Chapter 3, these are defined by first fixing to Landau gauge, and then removing the gauge links from the non-local operators. This is a well defined prescription in perturbation theory, but non-perturbatively there are Gribov copies, so the prescription is ambiguous. In practice, one simply defines “Landau gauge” as the result of using a particular algorithm for a certain number of iterations. Since the operators only extend over a hypercube, we expect that any problem from Gribov copies should vanish as a power of the lattice spacing, and should not influence the continuum limit. It may, however, increase the size of $O(a)$ corrections. Indeed the values for $\Lambda_{1,2}$ are twice as large as those obtained from a study of flavor symmetry restoration [14].
Another problem of Landau gauge is that its spectrum contains unphysical

states. For example, there may be quark and gluon states in addition to hadrons. In the calculations which use Landau gauge wall sources (those at $\beta = 6.2$ and $\beta = 6.4$ in Fig. 8.9), it is, in principle, possible that the matrix element being measured is contaminated by unphysical contributions. An uncorrelated quark–antiquark pair is likely to be the unphysical state with smallest energy which can contribute. In practice, however, it is found that the energy of this pair is close to the rho-meson mass, and far exceeds the pion mass [15]. Thus the contamination, if present, is exponentially suppressed.

The uncertainty due to gauge fixing is the least well understood, and requires further study. The calculation should be repeated using gauge invariant operators.

Another way of improving the reliability of the lattice results is to use smeared operators in which the parts proportional to a are suppressed by an additional power of α_s . As discussed in Chapter 3, it is relatively simple to construct such operators. Calculations using these operators are underway [14].

8.5.4 Quark Mass Dependence

We end this subsection by discussing the following issue: the quarks comprising the lattice kaons have masses much closer to each other than those of the physical kaon. A useful measure of the quark mass difference is $\delta = (m_s - m_d)^2 / (m_s + m_d)^2$. This is nearly unity for physical kaons, while ranging from zero (degenerate quarks) to 0.25 for the lattice kaons. To obtain the physical result we have to extrapolate in δ . To aid in this extrapolation, we recall the discussion of the chiral behavior of B_K given in Chapter 3. Defining $y = m_K^2 / (4\pi f_\pi)^2$, the result is

$$B_K = B_0 [1 + by + cy\delta - (3 + \delta)y \ln y] , \quad (8.5)$$

where b and c are unknown constants [16]. The last term is the chiral logarithm, the expression for which is an approximation valid for $\delta \ll 1$, and reasonably accurate for $\delta \sim 1$. As explained in Chapter 3, there are unresolved problems due to loops of flavor singlet pions in the quenched theory, which may lead to additional terms proportional to δ . Finally we note that in the full theory the expression is the same, except that $(3 + \delta) \rightarrow (3 + \delta/3)$.

The best test of the quark mass dependence comes from the results at $\beta = 6$ on $L = 24$ lattices. The available quark masses are 0.01, 0.02, 0.03, which we label 1, 2, 3 respectively. The quark masses are then written as $[m_d m_s, m'_d m'_s]$, where the primes distinguish the masses in one kaon from those in the other. Thus, for example, [13, 13] means that $m_d = m'_d = 0.01$ and $m_s = m'_s = 0.03$. The results are shown in Fig. 8.10. The issue is whether [11, 11], [22, 22], and [33, 33] lie on the same line as [12, 12], [13, 13] and [23, 23]. In addition, there are two points, [11, 13] and [11, 33], for which the two kaons are not degenerate, so that the weak operator inserts momentum. The chiral behavior of Eq. 8.5 still applies, with m_K^2 replaced by $m_{K'} m_K$ in y , except that there are additional terms proportional to $m_{K'}^2 - m_K^2$.

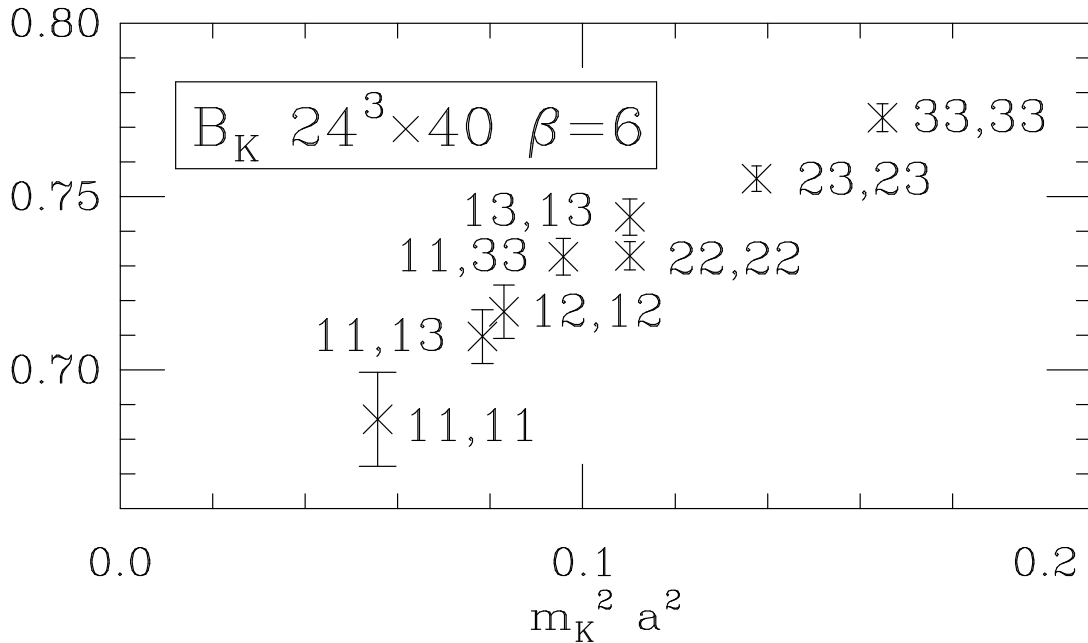


Figure 8.10: B_K for various combinations of quark masses [6].

The results show that the terms in Eq. 8.5 dependent on y alone give the dominant non-leading chiral correction. There is some indication, however, of an increase in B_K with δ , though it is as yet of marginal significance. To give an idea of the possible magnitude of this effect, we take seriously the difference of ~ 0.01 between [22,22] ($\delta = 0$) and [13,13] ($\delta = 0.25$). Linearly extrapolating to the physical value $\delta = 1$, B_K increases by ~ 0.04 , roughly a 5% increase. This is for a lattice kaon somewhat heavier than the physical kaon. According to Eq. 8.5 the effect is roughly proportional to $y\delta \propto m_K^2\delta$, and so will be smaller for the physical kaon. Using $a^{-1} = 1.9$ GeV, the reduction is by a factor of 1.7, so that the increase in B_K is roughly 3% for the physical kaon. This number is illustrative only, but it shows that the issue deserves further study. The conclusion of Ref. [1] that the effect on B_K of extrapolating to $\delta = 1$ was less than 1% was over-optimistic.

8.6 $K \rightarrow \pi\pi$ AMPLITUDES

We are interested in both the CP-invariant parts (which are the real parts in our convention) and the CP-violating imaginary parts of the $K \rightarrow \pi\pi$ amplitudes. The real parts exhibit the puzzling $\Delta I = 1/2$ rule, $\mathcal{A}_0/\mathcal{A}_2 \approx 22$, where \mathcal{A}_I is the amplitude for kaon decays to pions of isospin I . The part of the effective weak Hamiltonian responsible for this decay is completely known, and shows a mild enhancement of \mathcal{A}_0 over \mathcal{A}_2 , but the bulk of the enhancement must be due to QCD effects. Establishing that this is indeed so is an important challenge for lattice calculations.

The imaginary part of the amplitude can be measured experimentally by observ-

ing a non-zero ϵ' . The present experimental situation is confused, which allows the exciting possibility of a prediction of ϵ' . Here the effective weak Hamiltonian is not completely known, due to the uncertainty in m_t (the dominant contributions to ϵ' involve internal top quarks) and in the CP-violating angle δ . These uncertainties are being steadily reduced, however, so that the accuracy of a prediction, if one could be made, is improving.

What we must calculate are matrix elements of the form $\langle K|\mathcal{O}|\pi\pi\rangle$, where \mathcal{O} is one of the four-fermion operators in the effective weak Hamiltonian. Present calculations with staggered fermions do not attempt the direct calculation of this amplitude, but aim to calculate its value (up to phase space factors) in the chiral limit. As explained in Chapter 3, to do this one need only calculate $\langle K|\mathcal{O}|\pi\rangle$ and $\langle K|\mathcal{O}|0\rangle$. It is important to realize, however, that there are likely to be large higher order terms in the chiral expansion. The dominant such terms are probably due to final state interactions between the pions. In model calculations these increase $I = 0$ amplitudes by as much as a factor of 2, and reduce $I = 2$ similarly [17]. Nevertheless, a calculation of the amplitudes in the chiral limit would be an important first step.

8.6.1 CP Violating Amplitudes

The calculation of the imaginary parts of the amplitudes is more advanced than that of the real parts. A large contribution comes from the “strong-penguin” operators

$$\mathcal{O}_5 = -2 \sum_{q=u,d,s} \bar{s}_a(1-\gamma_5)q_b \bar{q}_b(1+\gamma_5)d_a , \quad (8.6)$$

$$\mathcal{O}_6 = -2 \sum_{q=u,d,s} \bar{s}_a(1-\gamma_5)q_a \bar{q}_b(1+\gamma_5)d_b . \quad (8.7)$$

These have been written in Fierz rearranged form, for the dominant contractions are those involving scalar and pseudoscalar bilinears. The matrix elements of \mathcal{O}_6 are discussed at length in Chapter 3, and the discussion can be taken over without change to \mathcal{O}_5 . The upshot is that one has to calculate eight-diagrams, eye-diagrams and the diagrams needed for subtractions. The general form of the on-shell matrix elements is

$$\langle K|\mathcal{O}_{5,6}|\pi\rangle = \alpha' - \beta'_\pi m_\pi^2 - \beta'_K m_K^2 + \gamma m_K m_\pi + O(m_K^4 \ln m_K) + O(m_K^4) . \quad (8.8)$$

The primes indicate that the coefficients differ slightly from those used in Chapter 3, in that they do not depend on the quark masses. The result of Chapter 3 is that all the coefficients are non-zero for the eight and eye diagrams separately, so that neither diagram vanishes in the chiral limit. When one adds these diagrams, however, the α' and β'_π terms vanish, so that the sum goes to zero in the chiral limit. The subtraction term by itself also has only β'_K and γ terms non-zero. When added to the sum of eights and eyes, however, the β'_K term vanishes. The total amplitude,

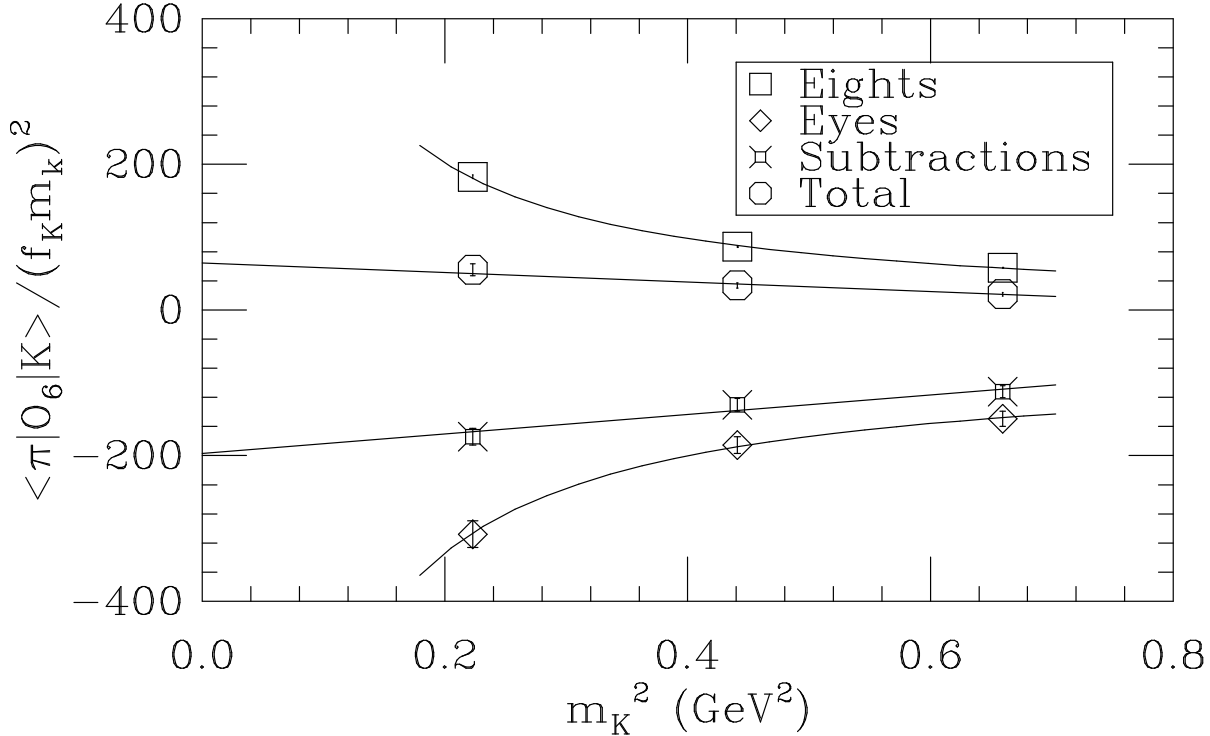


Figure 8.11: Matrix elements of \mathcal{O}_6 for $L = 24$, $\beta = 6$ lattices, using $a^{-1} = 2$ GeV [5]. The eights and eyes are fit to a form $b/m_K^2 + c$, while the subtractions and total are fit to $b + cm_K^2$.

therefore, contains only the term proportional to $m_K m_\pi$. As shown in Chapter 3, its coefficient γ is related in a known way to the chiral limit of $\langle K | \mathcal{O} | \pi\pi \rangle$.³

These cancellations are clear in Fig. 8.11, which shows the matrix element divided by $m_K^2 f_K^2$ [5]. If $\alpha' \neq 0$, the result should diverge like $1/m_K^2$. As expected, this is true for both eights and eyes. Both the subtraction and the total should not diverge, and the results are consistent with this expectation. Because the calculation is done with all quarks degenerate, so that $m_K = m_\pi$, it is not possible to distinguish β'_π , β'_K and γ terms. Thus we do not expect the results for the subtraction and total matrix element to look different in shape. We do, however, expect there to be a significant numerical cancellation, since the subtraction is an unphysical, quadratically divergent quantity, whereas the total amplitude is physical. This expectation is borne out by the results: the cancellation among the three contributions reduces the matrix element by about an order of magnitude.

Figure 8.11 does not demonstrate convincingly that the total matrix element has the correct chiral behavior. This is partly because the quark masses are relatively large ($m_s/2 < m_q < 3m_s/2$), so that higher order terms may be significant. These terms are reduced in importance by considering ratios of matrix elements. One can calculate the matrix elements of \mathcal{O}_5 and \mathcal{O}_6 in lattice vacuum saturation approxima-

³Strictly speaking, this has only been fully demonstrated for gauge invariant operators, and not for Landau gauge operators. This hardly affects the results for B_5 and B_6 given below, since the dominant contribution is from gauge invariant operators. It might have some effect on the results for \mathcal{A}_0 , but, as will be seen, these results are not statistically significant.

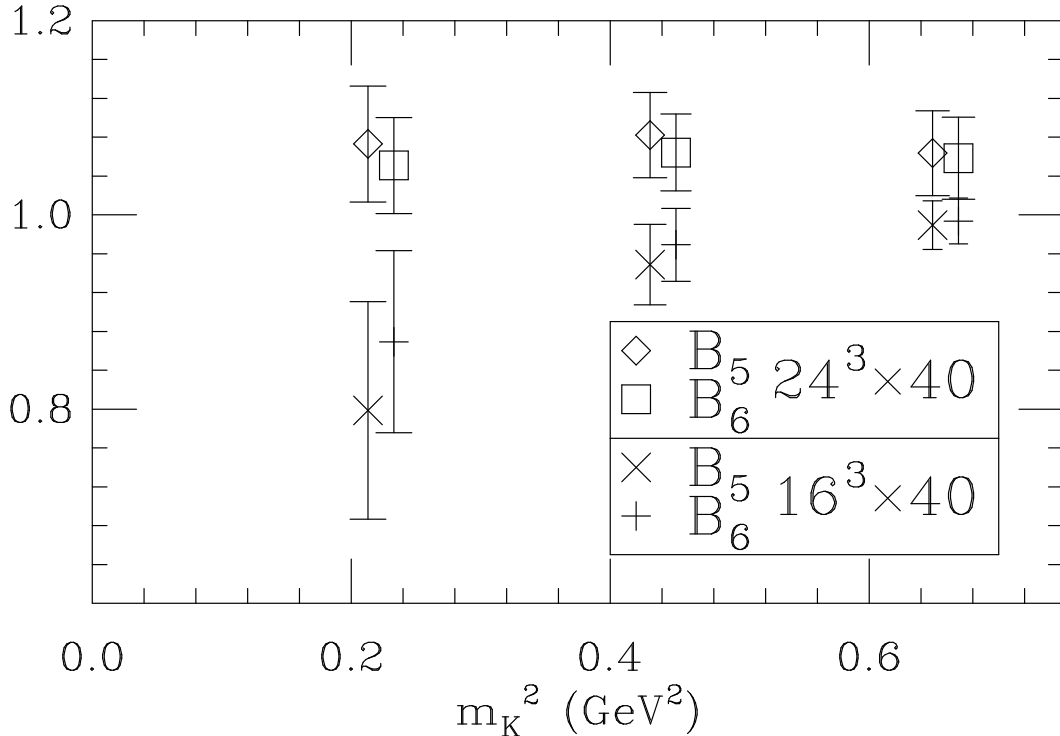


Figure 8.12: B_5 and B_6 at $\beta = 6$ on two lattice sizes, using $a^{-1} = 2$ GeV [6].

tion [18, 19, 20]. Taking the ratio of the matrix elements to their respective values in vacuum saturation approximation defines B_5 and B_6 . These B -parameters should tend to a constant in the chiral limit. The results are displayed in Fig. 8.12, and indeed show a smoother chiral limit than the matrix elements themselves. The results show some finite volume dependence, although improved statistics are needed to establish this convincingly. We conclude that the subtraction method works for staggered fermions, and that B_5 and B_6 are both close to unity in the chiral limit.

It is important to distinguish the two types of prediction made by the vacuum saturation approximation: (1) the overall magnitude of the matrix elements, e.g. $B_6 = 1$; and (2) the ratios of matrix elements with different color index contractions, e.g. $B_5 = B_6$. If the latter relation holds, then the matrix element of \mathcal{O}_6 is three times that of \mathcal{O}_5 , which is the expectation based upon the color Fierz factor and factorization. Large N_c arguments suggest that the second type of prediction should be less reliable than the first [21]. Instead, the results show that the latter predictions are more accurate. This presents an interesting challenge to large N_c calculations. The fact that vacuum saturation is a better approximation for $B_{5,6}$ than for B_K may well be due to the complete failure of the approximation for the two parts of B_K , i.e. B_V and B_A . The predictions $B_V = 0$ and $B_A = 1$ fail because of the enhanced chiral logarithms (discussed in Chapter 3). There are no such logarithms for the components of B_5 or B_6 .

The most reasonable way of using these results in phenomenological studies of ϵ' is to take the lattice B_5 and B_6 and multiply them by the matrix elements evaluated in continuum vacuum saturation approximation [22]. This is the approach used in

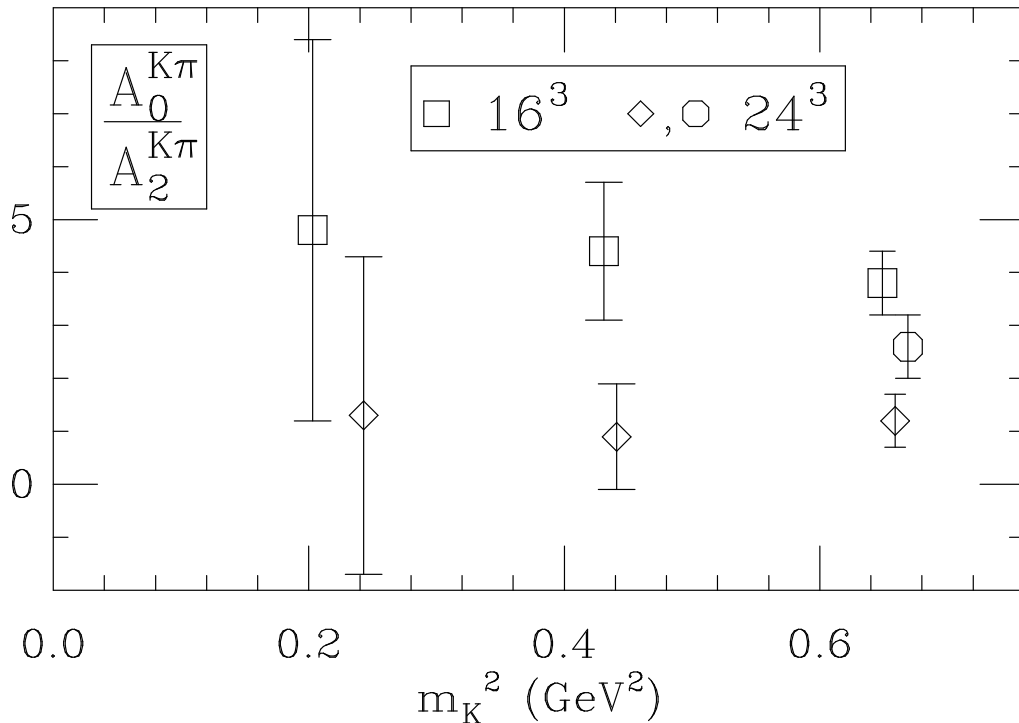


Figure 8.13: Results for $\mathcal{A}_0/\mathcal{A}_2$ at $\beta = 6$ using $a^{-1} = 2$ GeV. The 24^3 results come from the sample of 15 lattices, except at the highest mass where there are also results from the independent sample of 9 lattices [6].

various recent analyses, for example that of Ref. [13]. It has three advantages over a direct lattice calculation of the matrix elements: (1) the uncertainty in the lattice spacing only enters through the anomalous dimensions of the operators; (2) the matrix element in vacuum saturation approximation turn out to be proportional to $1/m_s$ [22], and, since the lattice value for m_s in the quenched approximation differs substantially from the continuum value, it is better to use the continuum m_s ; (3) the perturbative corrections are large (see Chapter 3) but substantially cancel in the B -parameters. In fact, the perturbative corrections are not included in the results of Fig. 8.12. The main disadvantage of this approach is that the higher order chiral effects (e.g. final state interactions) are not included, for these do not appear in the vacuum saturation estimate of $K \rightarrow \pi\pi$ amplitudes.

8.6.2 CP Conserving Amplitudes

We close this chapter with a brief summary of the status of the calculation of the real parts of the kaon decay amplitudes. As for the imaginary parts, present calculations only attempt to extract the value of these amplitudes in the chiral limit using $\langle K|\mathcal{O}|\pi\rangle$ and $\langle K|\mathcal{O}|0\rangle$. The real part of \mathcal{A}_2 requires only eight diagrams (the calculation is essentially the same as for B_K), and is known with small errors. To calculate \mathcal{A}_0 , however, requires eye diagrams and subtractions. The bilinears appearing in the operators are vectors and axial-vectors, and it turns out that the

signal for these is much worse than for scalar and pseudoscalar bilinears which dominate B_5 and B_6 . The collected results are shown in Fig. 8.13 (Ref. [6]). There appears to be a significant finite volume effect at the highest quark masses, but the disagreement between the two independent $L = 24$ calculations suggests that the statistical errors may have been underestimated. It is clear that to extract a reliable chiral limit much improved statistics are needed.

One tentative conclusion that can be drawn from these results is that $\mathcal{A}_0/\mathcal{A}_2$ is not large in the chiral limit.⁴ It seems unlikely that the result will exceed $\mathcal{A}_0/\mathcal{A}_2 = 10$. If so, then the experimental value of ≈ 22 can only be reached if there are large higher order chiral corrections to $K \rightarrow \pi\pi$ amplitudes.

A possible source of such corrections is the final state interactions between the two pions. This motivates a study of $\pi\pi$ interactions, as a preliminary step towards the calculation of the full $K \rightarrow \pi\pi$ amplitude. The calculation has been done for the $I = 2$ channel, which involves quark or antiquark exchange only [23, 24, 25]. The results for the scattering amplitude at threshold are in good agreement with the current algebra predictions of Weinberg. It will be interesting to repeat the calculation for the more challenging $I = 0$ channel, for which one must include quark annihilation.

ACKNOWLEDGEMENTS

I thank Rajan Gupta, Greg Kilcup and Guido Martinelli for comments. This work is supported in part by an OJI award through grant DE-FG09-91ER40614 and an Alfred P. Sloan Fellowship.

⁴For a discussion of the various contributions to $\mathcal{A}_0/\mathcal{A}_2$ see Ref. [6].

Bibliography

- [1] Kilcup, G., Sharpe, S., Gupta R. and Patel, A., Phys. Rev. Lett. 64,25(1990).
- [2] Gupta, R., Guralnik, G., Kilcup G. and Sharpe, S., Phys. Rev. D43,2003(1991).
- [3] Sharpe, S., Proc. “LATTICE 89”, Capri, Italy, Sept. 1989, Nucl. Phys. B (Proc. Suppl.)17,146(1990).
- [4] Kilcup, G., Proc. “LATTICE 89”, Capri, Italy, Sept. 1989, Nucl. Phys. B (Proc. Suppl.)17,533(1990).
- [5] Kilcup, G., Proc. “LATTICE 90”, Tallahassee, USA, Oct. 1990, Nucl. Phys. B (Proc. Suppl.)20,417(1991).
- [6] Sharpe, S., Proc. “LATTICE 90”, Tallahassee, USA, Oct. 1990, Nucl. Phys. B (Proc. Suppl.)20,429(1991).
- [7] Gupta, R., Guralnik, G., Kilcup, G., Patel, A., Sharpe S. and Warnock, T., Phys. Rev. D36,2183(1987).
- [8] Gasser J. and Leutwyler, H., Phys. Lett. 188B,477(1987).
- [9] Gasser J. and Leutwyler, H., Phys. Rep. 87,77(1982).
- [10] Lepage, G.P. and Mackenzie, P., Proc. “LATTICE 90”, Tallahassee, USA, Oct. 1990, Nucl. Phys. B (Proc. Suppl.)20,173(1991).
- [11] Cabasino, S. *et al*, (APE Collaboration) Phys. Lett. 258B,202(1991).
- [12] Chen, H., Proc. “LATTICE 90”, Tallahassee, USA, Oct. 1990, Nucl. Phys. B (Proc. Suppl.)20,370(1991).
- [13] Lusignoli, M., Maiani, L., Martinelli, G. and Reina, L., Rome Prep.N.792 (March 1991).
- [14] Sharpe, S., Proc. “LATTICE 91”, Tsukuba, Japan, Nov. 1991, Nucl. Phys. B (Proc. Suppl.),(1992), to appear, CEBAF preprint TH-92-01.
Gupta, R., Kilcup, G. and Sharpe, S., in preparation.

- [15] Bernard, C., Soni, A. and Yee, K., Proc. "LATTICE 90", Tallahassee, USA, Oct. 1990, Nucl. Phys. B (Proc. Suppl.)20,410(1991).
- [16] Sharpe, S., in preparation.
- [17] Isgur, N., Maltman, K., Weinstein J. and Barnes, T., Phys. Rev. Lett. 64,161(1990).
- [18] Kilcup, G. and Sharpe, S., Nucl. Phys. B283,493(1987).
- [19] Sharpe, S., Gupta, R., Guralnik, G., Kilcup, G. and Patel, A., Phys. Lett. 192B,149(1987).
- [20] Sharpe, S., Patel, A., Gupta, R., Guralnik G. and Kilcup, G., Nucl. Phys. B286,253(1987).
- [21] Buras A. and Gérard, J.-M., Phys. Lett. 203B,272(1988).
- [22] Chivukula, R.S., Flynn J. and Georgi, H., Phys. Lett. 171B,453(1982).
- [23] Guagnelli, M., Marinari E. and Parisi, G., Phys. Lett. 240B,188(1990).
- [24] Sharpe, S., Proc. "LATTICE 90", Tallahassee, USA, Oct. 1990, Nucl. Phys. B (Proc. Suppl.)20,406(1991).
- [25] Sharpe, S., Gupta, R. and Kilcup, G., University of Washington preprint, DOE/ER/40423-23 (March 1992).